NASA CONTRACTOR REPORT

NASA CR-1057

NASA CR-1057

THE DIELECTRIC CLAD AXIAL SLOT ANTENNA

by C. M. Knop, J. J. Meier, and O. K. Kim

Prepared by
ANDREW CORPORATION
Chicago, Ill.
for Langley Research Center

NATIONAL AERONAUTICS AND SPACE ADMINISTRATION • WASHINGTON, D. C. • JUNE 1968

NASA CR-1057

THE DIELECTRIC CLAD AXIAL SLOT ANTENNA

By C. M. Knop, J. J. Meier, and O. K. Kim

Prepared under Contract No. NAS 1-6242 by
ANDREW CORPORATION
Chicago, Ill.

for Langley Research Center

NATIONAL AERONAUTICS AND SPACE ADMINISTRATION

For sale by the Clearinghouse for Federal Scientific and Technical Information
Springfield, Virginia 22151 – CFSTI price $3.00

"Beauty is truth, truth beauty",—that is all
Ye know on earth, and all ye need to know.

Ode on a Grecian Urn

John Keats

TABLE OF CONTENTS

TABLE OF CONTENTS (Continued)

TABLE OF CONTENTS (Continued)

LIST OF FIGURES

LIST OF FIGURES (Continued)

LIST OF FIGURES (Continued)

LIST OF TABLES

THE DIELECTRIC CLAD AXIAL SLOT ANTENNA

By
C. M. Knop, J. J. Meier, and O. K. Kim

SUMMARY

The input admittance of a rectangular waveguide whose opening forms an axial slot on a metal cylinder of outer radius, a, which is coated with a concentric layer of homogeneous dielectric of outer radius, b, and of relative dielectric constant, ε_r, is analyzed. The analysis is accomplished by relating this input admittance to the external admittance by equating the complex power flow on each side of the slot. The external admittance is found by expanding the fields in the exterior of the cylinder in the form of a Fourier mode expansion following Wait, and casting the expression for the integration of Poynting's vector over the physical space of the slot into one over mode space via Parseval's theorem. The slot width is made small enough so that the higher order modes produced at the slot in the waveguide due to the slot-cylinder transition are negligible. Additionally, the guide is dielectric loaded, so as to realize sufficiently high attenuation at the slot location of the higher order modes produced at the excitation point for a given length of guide.

Consideration to both the axial and azimuthal surface waves which can exist and which are excited on the dielectric coated cylinder is given. The cutoff conditions for the axial surface wave modes which can be excited are derived by the determination of the singularities in the integrand

expression for the external admittance. By comparing these results with those for an unslotted dielectric coated cylinder, it is shown that TM and hybrid EH axial surface wave modes are not excited by this thin axial slot and that only TE and hybrid HE axial surface wave modes can be excited. The dominant of these is shown to be the TE_o mode. The coating thickness for the given dielectric constant and frequency range is then chosen under the thickness required for this mode to exist, so that no axial surface waves are excited.

Examination of the azimuthal surface waves which can exist shows that the lowest order TM_o mode has a zero cutoff frequency and is excited. However, it is shown that this and all other possible azimuthal surface waves which can exist appear as leakage radiation and the contribution they make to the conductance is already taken into account in the external admittance expression, i.e., they are not singularity contributions.

Using the derived expressions, computations of input admittance were made over the range of frequencies corresponding to $1.40 \leq C \leq 1.60$, with a center frequency corresponding to C=1.50 (f=1.905 gc for a=1.482 inches), where $C=\beta_v a = \frac{2\pi a}{\lambda_v}$ is the circumference in free space wavelengths of the metal cylinder. The following coating conditions were considered: no coating, a Teflon coating ($\varepsilon_r=2.10$) of several thicknesses corresponding to W=b/a=1.0,

1.2 and 1.5; and a plasma coating ($0 \leq \varepsilon_r \leq 1$) of the same thickness.

The measured values for the input admittance seen by the coaxial feed line and the theoretical values for this admittance (obtained from the theoretical value of waveguide input admittance and the measured values of the scattering matrix elements) were obtained and compared. The measured and computed values for this admittance for the no coating case agree within 10% for conductance values over the entire 10% bandwidth (1.80 to 2.00 gc) and within 10% for susceptance values over approximately a 2% bandwidth (1.945 to 1.980 gc).

A comparison for the coating case could not be made, since only the external conductance was computed, and in going from the waveguide admittance to the coaxial line admittance, both external conductance and susceptance are required. However, since the measured values of input admittance for the Teflon coating case have a smoother behavior with respect to frequency, as compared to the no coating case, it is anticipated that equally good or better agreement with theory will be found. The computed external conductance values were checked by considering the limiting case of zero coating thickness (W=1.00) which gave, as should be, the no coating results.

It is shown that an admittance comparison of theory and experiment cannot meaningfully be made in waveguide, due to the nature of the scattering matrix elements and

the high value of reflection coefficient in this guide. Comparison with theory and experiment should only be made in the coaxial line.

Equatorial plane radiation patterns, both computed and measured, are in excellent agreement for both the no coating case and the Teflon coating cases.

Generalizing from the given findings, it is concluded that the analyses given for both the input admittance and equatorial plane radiation patterns of the axial slot waveguide fed dielectric clad antenna are accurate enough for predicting these quantities a priori within state-of-the-art accuracies. Application of this knowledge to plasma diagnostics is then discussed.

I. INTRODUCTION

The radiating structure considered consists of an axial slot-dielectric clad cylinder, where the slot is the open end of a rectangular waveguide, as depicted in Fig. 1, which defines all the dimensions. The basic problem is to determine the normalized input waveguide admittance, y_{in}, as a function of all the parameters. To accomplish this the idealized model of an infinitely long perfectly conducting cylinder is adopted and an assumed form for the tangential electric fields across the slot is made. Following the work of Wait [1], the fields exterior to the cylinder, i.e., $\rho \geq a$, are then expanded in their appropriate Fourier mode representation as a standing radial wave in the coating region, $a \leq \rho \leq b$, and as a traveling radial wave in the air region $b \leq \rho \leq \infty$. These total fields contain six unknown mode transform coefficients which are determined by applying the six tangential boundary conditions (two at $\rho=a$ and four at $\rho=b$). This then determines all the field transforms in the coating and air regions in terms of the tangential field transforms across the slot. The pertinent tangential electric and magnetic fields across the slot give the power flow through the slot. This power is the same on either side of the slot. This fact enables one to relate the input admittance in the guide to the external admittance of the slot. This is facilitated by using Parseveal's theorem to express the required Poynting vector integration over physical space to one over mode space.

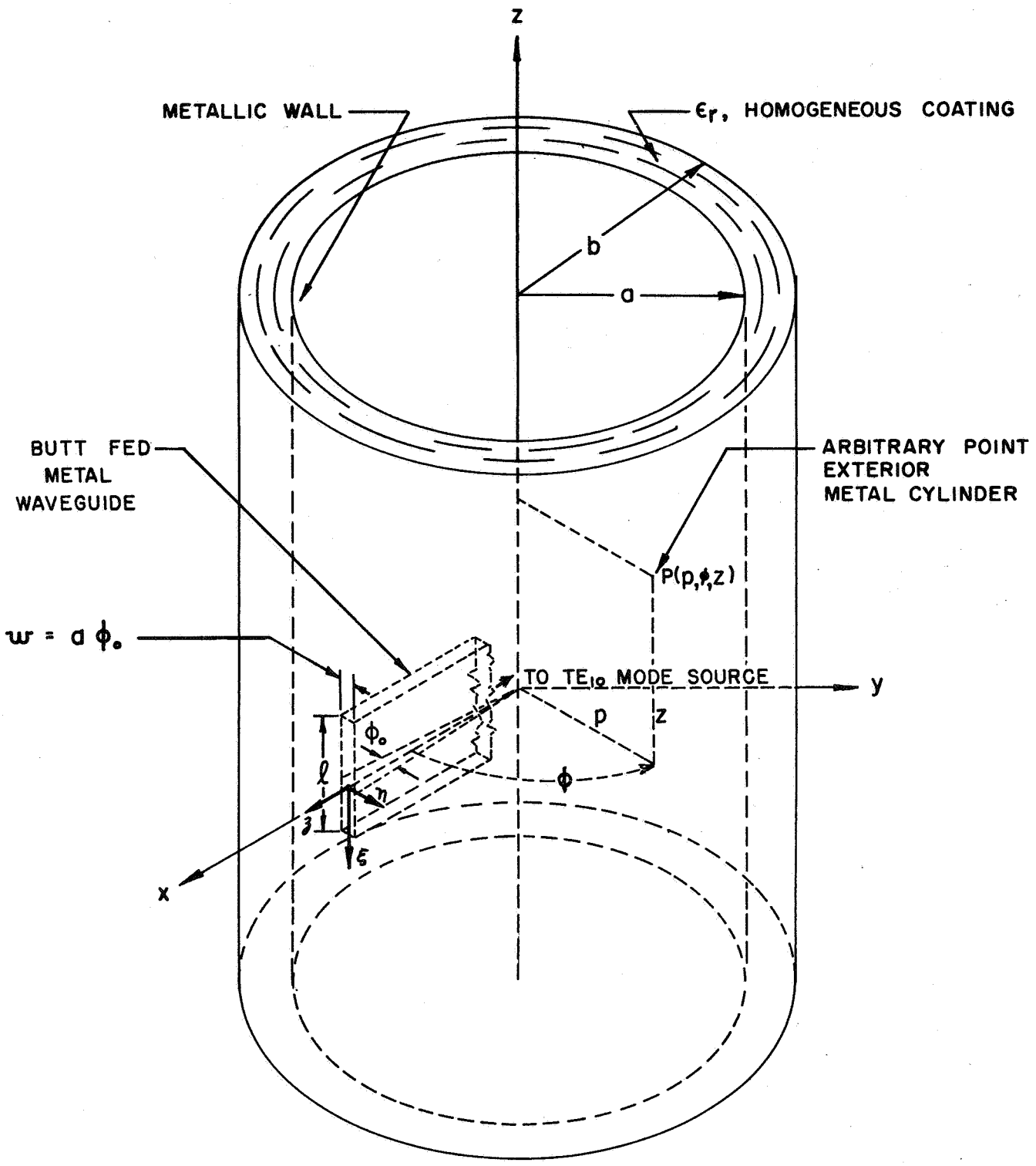

FIG. I GEOMETRY OF THE DIELECTRIC CLAD AXIAL SLOT CYLINDER ANTENNA

The expression for y_{in} is so obtained and the significance of the singularities in the integrand of this expression as related to axial surface waves is brought out, and the cut-off conditions of these axial surface waves are derived. It is shown that the contribution of the axial surface waves to the conductance appear as explicit pole contributions in the form of residues at these singularities. Azimuthal surface waves can and do also exist, but their contribution to the conductance does not appear explicitly, since it is already included in the integration. The physical reason for this is that, whereas axial surface waves carry power only axially, azimuthal surface waves radiate into the air region.

The expression for y_{in} is then rationalized into real and imaginary parts representing the conductance and susceptance, respectively. These parts take on different forms for each coating case considered: no coating, Teflon coating, and a plasma coating, and are explicitly given in a normalized form ready to be programmed and computed.

Computations for these cases are given, where in all cases the coating thickness is chosen sufficiently thin, so that no axial surface waves exist. Experimental results for the no coating and Teflon coating cases are given and compared with computations. A sufficiently detailed description of the antenna construction and measurement method is given to ascertain their validity. Generalizations based

on these comparisons between theory and experiment are then made.

II. FORMAL SOLUTION PROCEDURE

a. Formulation of External Admittance Expression

Since the method of expanding the fields in terms of cylindrical Fourier transforms is clearly described in Wait [1], it will only be outlined, as required, here. If we let $\psi(\rho,\phi,z)$ represent any scalar component of either $\mathbf{E}$ or $\mathbf{H}$, then it can be represented by

$$\psi(\rho,\phi,z) = \sum_{m=-\infty}^{m=+\infty} \int_{-\infty}^{\infty} \bar{\psi}_m(h,\rho) e^{-jhz}\, dh \quad e^{-jm\phi} \tag{1}$$

where $\bar{\psi}_m(h,\rho)$ is the transform of ψ, and is

$$\bar{\psi}_m(h,\rho) = \frac{1}{(2\pi)^2} \int_{-\pi}^{\pi} \int_{-\infty}^{\infty} \psi(\rho,\phi,z) e^{+jhz} dz\, e^{+jm\phi} d\phi. \tag{2}$$

Referring to Fig. 1, if it is assumed that the tangential electric fields are

$$E_\phi(a,\phi,z) = \begin{cases} 0 & \text{off slot} \\ E_o \cos\left(\frac{\pi z}{\ell}\right) & \text{on slot} \end{cases}, \tag{3}$$

$$E_z(a,\phi,z) = 0 \tag{4}$$

then the corresponding transforms are

$$\bar{E}_{\phi m}(h,a) \equiv \bar{E}_{\phi} = - \frac{\sqrt{a_m}\, V_o \cos(\frac{h\ell}{2})}{2\pi\ (\frac{a}{\ell})\,(h^2\ell^2-\pi^2)} \tag{5}$$

where $V_o = E_o w$ = voltage across center of slot, and

$$a_m = \left[\frac{\sin(\frac{m\phi_o}{2})}{(\frac{m\phi_o}{2})} \right]^2$$

From (339) of Wait, the transform of $H_z(a,\phi,z)$ is then

$$\bar{H}_{zm}(h,a) \equiv \bar{H}_z = u^2\ [b_m\ H_m^{(2)}(ua) + B_m\ J_m(ua)] \tag{6}$$

Similarly, all the required fields in both the coating region ($a \leq \rho \leq b$) and the air region ($b \leq \rho \leq \infty$) are given by (336), (337), (339), (340) and (342), (343), (345), (346) of Wait, respectively. For the sake of brevity, these expressions will not be rewritten here, but it is noted that the following difference in notation is used:

Wait's Notation	Notation of this paper
μ	μ_v
u_o	u_v
k_o	β_v

Furthermore, it is noted that in Table I of Wait (p. 128), that the coefficient b_{m1} should be multiplied by u, and the coefficient a_{m5} is lacking a minus sign.

The complex power, P, flowing through the slot is

$$P = \frac{1}{2} \iint_{slot} \overset{*}{E}_{slot} \times H_{slot} \; d\$_{slot} \tag{7}$$

which can, by Parseveal's theorem, Knop and Swift [2], can be cast into the form

$$P = \frac{a}{2} (2\pi)^2 \sum_{m=-\infty}^{m=+\infty} \int_{-\infty}^{\infty} \overset{*}{E}_{\phi} \, \overline{H}_z \, dh. \tag{8}$$

Using the six tangential boundary conditions (continuity of E_ϕ, E_z, H_ϕ, H_z at $\rho=b$ and continuity of E_ϕ and E_z at $\rho=a$) and determinants gives expressions for B_m, b_m and D_m, respectively, where D_m is the determinant formed by the coefficients a_{mp}, etc., in Table I, p. 128, of Wait. Explicitly solving for B_m, b_m, and D_m (see Reference 3) and substituting into P gives for the normalized external slot admittance, y_c, defined by

$$y_c = Y_c \eta_v \tag{9a}$$

where Y_c is the external slot admittance defined by

$$Y_c = \frac{2P}{|V_o|^2} \tag{9b}$$

the expression,

$$y_c = \frac{4}{(\beta_v \ell)^2 C} \sum_{m=0}^{m=+\infty} j \, \frac{a_m}{(1+\delta_o^m)} \int_o^{\infty} \frac{\sqrt{N^2-y^2} \, \cos^2\left(\frac{\beta_v \ell}{2} y\right) n_m(y) \, dy}{\left[y^2 - \left(\frac{\pi}{\beta_v \ell}\right)^2\right]^2 d_m(y)} \tag{10}$$

where

$$n_m(y)=(N^2-y^2)(1-y^2)(CW)^2[N^2\sqrt{1-y^2}U_mH_m-\sqrt{N^2-y^2}V_mH_m']\cdot \quad (11)$$

$$[\sqrt{1-y^2}U_mH_m-\sqrt{N^2-y^2}V_mH_m']-(my)^2(N^2-1)^2V_m^2H_m^2$$

$$d_m(y)=(N^2-y^2)^2(1-y^2)(CW)^2[N^2\sqrt{1-y^2}U_mH_m-\sqrt{N^2-y^2}V_mH_m']\cdot \quad (12)$$

$$[\sqrt{1-y^2}T_mH_m-\sqrt{N^2-y^2}L_mH_m']-(my)^2(N^2-1)^2V_mL_mH_m^2$$

with

$$\begin{cases} U_m = J_m(ua)H_m^{(2)\prime}(ub)-J_m'(ub)H_m^{(2)}(ua) \\ V_m = J_m(ua)H_m^{(2)}(ub)-J_m(ub)H_m^{(2)}(ua) \\ L_m = J_m(ub)H_m^{(2)\prime}(ua)-J_m'(ua)H_m^{(2)}(ub) \\ T_m = J_m'(ub)H_m^{(2)\prime}(ua)-J_m'(ua)H_m^{(2)\prime}(ub) \\ u = \beta_v\sqrt{\varepsilon_r-y^2} \\ H_m = H_m^{(2)}(u_vb) \\ u_v = \beta_v\sqrt{1-y^2},\ y=h/\beta_v,\ \delta_o^m=\begin{cases}1 & m=0\\ 0 & m\neq 0\end{cases},\quad N^2=\varepsilon_r \end{cases} \quad (13)$$

Prime denotes differentiation with respect to entire argument, e.g., $H_m^{(2)\prime}(ub)=\left.\dfrac{dH_m^{(2)}(X)}{dx}\right|_{x=ub}$

To obtain (10) the relations

$$J_{-m}(X)=(-1)^m J_m(X),\ Y_{-m}(X)=(-1)^m Y_m(X),\ \text{and} \tag{14}$$

$$H_{-m}^{(2)}(X)=(-1)^m H_m^{(2)}(X),\ n_{-m}(y)=n_m(y),\ d_{-m}(y)=d_m(y)$$

were used, as well as the symmetry of all functions with respect to y.

It is noted that both $n_m(y)$ and $d_m(y)$ are complex functions of the real variable y, and hence, (10) must be rationalized to obtain the real and imaginary parts, g_c and b_c, respectively, of y_c ($y_c=g_c+j\ b_c$). Before doing this, however, let us obtain the expression relating the normalized input waveguide admittance to the normalized external admittance.

b. Relation of External to Waveguide Input Admittance

The pertinent fields which exist in the waveguide are,

$$E_\eta(\xi,\eta,z)=\vec{E}_o\ e^{-j\beta_1 z}\cos\left(\frac{\pi\xi}{\ell}\right)(1+\Gamma e^{j2\beta_1 z})+(h.t.)_E \tag{15}$$

$$H_\xi(\xi,\eta,z)=-Y_{10}\vec{E}_o\ e^{-j\beta_1 z}\cos\left(\frac{\pi\xi}{\ell}\right)(1-\Gamma e^{j2\beta_1 z})+(h.t.)_H \tag{16}$$

where Γ is the reflection coefficient of the dominant TE_{10} mode in the waveguide, β_1 is the guide wavelength of this mode, and Y_{10} is the characteristic waveguide admittance of this mode. $\vec{E}_o$ is the arbitrary source constant for the exciting TE_{10} mode and is the only specified quantity.

The reflection coefficient, Γ, and the magnitude and phase of the higher order mode dielectric $(h.t.)_E$ and magnetic, $(h.t.)_H$, are unknown. The problem is to determine Γ or the input wave admittance, Y_{in}, of the TE_{10} mode which is related to Γ through the relation

$$Y_{in} = G_{in}+jB_{in} \equiv - \left.\frac{H_\xi(\xi,\eta,0)}{E_\eta(\xi,\eta,0)}\right|_{TE_{10}\ mode} = Y_{01}\,\frac{(1-\Gamma)}{(1+\Gamma)} \qquad (17)$$

It is convenient to define the normalized input waveguide admittance, y_{in}, by

$$y_{in} \equiv \frac{Y_{in}}{Y_{10}} = g_{in}+j\ b_{in} = \frac{1-\Gamma}{1+\Gamma}\ . \qquad (18)$$

Assuming that the higher order terms vanish, i.e., $(h.t.)_E=(h.t.)_H=0$, (the validity of this assumption will be discussed shortly), the complex power flowing through the slot in terms of the fields inside the guide is

$$P = |\vec{E}_o|^2 (1+\Gamma^*)(1-\Gamma)\, Y_{10}\,\frac{w\ell}{4} \qquad (19)$$

which is obtained by integration of the complex Poynting vector over a cross-section of the guide. Using the relation defining Γ,

$$E_o = \frac{V_o}{w} = \vec{E}_o(1+\Gamma) \qquad (20)$$

gives

$$Y_c = \frac{2P}{|V_o|^2} = \frac{\ell}{2w} \frac{(1-\Gamma)}{(1+\Gamma)} Y_{10} \tag{21}$$

thus,

$$y_{in} = 2\left(\frac{w}{\ell}\right)\left(\frac{\lambda_g}{\lambda_v}\right) y_c \tag{22}$$

which relates the normalized input admittance (a measurable quantity) to the normalized external admittance (a quantity which can be computed via (10)).

c. Application to Specific Coatings

The expression (10) holds for any ε_r, real or complex, but, as pointed out, both $n_m(y)$ and $d_m(y)$ can be complex, and it remains to rationalize (10) to obtain g_c and b_c. This rationalization differs for each coating type and each will be described separately. However, regardless of what coating is considered, the fact that the radial portion of the wave must be outward-going and bounded means that the choice of positive real parts and negative imaginary parts of the corresponding propagation factors must be made, i.e., one must choose

$$\begin{aligned} &R_e\sqrt{\varepsilon_r - y^2} > 0 \qquad && R_e\sqrt{1-y^2} > 0 \\ &I_m\sqrt{\varepsilon_r - y^2} < 0 \qquad && I_m\sqrt{1-y^2} < 0 \end{aligned} \tag{23}$$

for all values of ε_r and y^2.

1. Dielectric Coating (ε_r real and $\varepsilon_r \geq 1$)

For this case the range of integration over $0 \leq y \leq \infty$ can be split into the three regions; $0 \leq y \leq 1$, $1 \leq y \leq \varepsilon_r$, and $\varepsilon_r \leq y \leq \infty$.

In the range $0 \leq y \leq 1$, both $\sqrt{1-y^2}$ and $\sqrt{\varepsilon_r - y^2}$ are greater than zero and (23) with (10) gives both a real, g_{c1}, and an imaginary, b_{c1}, contribution to y_c as given by (I) and (V), respectively, of Table I, in this range.

In the range $1 \leq y \leq \varepsilon_r$, $\sqrt{1-y^2} = -j\sqrt{y^2-1}$, causing $H_m^{(2)}[CW\sqrt{1-y^2}] = (2/\pi)\, j^{m+1} K_m[CW\sqrt{y^2-1}]$ and $H_m^{(2)'}[CW\sqrt{1-y^2}] = -(2/\pi)\, j^m K_m'[CW\sqrt{y^2-1}]$. Examination of (10) then gives a purely imaginary contribution, $j\, b_{c2}$, to y_c in this range, as given by (VII) of Table I.

In the range $1 \leq y \leq \infty$, the term $\sqrt{\varepsilon_r - y^2} = -j\sqrt{y^2-\varepsilon_r}$ and also $\sqrt{1-y^2} = -j\sqrt{y^2-1}$, causing the appropriate Hankel functions to become modified Bessels (as above) and thus (10) gives a purely imaginary contribution, $j\, b_{c3}$, as given by (IX) of Table I, to y_c in this range.

Thus, for ε_r real and $\varepsilon_r \geq 1$, the total external admittance is given by

$$y_c\Big|_{\varepsilon_r \geq 1} = g_c + j(b_{c1} + b_{c2} + b_{c3}) \qquad (24)$$

as given in Table I.

2. Plasma Coating

For the case of a lossless plasma coating having $\epsilon_r = 1-\omega_p^2/\omega^2$ with $0 \leq (\omega_p/\omega)^2 \leq 1$, i.e., for $0 \leq \epsilon_r \leq 1$, the expression (10) can be split into the ranges $0 \leq y \leq \sqrt{\epsilon_r}$, $\sqrt{\epsilon_r} \leq y \leq 1$, and $1 \leq y \leq \infty$.

In the range $0 \leq y \leq \sqrt{\epsilon_r}$, both $1-y^2$ and $\epsilon_r - y^2$ are greater than zero and (10) gives both a real, g_{cp1}, and an imaginary, b_{cp1}, (subscript p for plasma) contribution to y_c, as given by (XII) and (XV), respectively, of Table I.

In the range $\sqrt{\epsilon_r} \leq y \leq 1$, $\sqrt{\epsilon_r - y^2} = -j\sqrt{y^2-\epsilon_r}$, causing the Hankel functions to become Modified Bessels, as above, and causing (10) to have both a real, g_{cp2}, and an imaginary, b_{cp2}, part as given by (XIII) and (XVI), respectively, of Table I.

In the range $1 \leq y \leq \infty$, $\sqrt{\epsilon_r - y^2} = -j\sqrt{y^2-\epsilon_r}$ and $\sqrt{1-y^2} = -j\sqrt{y^2-1}$, causing similar changes of Hankels to Modified Bessels and causing (10) to only have an imaginary part, b_{cp3}, as given by (XVIII) of Table I.

Thus, for the plasma coating, the total external admittance is

$$y_c \Big|_{0 \leq \epsilon_r \leq 1} = y_{cp} = g_{cp1} + g_{cp2} + j(b_{cp1} + b_{cp2} + b_{cp3}) = g_{cp} + j\, b_{cp} \qquad (25)$$

as given in Table I.

3. No Coating

For no coating (i.e., for a coating of $\varepsilon_r=1$, free space, and/or a coating of zero thickness, W=1), the limiting form of the above two cases give the result

$$Y_c \Big|_{\substack{\varepsilon_r=1 \\ \text{and/or } W=1}} \equiv Y_{cv} = g_{cv}+j\, b_{cv} \tag{26}$$

where the subscript v is for vacuum (free space) and where g_{cv} and b_{cv} are given by (XIX) and (XXI) of Table I. In this limiting process use is made of the Wronskian relations,

$$J_m(X)Y_m'(X)-J_m'(X)Y_m(X) = \frac{2}{\pi X} \tag{27}$$

and

$$I_m(X)K_m'(X)-I_m'(X)K_m(X) = -\frac{1}{X} \tag{28}$$

The result (26) is identical with that obtained by considering the no coating case initially [4] and, hence, serves as a partial check on all the admittance expressions for the dielectric and plasma cases.

TABLE I - EXTERNAL ADMITTANCE EXPRESSIONS

NORMALIZED RADIATION CONDUCTANCE, g_c, OF AXIAL SLOT ON DIELECTRIC COATED CYLINDER, $\epsilon_r \geq 1$

$$(I)\quad g_c = \frac{32}{\pi^3 C^4 \left(\frac{\ell}{a}\right)^2} \sum_{m=0}^{\infty} \frac{a_m}{(1+\delta_o^m)} \int_o^1 \frac{(\epsilon_r-y^2)(1-y^2)\cos^2\left[\frac{C}{2}\left(\frac{\ell}{a}\right)y\right]\left\{(\epsilon_r-y^2)(1-y^2)(CW)^2\left|\epsilon_r\sqrt{1-y^2}\,\bar{U}H-\sqrt{\epsilon_r-y^2}\,\bar{V}H'\right|^2+(my)^2(\epsilon_r-1)^2|H|^2\bar{V}^2\right\}dy}{\left[y^2-\frac{\pi^2}{C^2\left(\frac{\ell}{a}\right)^2}\right]^2\left|(\epsilon_r-y^2)(1-y^2)(CW)^2\left[\epsilon_r\sqrt{1-y^2}\,\bar{U}H-\sqrt{\epsilon_r-y^2}\,\bar{V}H'\right]\left[\sqrt{1-y^2}\,\bar{T}H-\sqrt{\epsilon_r-y^2}\,\bar{L}H'\right]-(my)^2(\epsilon_r-1)^2\bar{V}\,\bar{L}H^2\right|^2}$$

where:

$$(II)\quad \begin{cases} a_m = \left[\dfrac{\sin\left(\frac{m\phi_o}{2}\right)}{\left(\frac{m\phi_o}{2}\right)}\right]^2 \\ \delta_o^m = \text{Kronecker Delta} = \begin{cases} 1 & m = 0 \\ 0 & m \neq 0 \end{cases} \\ H = H_m^{(2)}\left[CW\sqrt{1-y^2}\right],\quad H' = \left.\dfrac{d\,H_m^{(2)}(x)}{dx}\right|_{x=CW\sqrt{1-y^2}} \end{cases}$$

$$(III)\quad \begin{cases} \bar{U} = \bar{U}_m = J_m\left(\frac{z}{W}\right)Y_m'(z) - J_m'(z)Y_m\left(\frac{z}{W}\right) \\ \bar{V} = \bar{V}_m = J_m\left(\frac{z}{W}\right)Y_m(z) - J_m(z)Y_m\left(\frac{z}{W}\right) \\ \bar{L} = \bar{L}_m = J_m(z)Y_m'\left(\frac{z}{W}\right) - J_m'\left(\frac{z}{W}\right)Y_m(z) \\ \bar{T} = \bar{T}_m = J_n'(z)Y_m'\left(\frac{z}{W}\right) - J_m'\left(\frac{z}{W}\right)Y_m'(z) \\ z = CW\sqrt{\epsilon_r-y^2} \end{cases}$$

Prime denotes differentiation with respect to entire argument, e.g., $J_m'\left(\frac{z}{W}\right) = \left.\dfrac{d\,J_m(x)}{dx}\right|_{x=\frac{z}{W}}$, etc.

ϕ_o, C, W, and $\left(\frac{\ell}{a}\right)$ are real, positive, specified parameters.

ϵ_r real positive number greater than or equal to unity, $\epsilon_r \geq 1$.

$J_m(x)$ = Bessel function of first kind, order m, argument x.

$Y_m(x)$ = Bessel function of second kind, order m, argument x (Neumann Function).

$H_m^{(2)}(x) = J_m(x) - jY_m(x)$ = Hankel function of second kind, order m, argument x.

NORMALIZED RADIATION SUSCEPTANCE, b_c, OF AXIAL SLOT ON DIELECTRIC COATED CYLINDER, $\epsilon_r \geq 1$

(IV) $b_c = b_{c1} + b_{c2} + b_{c3}$

(V) $$b_{c1} = \frac{4}{C^3\left(\frac{\ell}{a}\right)^2} \sum_{m=0}^{\infty} \frac{a_m}{(1+\delta_o^m)} \int_0^1 \frac{\sqrt{\epsilon_r - y^2}\, \cos^2\left[\frac{C}{2}\left(\frac{\ell}{a}\right) y\right] f_1(y)\, dy}{\left[y^2 - \frac{\pi^2}{C^2\left(\frac{\ell}{a}\right)^2}\right]^2}$$

where:

(VI) $$f_1(y) = \left\{ (\epsilon_r - y^2)^2 (1-y^2)^2 (CW)^4 \left| \epsilon_r \sqrt{1-y^2}\, \overline{U} H - \sqrt{\epsilon_r - y^2}\, \overline{V} H' \right|^2 \left[(1-y^2) \overline{U}\, \overline{T} |H|^2 - \sqrt{1-y^2}\sqrt{\epsilon_r - y^2}\, (JJ' + YY')(\overline{U}\, \overline{L} + \overline{V}\, \overline{T}) + (\epsilon_r - y^2) \overline{V}\, \overline{L} |H'|^2 \right] \right\} - (my)^2 (\epsilon_r - 1)^2 \overline{V} (\epsilon_r - y^2)(1-y^2)(CW)^2 \left\{ \epsilon_r \overline{U} (1-y^2) |H|^4 (\overline{V}\, \overline{T} + \overline{U}\, \overline{L}) - \sqrt{1-y^2}\sqrt{\epsilon_r - y^2} |H|^2 (JJ' + YY') \overline{V} \left[\overline{U}\, \overline{L} (2\epsilon_r + 1) + \overline{V}\, \overline{T} \right] + 2L (\epsilon_r - y^2) \overline{V}^2 \left[(JJ' + YY')^2 - \frac{4}{\pi (CW)^2 \sqrt{1-y^2}} \right] \right\} + (my)^4 (\epsilon_r - 1)^4 \overline{V}^3 \overline{L} |H|^4 \Bigg\} \cdot \left| (\epsilon_r - y^2)(1-y^2)(CW)^2 \left[\epsilon_r \sqrt{1-y^2}\, \overline{U} H - \sqrt{\epsilon_r - y^2}\, \overline{V} H' \right] \left[\sqrt{1-y^2}\, \overline{T} H - \sqrt{\epsilon_r - y^2}\, \overline{L} H' \right] - (my)^2 (\epsilon_r - 1)^2 \overline{V}\, \overline{L} H^2 \right|^{-2}$$

with all symbols defined by (II) and (III); arguments of J, J', Y, Y' are $CW\sqrt{1-y^2}$.

(VII) $$b_{c2} = \frac{4}{C^3\left(\frac{\ell}{a}\right)^2} \sum_{m=0}^{\infty} \frac{a_m}{(1+\delta_o^m)} \int_1^{\sqrt{\epsilon_r}} \frac{\sqrt{\epsilon_r - y^2}\, \cos^2\left[\frac{C}{2}\left(\frac{\ell}{a}\right) y\right] \left\{ (\epsilon_r - y^2)(y^2-1)(CW)^2 \left[\epsilon_r \sqrt{y^2-1} \left(\frac{K}{K'}\right) \overline{U} + \sqrt{\epsilon_r - y^2}\, \overline{V} \right] \left[\sqrt{y^2-1}\, \overline{U} \left(\frac{K}{K'}\right) + \sqrt{\epsilon_r - y^2}\, \overline{V} \right] - (my)^2 (\epsilon_r - 1)^2 \overline{V}^2 \left(\frac{K}{K'}\right)^2 \right\} dy}{\left[y^2 - \frac{\pi^2}{C^2\left(\frac{\ell}{a}\right)^2}\right]^2 \left\{ (\epsilon_r - y^2)(y^2-1)(CW)^2 \left[\epsilon_r \sqrt{y^2-1} \left(\frac{K}{K'}\right) \overline{U} + \sqrt{\epsilon_r - y^2}\, \overline{V} \right] \left[\sqrt{y^2-1}\, \overline{T} \left(\frac{K}{K'}\right) + \sqrt{\epsilon_r - y^2}\, \overline{L} \right] - (my)^2 (\epsilon_r - 1)^2 \overline{V}\, \overline{L} \left(\frac{K}{K'}\right)^2 \right\}}$$

(VIII) $K = K_m\left[CW\sqrt{y^2-1}\right]$

$K' = \left.\frac{d\, K_m(x)}{dx}\right|_{x = CW\sqrt{y^2-1}}$, $\overline{U}, \overline{V}, \overline{L}, \overline{T}$ defined in (III), $K_m(x)$ = Modified Bessel function of second kind, order m, argument x.

(IX) $$b_{c3} = \frac{-4}{C^3\left(\frac{\ell}{a}\right)^2} \sum_{m=0}^{\infty} \frac{a_m}{(1+\delta_o^m)} \int_{\sqrt{\epsilon_r}}^{\infty} \frac{\sqrt{y^2 - \epsilon_r}\, \cos^2\left[\frac{C}{2}\left(\frac{\ell}{a}\right) y\right] \left\{ (y^2 - \epsilon_r)(y^2-1)(CW)^2 \left[\epsilon_r \sqrt{y^2-1} \left(\frac{K}{K'}\right) \overline{\overline{U}} + \sqrt{y^2 - \epsilon_r}\, \overline{\overline{V}} \right] \left[\sqrt{y^2-1}\, \overline{\overline{U}} \left(\frac{K}{K'}\right) + \sqrt{y^2 - \epsilon_r}\, \overline{\overline{V}} \right] - (my)^2 (\epsilon_r - 1)^2 \overline{\overline{V}}^2 \left(\frac{K}{K'}\right)^2 \right\} dy}{\left[y^2 - \frac{\pi^2}{C^2\left(\frac{\ell}{a}\right)^2}\right]^2 \left\{ (y^2 - \epsilon_r)(y^2-1)(CW)^2 \left[\epsilon_r \sqrt{y^2-1} \left(\frac{K}{K'}\right) \overline{U} + \sqrt{y^2 - \epsilon_r}\, \overline{V} \right] \left[\sqrt{y^2-1}\, \overline{\overline{T}} \left(\frac{K}{K'}\right) - \sqrt{y^2 - \epsilon_r}\, \overline{\overline{L}} \right] + (my)^2 (\epsilon_r - 1)^2 \overline{\overline{V}}\, \overline{\overline{L}} \left(\frac{K}{K'}\right)^2 \right\}}$$

where:

(X)
- K and K' defined by (VII)
- $\overline{\overline{V}} = \frac{2}{\pi} \left[I_m(\alpha) K_m\left(\frac{\alpha}{w}\right) - I_m\left(\frac{\alpha}{w}\right) K_m(\alpha) \right]$
- $\overline{\overline{T}} = \frac{2}{\pi} \left[I_m'(\alpha) K_m'\left(\frac{\alpha}{w}\right) - I_m'\left(\frac{\alpha}{w}\right) K_m'(\alpha) \right]$
- $\overline{\overline{U}} = \frac{2}{\pi} \left[I_m\left(\frac{\alpha}{w}\right) K_m'(\alpha) - I_m'(\alpha) K_m\left(\frac{\alpha}{w}\right) \right]$
- $\overline{\overline{L}} = \frac{2}{\pi} \left[I_m(\alpha) K_m'\left(\frac{\alpha}{w}\right) - I_m'\left(\frac{\alpha}{w}\right) K_m(\alpha) \right]$
- $\alpha = CW\sqrt{y^2 - \epsilon_r}$

$I_m(X)$ = Modified Bessel function of first kind, order m, argument X.

$I_m'(X) = \frac{d\, I_m(X)}{dx}$

NORMALIZED RADIATION CONDUCTANCE, g_{c_p}, OF AXIAL SLOT ON PLASMA COATED CYLINDER, $0 \le \epsilon_r \le 1$

(XI) $g_{cp} = g_{cp_1} + g_{cp_2}$

(XII) $g_{cp_1} = g_c$ of (I), with (II) and (III), but with integration range changed to $0 \le y \le \sqrt{\epsilon_r}$.

(XIII)
$$g_{cp_2} = \frac{32}{\pi^3 C^4 \left(\frac{\ell}{a}\right)^2} \sum_{m=0}^{\infty} \frac{a_m}{(1+\delta_o^m)} \int_{\sqrt{\epsilon_r}}^{1} \frac{(y^2-\epsilon_r)(1-y^2)\cos^2\left[\frac{C}{2}\left(\frac{\ell}{a}\right)y\right]\left\{(y^2-\epsilon_r)(1-y^2)(CW)^2\left|\epsilon_r\sqrt{1-y^2}\,\bar{\bar{U}}\,H-\sqrt{y^2-\epsilon_r}\,\bar{\bar{V}}\,H'\right|^2+(my)^2(\epsilon_r-1)^2\bar{\bar{V}}^2|H|^2\right\}}{\left[y^2-\frac{\pi^2}{C^2\left(\frac{\ell}{a}\right)^2}\right]^2\left|(y^2-\epsilon_r)(1-y^2)(CW)^2\left[\epsilon_r\sqrt{1-y^2}\,\bar{\bar{U}}\,H-\sqrt{y^2-\epsilon_r}\,\bar{\bar{V}}\,H\right]\left[\sqrt{1-y^2}\,\bar{\bar{T}}\,H+\sqrt{y^2-\epsilon_r}\,\bar{\bar{L}}\,H'\right]+(my)^2(\epsilon_r-1)^2\bar{\bar{V}}\,\bar{\bar{L}}\,H^2\right|^2}$$

where:

a_m, δ_o^m, H and H' are defined by (II)

$\bar{\bar{U}}, \bar{\bar{V}}, \bar{\bar{T}}$ and $\bar{\bar{L}}$ are defined by (X)

NORMALIZED RADIATION SUSCEPTANCE, b_{cp}, OF AXIAL SLOT ON PLASMA COATED CYLINDER, $0 \le \epsilon_r \le 1$

(XIV) $b_{cp} = b_{cp_1} + b_{cp_2} + b_{cp_3}$

(XV) $b_{cp_1} = b_{c1}$ of (V), with (VI), but with integration range changed to $0 \le y \le \sqrt{\epsilon_r}$.

(XVI)
$$b_{cp_2} = -\frac{4}{C^3\left(\frac{\ell}{a}\right)^2} \sum_{m=0}^{\infty} \frac{a_m}{(1+\delta_o^m)} \int_{\sqrt{\epsilon_r}}^{1} \frac{\sqrt{y^2-\epsilon_r}\cos^2\left[\frac{C}{2}\left(\frac{\ell}{a}\right)y\right] f_2(y)\,dy}{\left[y^2-\frac{\pi^2}{C^2\left(\frac{\ell}{a}\right)^2}\right]^2}$$

where:

(XVII)
$$f_2(y) = \left[(y^2-\epsilon_r)^2(1-y^2)^2(CW)^4\left|\epsilon_r\sqrt{1-y^2}\,\bar{\bar{U}}\,H-\sqrt{y^2-\epsilon_r}\,\bar{\bar{V}}\,H'\right|^2\left[(1-y^2\,\bar{\bar{U}}\,\bar{\bar{T}}|H|^2-\sqrt{1-y^2}\sqrt{y^2-\epsilon_r}\,(-\bar{\bar{U}}\,\bar{\bar{L}}+\bar{\bar{V}}\,\bar{\bar{T}})(JJ'+YY')-(y^2-\epsilon_r)\bar{\bar{V}}\,\bar{\bar{L}}|H'|^2\right]-(my)^2(\epsilon_r-1)^2(y^2-\epsilon_r)(1-y^2)(CW)^2\bar{\bar{V}}\left\{\epsilon_r\,(1-y^2)|H|^4\bar{\bar{U}}(\bar{\bar{V}}\,\bar{\bar{T}}-\bar{\bar{L}}\,\bar{\bar{U}})-\sqrt{y^2-\epsilon_r}\sqrt{1-y^2}|H|^2(JJ'+YY')\right.$$
$$\left.\bar{\bar{V}}\left[-\bar{\bar{U}}\,\bar{\bar{L}}(2\epsilon_r+1)+\bar{\bar{V}}\,\bar{\bar{T}}\right]-2(y^2-\epsilon_r)\bar{\bar{V}}^2\bar{\bar{L}}\left[(JJ'+YY')^2-\frac{4}{\pi^2C^2W^2(1-y^2)}\right]\right\}-(my)^4(\epsilon_r-1)^4\bar{\bar{V}}^3\bar{\bar{L}}|H|^4\Big] \cdot \left|(y^2-\epsilon_r)(1-y^2)(CW)^2\left[\epsilon_r\sqrt{1-y^2}\,\bar{\bar{U}}\,H-\sqrt{y^2-\epsilon_r}\,\bar{\bar{V}}\,H'\right]\cdot\left[\sqrt{1-y^2}\,\bar{\bar{T}}\,H+\sqrt{y^2-\epsilon_r}\,\bar{\bar{L}}\,H'\right]+(my)^2(\epsilon_r-1)^2\bar{\bar{V}}\,\bar{\bar{L}}\,H^2\right|^{-2}$$

where: a_m, δ_o^m, H, and H' are defined by (II)

$\bar{\bar{U}}$, $\bar{\bar{V}}$, $\bar{\bar{L}}$, $\bar{\bar{T}}$ are defined by (X)

arguments of J, J', Y, Y' are $CW\sqrt{1-y^2}$

(XVIII) $b_{c3_p} = b_{c3}$ of (IX) with (X), but with integration range changed to $1 \le y \le \infty$.

NORMALIZED RADIATION CONDUCTANCE, g_{cv}, AND NORMALIZED RADIATION SUSCEPTANCE, b_{cv}, OF AXIAL SLOT ON NON-COATED CYLINDER, (ε_r=1 and/or W=1)

(XIX) $$g_{cv} = \frac{8}{\pi C^4 \left(\frac{\ell}{a}\right)^2} \sum_{m=0}^{\infty} \frac{a_m}{(1+\delta_o^m)} \; I_{mg}$$

(XX) $$I_{mg} = \int_o^1 \frac{\cos^2\left[\frac{C}{2}\left(\frac{\ell}{a}\right)y\right] dy}{\left[y^2 - \frac{\pi^2}{C^2\left(\frac{\ell}{a}\right)^2}\right] \left|H_m^{(2)\prime}\left[C\sqrt{1-y^2}\right]\right|^2}$$

(XXI) $$b_{cv} = \frac{4}{C^3\left(\frac{\ell}{a}\right)^2} \sum_{m=0}^{\infty} \frac{a_m}{(1+\delta_o^m)} \; (I_{1m} - I_{2m})$$

(XXII) $$I_{1m} = \int_1^{\infty} \frac{\sqrt{y^2-1}\,\cos^2\left[\frac{C}{2}\left(\frac{\ell}{a}\right)y\right] K_m\left[C\sqrt{y^2-1}\right] dy}{\left[y^2 - \frac{\pi^2}{C^2\left(\frac{\ell}{a}\right)^2}\right]^2 K_m'\left[C\sqrt{y^2-1}\right]}$$

(XXIII) $$I_{2m} = \int_o^1 \frac{\sqrt{1-y^2}\,\cos^2\left[\frac{C}{2}\left(\frac{\ell}{a}\right)y\right]\left[J_m(X)J_m'(X) + Y_m(X)Y_m'(X)\right] dy}{\left[y^2 - \frac{\pi^2}{C^2\left(\frac{\ell}{a}\right)^2}\right]^2 \left|H_m^{(2)\prime}(X)\right|^2}$$

where a_m, δ_o^m are given by (II), $X = C\sqrt{1-y^2}$

III. AXIAL SURFACE WAVES

The dielectric clad metallic cylinder can act as a waveguide, since it can support surface modes travelling along the axis of the cylinder (axial surface waves). The cutoff conditions for these modes can be obtained by considering an infinite metal cylinder (with no slots) coated with the given dielectric and insisting that the boundary conditions be satisfied, i.e., treating the waveguide problem, as is done in Appendix I. However, not all of these allowable modes are excited by a thin finite axial slot cut in the metal cylinder. The modes excited by this slot are determined by an examination of the integrand of the external admittance expression (10); any singularities which exist are due to axial surface waves.

Intuitively, one would anticipate that, since the axial slot is assumed very thin and, hence, has no exciting E_z component, that modes having only axial electric or predominantly axial electric fields, i.e., either TM or hybrid EH modes, respectively, will not be excited. As will be shown, this is precisely what is revealed by the integrand singularities.

a. Cutoff Condition Equations

The essential quantity in (10) is $n_m(y)/dm(y)$, since no singularities can occur due to the other quantities. By factoring out the term $(H_m')^2$ in both $n_m(y)$ and $dm(y)$, as defined by (11) and (12), and realizing that singularities can only occur in the surface wave range of $1 \leq y \leq \sqrt{\epsilon_r}$,

since the surface wave is a slow wave, causing the factors U_m, V_m, L_m, and T_m to become $-j\bar{U}_m$, $-j\bar{V}_m$, $-j\bar{L}_m$, and $-j\bar{T}_m$, respectively, as defined in Table I, and causing H_m/H_m' to become $-jK_m(pb)/K_m'(pb)$, and $\sqrt{1-y^2} = -jP/\beta_v$, the ratio $n_m(y)/dm(y)$ becomes

$$\left.\frac{n_m(y)}{dm(y)}\right|_{1\leq y\leq \varepsilon_r} = \frac{p^2\beta_v{}^2u^2\left[\varepsilon_r\, p\bar{U}\,\frac{K}{K'}+u\bar{V}\right]\left[p\bar{U}\,\frac{K}{K'}+u\bar{V}\right]}{p^2\beta_v{}^2u^2\left[\varepsilon_r\, p\bar{U}\,\frac{K}{K'}+u\bar{V}\right]\left[p\bar{T}\,\frac{K}{K'}+u\bar{L}\right]} \tag{29}$$

$$\frac{-\left(\frac{mh}{b}\right)^2\beta_v{}^4(\varepsilon_r-1)^2\bar{V}^2\left(\frac{K}{K'}\right)^2}{-\left(\frac{mh}{b}\right)^2\beta_v{}^4(\varepsilon_r-1)^2\bar{V}\,\bar{L}\left(\frac{K}{K'}\right)^2}$$

where the subscripts on the quantities $\bar{U}$, K, etc., are understood.

It is immediately noted that, if the denominator of this quantity is equated to zero, this gives the transcendental equation for the axial surface wave modes on an unslotted dielectric coated metal cylinder, as derived independently in Appendix I. However, what one must do here is equate (29) to ∞ to obtain the axial surface wave modes on the axially slotted dielectric coated metal cylinder. As we will see shortly, this will eliminate the TM and EH modes. For example, for m=0, (29) reduces to

$$\left.\frac{n_m(y)}{dm(y)}\right|_{m=0} = \frac{\left[p\bar{U}_o \frac{K_o}{K_o'} + u\bar{V}_o\right]}{\left[p\bar{T}_o \frac{K_o}{K_o'} + u\bar{L}_o\right]} \tag{30}$$

and examination of this quantity shows that the only way it can equal ∞ is for $p\bar{T}_o \frac{K_o}{K_o'} + u\bar{L}_o = 0$, which is the TE_o mode equation (see Appendix I). The equation for the TM_o mode, i.e., $\varepsilon_r p\bar{U}_o \frac{K_o}{K_o'} + u\bar{V}_o = 0$ has been eliminated, since this term also occurs in the numerator. Physically, this means that the TM_o mode cannot be excited by a thin axial slot (even though its cutoff frequency is zero, whereas that of the TE_o mode, as will be shown, is finite). This is because there is no exciting E_z component in the slot to excite this mode. It will also be shown that the hybrid modes having predominantly axial electric axial fields cannot be excited, i.e., no EH modes will be excited.

To prove this, consider first the case of finite frequency (C>0), for which all the factors $\bar{U}$, $\bar{V}$, $\bar{T}$, and $\bar{L}$ are bounded, and examine (29) for the cutoff condition of p=0. For this purpose, one notes that

$$\lim_{p \to 0} \frac{K_m(pb)}{K_m'(pb)} = -\left(\frac{pb}{m}\right) + \Delta_m \tag{31}$$

where Δ_m approaches zero faster than $(pb)^1$. Then it follows that (29) becomes

$$\lim_{\substack{p\to 0 \\ C>0}} \frac{n_m(y)}{dm(y)} = \tag{32}$$

$$\frac{p^2\beta_v{}^2u^2[u\bar{V}][u\bar{V}]-(\frac{mh}{b})^2\beta_v{}^4(\varepsilon_r-1)^2\bar{V}^2\left[\frac{(pb)^2}{m^2}-2(\frac{pb}{m})\Delta_m\right]}{p^2\beta_v{}^2u^2[u\bar{V}][u\bar{L}]-(\frac{mh}{b})^2\beta_v{}^4(\varepsilon_r-1)^2\bar{V}\,\bar{L}\left[(\frac{pb}{m})^2-2(\frac{pb}{m})\Delta_m\right]}$$

but as $p\to 0$, $h\to\beta_v$ and $u\to\beta_v\sqrt{\varepsilon_r-1}$, hence

$$\lim_{\substack{p\to 0 \\ C>0}} \frac{n_m(y)}{dm(y)} = \tag{33}$$

$$\frac{p^2\beta_v{}^6(\varepsilon_r-1)^2\bar{V}^2-p^2\beta_v{}^6(\varepsilon_r-1)^2\bar{V}^2+\frac{2pm}{b}\beta_v{}^6(\varepsilon_r-1)^2\bar{V}^2\Delta_m}{p^2\beta_v{}^6(\varepsilon_r-1)^2\bar{V}\,\bar{L}-p^2\beta_v{}^6(\varepsilon_r-1)^2\bar{V}\,\bar{L}+\frac{2pm}{b}\beta_v{}^6(\varepsilon_r-1)^2\bar{V}\,\bar{L}\Delta_m}$$

$$= \frac{\bar{V}_m\Big|_{p=0}}{\bar{L}_m\Big|_{p=0}}$$

Examination of (33) reveals that the only way $\frac{n_m(y)}{dm(y)}$ can become infinite for $C>0$, since $\bar{V}_m\Big|_{p=0}$ is bounded, is to have

$$\bar{L}_m\Big|_{p=0}=0=J_m(CW\sqrt{\varepsilon_r-1})Y_m'(C\sqrt{\varepsilon_r-1})-J_m'(C\sqrt{\varepsilon_r-1})Y_m(CW\sqrt{\varepsilon_r-1}) \tag{34}$$

which is recognized from Appendix I as the cutoff condition for the HE modes. The cutoff condition for the EH modes, namely $\bar{V}_m\Big|_{p=0}=0$, has, like that for the TM_o mode, been

suppressed because of the numerator.

Repeating the above procedure, but removing the restriction of bounded frequency, i.e., allowing the frequency to approach zero ($\beta_v \to 0$), and using the small argument approximations for $\bar{U}$, $\bar{V}$, $\bar{L}$, and $\bar{T}$, as given in Appendix II, and simplifying (29) for the cutoff condition ($p \to 0$) gives

$$\left.\frac{n_m(y)}{dm(y)}\right|_{\substack{p\to 0\\ \beta_v\to 0\\ m\geq 1}} = \frac{\beta_v a \left(\frac{1}{W^{m+1}} + W^{m-1}\right)}{m\left(W^{m-1} - \frac{1}{W^{m+1}}\right)} \tag{35}$$

which is seen to approach zero for all $m \geq 1$ and $W > 1$ and, hence, cannot be ∞; therefore, there can be no hybrid mode excited by the axial slot having a zero cutoff frequency. It is noted in Appendix I that the first hybrid EH_1 mode on the unslotted coated cylinder root has a zero cutoff frequency. This corresponds to the vanishing of $dm(y)\,|_{p=0,C=0,m=1}$, but for the axial slotted cylinder, here again the numerator term $n_m(y)$ nullifies this mode, since it vanishes with β_v also, but at a faster rate; hence, this EH_1 mode cannot exist on the axial slotted cylinder.

From the above, it is concluded that only the TE_o and HE modes can exist on the subject antenna consisting of a finite thin axial slot cut in the wall of a metal cylinder concentrically coated with dielectric. To determine if they actually do exist for a specified frequency and cylinder dielectric conditions, the cutoff conditions must be evaluated.

b. Cutoff Condition Computations

1. TE_o Mode

The TE_o mode transcendental equation was found to be $p\bar{T}_o K_o/K_o' + u\bar{L}_o = 0$, which can be written as

$$\frac{K_1(pb)}{(pb)K_o(pb)} = -\frac{\bar{T}_o}{(ub)\bar{L}_o} \tag{36}$$

Inspection of the L.H.S. of (36) shows that, as cutoff is approached ($p \to 0$), it becomes positively infinite. Inspection of the R.H.S. shows that it is bounded for $\beta_v = 0$ and, hence, the cutoff frequency of the TE_o modes are all finite. Inspection of $\bar{T}_o/ub$ shows that it is bounded for all $\beta_v > 0$; it follows that the only way the R.H.S. can become infinite is for the term $\bar{L}_o\big|_{p=0}$ to vanish. Thus, the cutoff condition for the TE_o modes is

$$L_o\Big|_{p=0} = 0 = J_1(C\sqrt{\varepsilon_r - 1})\,Y_o(CW\sqrt{\varepsilon_r - 1}) - J_o(CW\sqrt{\varepsilon_r - 1})\,Y_1(C\sqrt{\varepsilon_r - 1}). \tag{37}$$

The first root of (37) will give the first TE_o mode and successive roots the successively higher TE_o roots, each with successively higher cutoff frequency. In this work, no second subscript will be used, since only the first roots are of interest.

The roots of (37) can be found graphically. Only the first root will be found here. A plot (using tabulated values of Bessel and Neumann functions [5] and a Friden calculating machine) of $\bar{L}_o\big|_{p=0}$ for a fixed value of W and

with $CW\sqrt{\varepsilon_r-1}$ as a variable was made and the value of $C\sqrt{\varepsilon_r-1}$ required for $\bar{L}_o\big|_{p=0}$ to vanish was determined graphically. This was then repeated for another value of W, etc. The corresponding $C\sqrt{\varepsilon_r-1}$ roots versus W are given in Table II for $1 \leq W \leq 2.4$, and are plotted in Fig. 2. From this curve, one can determine the cutoff thickness factor W for a specified frequency and dielectric constant factor $C\sqrt{\varepsilon_r-1}$. Suppose, for example, that the operating conditions correspond to $C\sqrt{\varepsilon_r-1}=3$; then from Fig. 2 it is seen that for any thickness of dielectric corresponding to $W \leq 1.575$, the TE_o mode cannot exist. Alternatively, for a specified W, the cutoff frequency can be found. For example, if W=2.0, then from Fig. 2, for any $C\sqrt{\varepsilon_r-1} < 1.80$, the TE_o mode cannot exist. Fig. 2 also shows a plot of $C\sqrt{\varepsilon_r-1} = \pi/2(W-1)$, which is the cutoff equation for the first TE root on a dielectric coated metal plane. This is seen as follows: The TE_o mode cutoff condition for a dielectric coated plane is that the thickness of the dielectric slab (b-a), is a quarter of a wavelength in the slab measured in the direction perpendicular to the surface and evaluated at cutoff $\lambda_v/\sqrt{\varepsilon_r-1}$, i.e., $(b-a) = \frac{1}{4}\frac{\lambda_v}{\sqrt{\varepsilon_r-1}}$, which can be rearranged to read $C\sqrt{\varepsilon_r-1} = \pi/2(W-1)$. It is seen that, as C becomes larger (larger cylinder radius for a given frequency), that the cutoff curve for the cylinder begins to coincide with that for the plane, as it should.

TABLE II

AXIAL SURFACE WAVE CUTOFF ROOTS FOR FIRST TE_o MODE

W	$CW\sqrt{\varepsilon_r-1}$	$C\sqrt{\varepsilon_r-1}$	Plane $\frac{\pi/2}{W-1}$
1.00	∞	∞	∞
1.10	17.619	16.0172	15.7079
1.20	9.772	8.1433	7.8539
1.40	5.875	4.1964	3.9269
1.50	5.103	3.402	3.1415
1.60	4.592	2.870	2.6179
1.80	3.961	2.2005	1.9634
2.00	3.586	1.7930	1.5707
2.20	3.295	1.4977	1.3089
2.40	3.171	1.3212	1.1219

2. HE_1 Mode

Repeating the above graphical procedure as for m=0, for m=1 to obtain the roots of $\bar{L}_1\big|_{p=0}=0$ of (34), gives the results of Table III for the first hybrid HE_1 mode, as also plotted in Fig. 2. It is noted that the cutoff condition for this first hybrid HE_1 mode is slightly higher than that for the first TE_o mode. For successively larger values of m, the corresponding curves have a higher $C\sqrt{\varepsilon_r-1}$ value for a given W and were not computed, since primary interest in this work was to determine the cutoff condition for the lowest order mode.

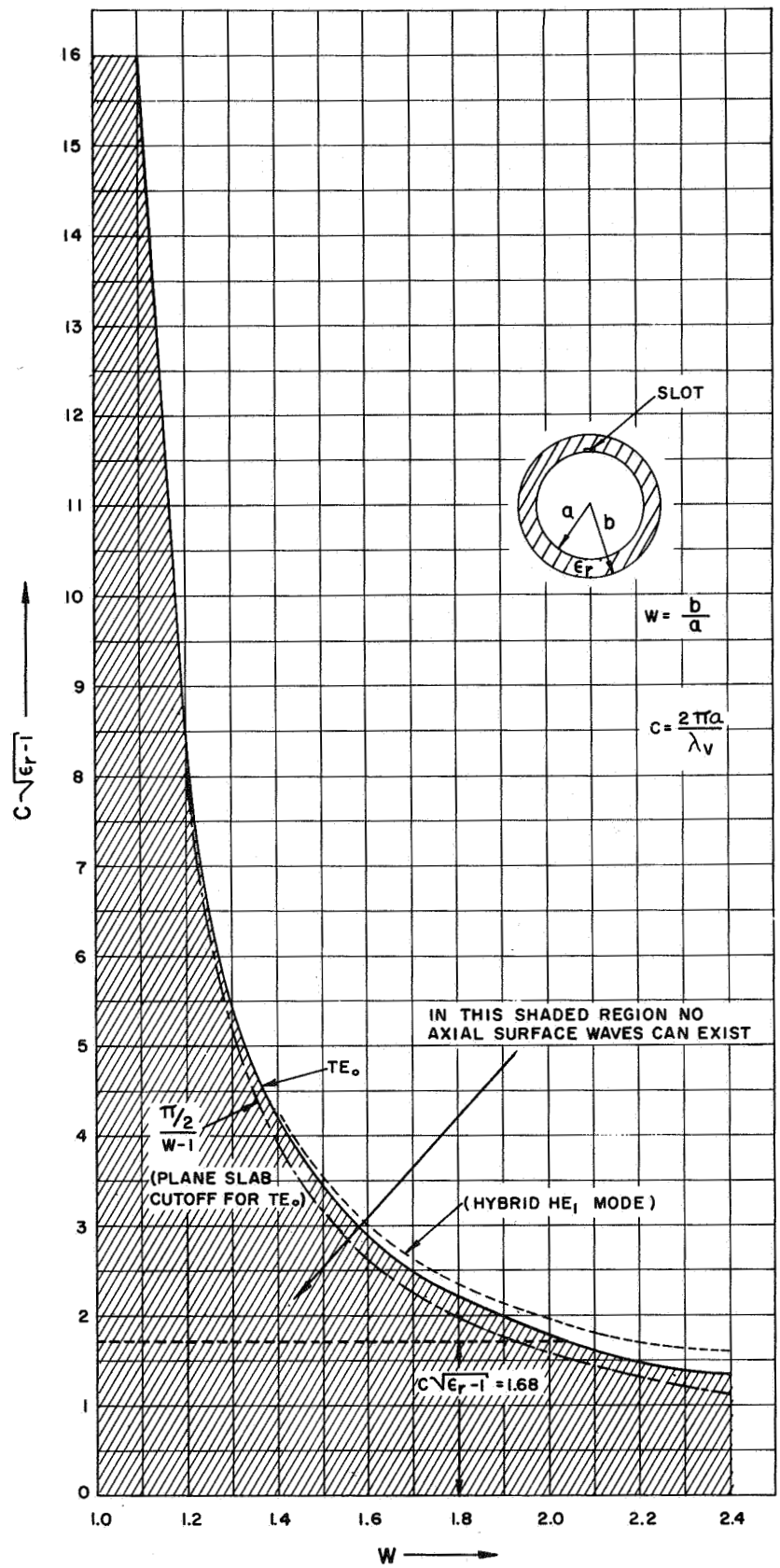

FIG. 2 CUTOFF CONDITIONS FOR LOWEST ORDER TE_0 AND HE_1 AXIAL SURFACE WAVE MODES ON DIELECTRIC COATED METAL CYLINDER EXCITED BY A THIN AXIAL SLOT

TABLE III

AXIAL SURFACE WAVE CUTOFF ROOTS FOR

FIRST HE_1 HYBRID MODE

W	$CW\sqrt{\epsilon_r-1}$	$C\sqrt{\epsilon_r-1}$
1.00	∞	∞
1.40	6.005	4.289
1.50	5.271	3.514
1.60	4.792	2.995
1.80	4.226	2.348
2.00	3.916	1.958
2.20	3.736	1.698
2.40	3.622	1.509

c. Conclusions for Axial Surface Waves

From the universal curves of Fig. 2, it is seen that if one chooses the operating frequency and cylinder-dielectric parameters (i.e., C, ϵ_r, and W), such as to fall in the shaded region, then no axial surface waves will exist on the axial slotted-dielectric coated metal cylinder.

IV. AZIMUTHAL SURFACE WAVES

The foregoing discussion has considered what types of axial surface waves can exist and are excited on the given structure. These axial surface waves propagate in the axial (z) direction.

The possibility of the structure supporting azimuthal (circumferential) surface waves also exists. These waves travel in the circumferential (ϕ) direction. In general, this type of wave, either of TM or TE type, will have the form $e^{-(\gamma b)\phi} f(\rho)g(z)$ where γb need not be an integer, and where $\gamma=\alpha+j\beta$ is the complex propagation constant for the azimuthal surface wave. For the case of no axial (z) variation, i.e., g(z) a constant, the transcendental equations governing the propagation factor γ for both the TM and TE waves has been obtained by Elliott [6], as reviewed by Walter [7]. Examination of these equations reveals that the lowest order TM azimuthal surface has a zero cutoff frequency, whereas the lowest order TE azimuthal surface wave has a cutoff frequency, fc_{TE}, of approximately (with the approximation improving for increasing C) $fc_{TE} \approx \frac{4c\sqrt{\epsilon_r - 1}}{d}$, corresponding to a coating thickness, d, at cutoff of a quarter of a wavelength in the radial direction.

For the axial slot antenna, examination of the field structure discloses that a strong E_ϕ component across the slot exists and this will excite the azimuthal TM surface wave. This TM wave will then be the dominant and only azimuthal surface wave for a coating thickness, T, satisfying

$$T < \frac{\lambda_v}{4\sqrt{\epsilon_r - 1}} .$$

The above work [6,7] also shows that for large $\beta_v a$, that γ is almost purely imaginary and is given approximately by the work of Baechle [7,8], but that the attenuation factor, α, though small, is not zero and represents radiation (α only vanishes for the limiting case of infinite cylinder radius, i.e., the plane case). This radiation contributes to the radiation field, which can be seen as follows.

In the axial slot antenna under consideration, one notes from symmetry, that azimuthal surface waves in both the forward-going and backward-going ϕ direction are excited in equal strengths and carry power densities of, say, S_ϕ^+ and S_ϕ^-, respectively, where

$$S_\phi^+ = \frac{S_o}{2} e^{-2(\alpha b)\phi}$$

$$S_\phi^- = \frac{S_o}{2} e^{-(2\alpha b)(2\pi - \phi)} \qquad (38)$$

S_o = Slot power density coupled into azimuthal surface wave.

Suppose one considers the total power conservation theorem, which states that within a closed area energy cannot be created or destroyed, and applies it to an arbitrary pie slice extending from $a \leq \rho \leq \rho_o$ and from $\phi_1 \leq \phi \leq \phi_2$, where $\phi_2 = \phi_1 + \Delta\phi$, as shown in Fig. 3. Assuming no field variation in the z direction (the allowance of variation in the z direction will not change the conclusions and only unnecessarily complicates the argument), then application of conservation principle gives

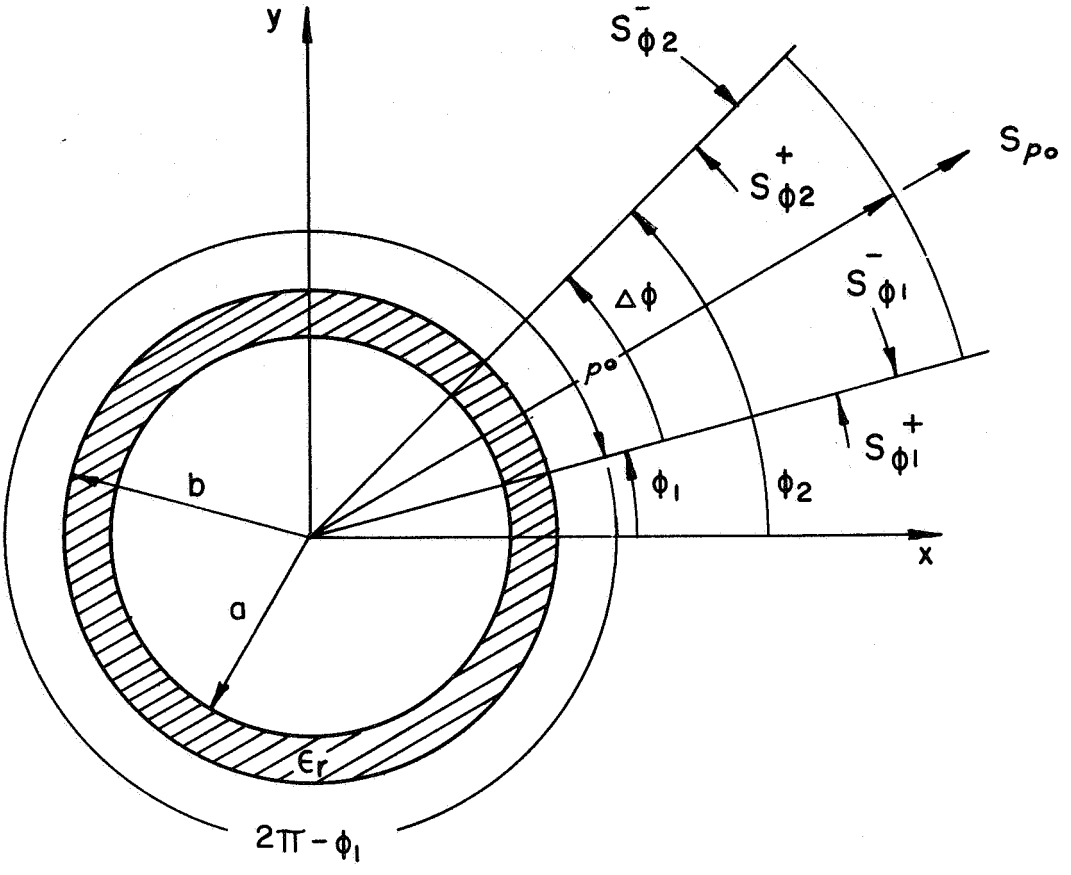

FIG. 3 POWER FLOW FOR AZIMUTHAL SURFACE WAVE

$$\ell \int_a^{\rho_o} (S_{\phi 1}^{+} - S_{\phi 1}^{-}) d\rho - \ell \int_a^{\rho_o} (S_{\phi 2}^{+} - S_{\phi 2}^{-}) \cdot d\rho = S_{\rho_o} \ell \rho_o \Delta\phi \qquad (39)$$

where ℓ is an arbitrary length in the z direction, and $S_{\rho o}$ is the radial power density at the radius ρ_o, i.e.,

$$\Delta P_\phi = \Delta P_r \qquad (40)$$

where ΔP_ϕ is the l.h.s. of (39) and ΔP_r is the r.h.s. of (39); that is, the difference in azimuthal power flow in the given sector appears as radial power flow, i.e., radiation.

It is noted that if $\alpha=0$, then $S_{\phi 1}^{+}=S_{\phi 1}^{-}$, $S_{\phi 2}^{+}=S_{\phi 2}^{-}$, i.e., $\Delta P_\phi=0$, and hence, $\Delta P_r=0$, i.e., no radiation would occur. Thus, the curved surface must have $\alpha>0$ (as it does) for radiation to occur due to the azimuthal surface wave.

As such, the effect of the azimuthal surface waves which exist contribute directly to the radiation conductance of the slot. No explicit pole contribution is made (as is the case for the axial surface waves which only carry power in the axial direction and do not radiate for the case of an infinite cylinder) in the form of a surface wave conductance. The conductance contributed by the azimuthal surface waves only exists in the radiation conductance term, and is already included in the conductance expression (equation (I) of Table II) obtained previously; indeed, the existence of the azimuthal surface wave is manifested by the dependence in shape of the radiation patterns on the coating parameters W and ε_r.

V. NUMERICAL COMPUTATIONS OF EXTERNAL ADMITTANCE

a. No Coating

After determining the pertinent antenna parameters (as discussed in Section VI), the computations of external admittance for the no coating case were performed. In particular, computations of g_{cv} and b_{cv}, as given by (XIX) and (XXI) of Table I, for $1.40 \leq C \leq 1.60$ in increments in C of $\Delta C=0.01$, and for $\ell/a=2.388$ (corresponding to $\ell=3.540$ inches and a=1.482 inches), with $\phi_o=0.1687$ radians (corresponding to w=0.250 inches and a=1.482 inches) were made. The programming* for both g_{cv} and b_{cv} are given in Appendix X. The results (rounded off to four significant figures) are tabulated in Table IV and plotted in Fig. 4. A partial check was made on these computer results (since these no coating results will later be used as a check on the cases for a coating by letting W=1.00) by manually computing both g_{cv} and b_{cv} for C=1.50. These manual computations are given in Appendix IV and agree within two significant figures for g_{cv} and within one significant figure for b_{cv}; as such,confidence in the computer results was established, so that the coating cases could then be considered.

It is noted that the values of g_{cv} are not too much different from a thin half wavelength slot on an infinite ground plane (g_{cv} = 0.388).

*All programming and associated analysis for this work was done by Dr. V. Gylys of IITRI.

TABLE IV

COMPUTED VALUES OF EXTERNAL ADMITTANCE - NO COATING

($\ell/a=2.388$, $\phi_o=0.1687$)

c	g_{cv}	b_{cv}
1.40	0.3511	0.3751
1.41	0.3562	0.3934
1.42	0.3613	0.4116
1.43	0.3664	0.4296
1.44	0.3716	0.4470
1.45	0.3768	0.4645
1.46	0.3820	0.4814
1.47	0.3873	0.4980
1.48	0.3926	0.5146
1.49	0.3980	0.5321
1.50	0.4034	0.5492
1.51	0.4088	0.5655
1.52	0.4142	0.5817
1.53	0.4200	0.5978
1.54	0.4252	0.6138
1.55	0.4307	0.6302
1.56	0.4363	0.6461
1.57	0.4418	0.6618
1.58	0.4474	0.6777
1.59	0.4531	0.6933
1.60	0.4587	0.7088

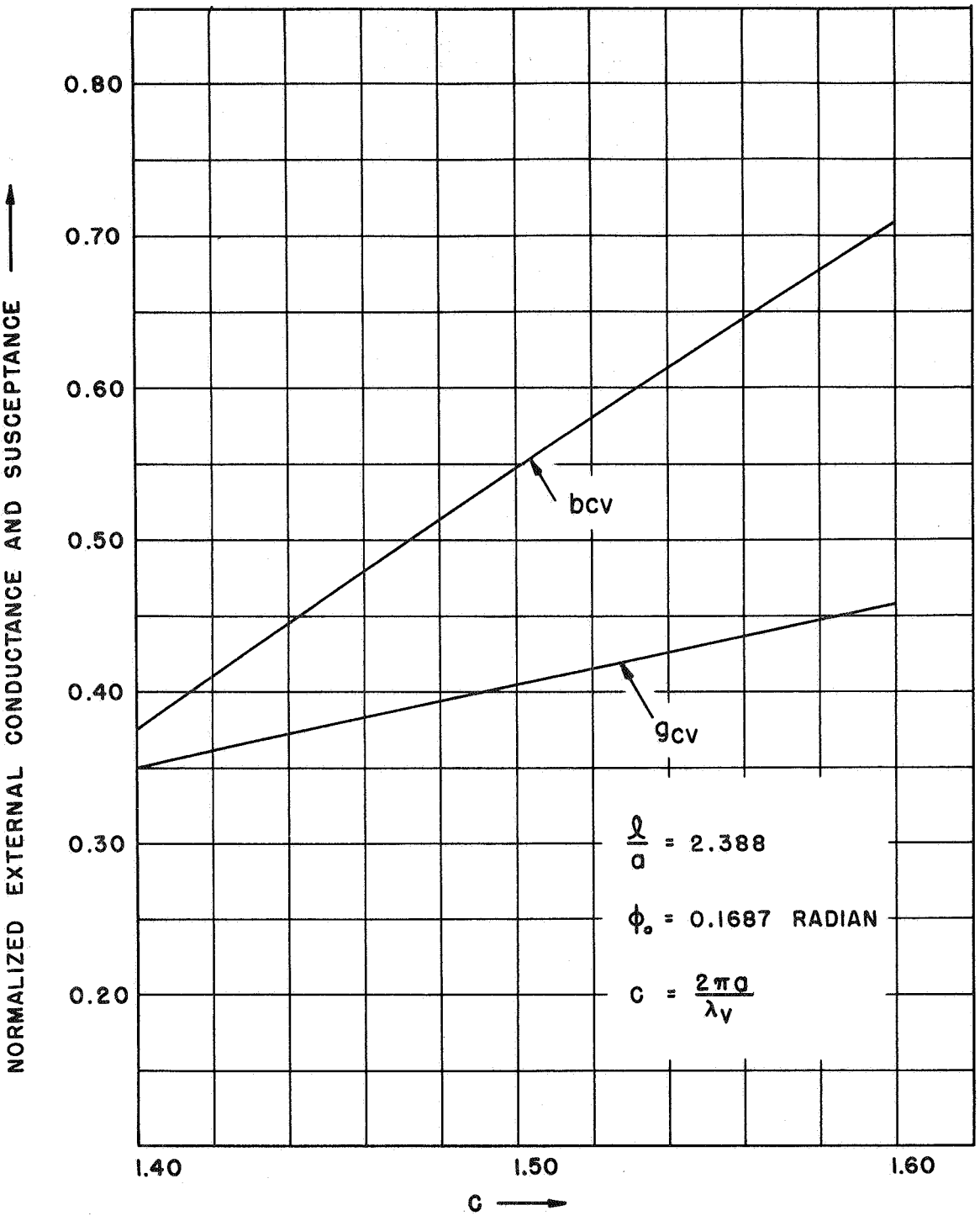

FIG. 4 COMPUTED NORMALIZED EXTERNAL CONDUCTANCE AND SUSCEPTANCE OF UNCOATED AXIAL SLOTTED CYLINDER

b. Teflon Coating

The external conductance, g_c, for a Teflon coating (ε_r=2.10), as given by (I) of Table I, was computed over the same frequency range as for the no coating case ($1.40 \leq C \leq 1.60$) for coating thicknesses corresponding to W=1.00, 1.20 and 1.50, respectively. The case of W=1.00 serves as a check on the computer program, since it represents the no coating case and must give (as it did) the same results as for g_{cv} of Fig. 4. The program for these coating cases is given in Appendix XI. The results are tabulated in Table V and are plotted in Fig. 5.

It is seen that the effect of the coating is to increase the external conductance as the coating thickness is increased. For infinite coating thickness, the expression for g_c reduces to that given in Appendix V which has, as yet, not been computed. For the sake of curiosity, the value of normalized admittance $\sqrt{\varepsilon_r}\, g_{cv}$, is also plotted in Fig. 5.

c. Plasma Coating

The external conductance, g_{cp}, and susceptance, b_{cp}, expressions for the case of a plasma coating having $0 \leq \varepsilon_r \leq 1$, (corresponding to a plasma frequency to operating frequency range of $0 \leq \omega_p/\omega \leq 1$, i.e., $\omega \geq \omega_p$ for the idealized plasma model of $\varepsilon_{rp}=1-\omega_p^2/\omega^2$) are given by (XI) and (XIV) of Table I.

Only two limiting cases were considered thus far.

TABLE V

COMPUTED VALUES OF g_c EXTERNAL CONDUCTANCE-TEFLON COATING

(ε_r=2.10, ℓ/a=2.388, ϕ_o=0.1687)

C	W=1.00	W=1.20	W=1.50
1.40	0.3511	0.4476	0.7002
1.41	0.3562	0.4551	0.7146
1.42	0.3613	0.4627	0.7291
1.43	0.3664	0.4703	0.7438
1.44	0.3716	0.4780	0.7586
1.45	0.3768	0.4857	0.7736
1.46	0.3820	0.4935	0.7887
1.47	0.3873	0.5013	0.8040
1.48	0.3926	0.5093	0.8194
1.49	0.3980	0.5171	0.8349
1.50	0.4034	0.5252	0.8506
1.51	0.4088	0.5375	0.8664
1.52	0.4142	0.5414	0.8824
1.53	0.4197	0.5496	0.8985
1.54	0.4252	0.5578	0.9147
1.55	0.4307	0.5660	0.9311
1.56	0.4363	0.5746	0.9477
1.57	0.4418	0.5826	0.9638
1.58	0.4474	0.5910	0.9812
1.59	0.4531	0.5994	0.9982
1.60	0.4587	0.6079	1.0154

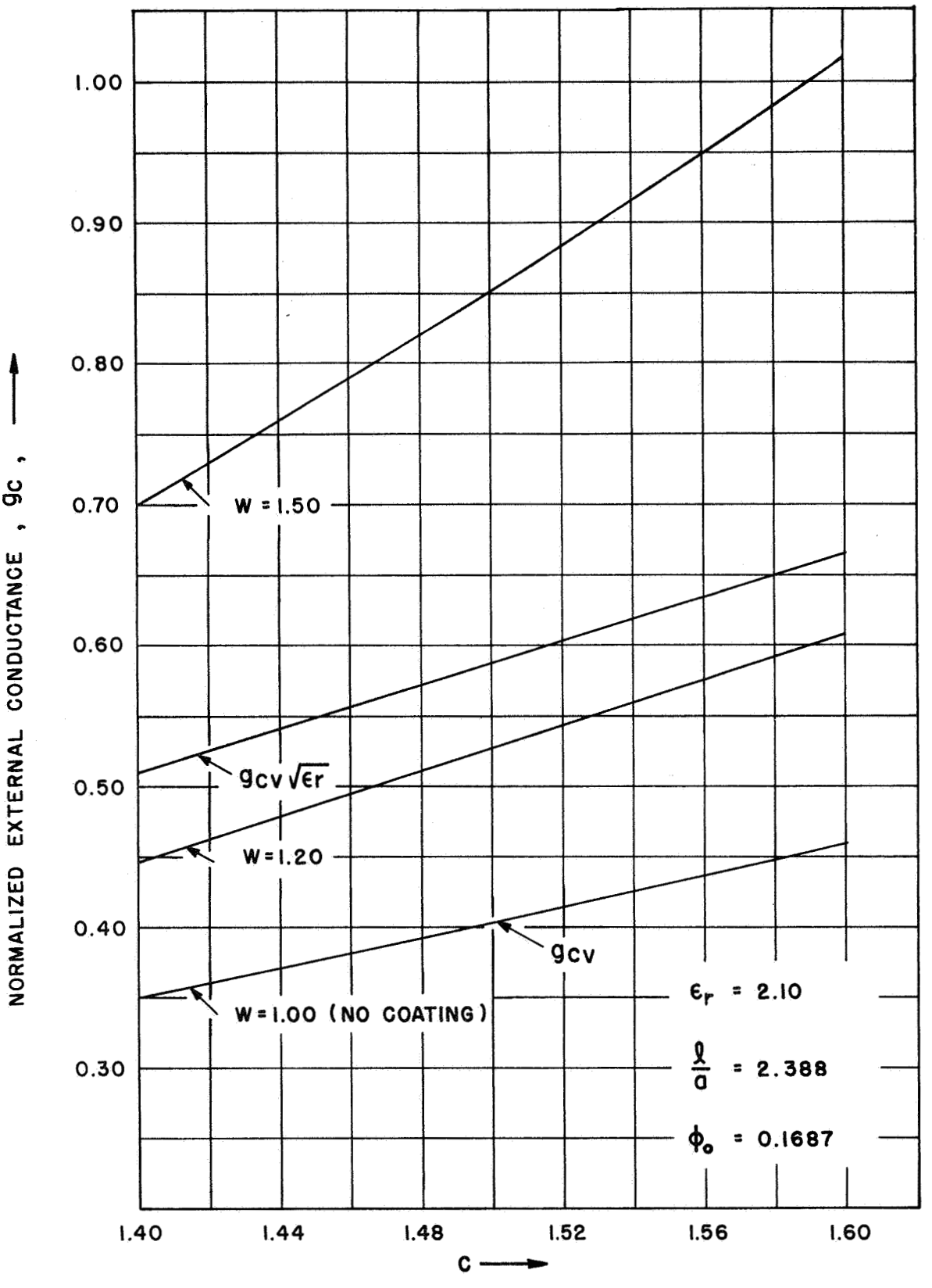

FIG. 5 COMPUTED NORMALIZED EXTERNAL CONDUCTANCE OF TEFLON COATED AXIAL SLOTTED CYLINDER

(1) Case of Zero Thickness (W=1) and/or Zero Plasma Frequency (ω_p=0)

For this case (W=1 and/or ε_r=1) the expressions (XI) and (XIV) of Table I reduce to (XIX) and (XXI) of Table I as they should, since this represents the no coating case.

(2) Case of Infinite Thickness at Plasma Resonance

For the case of infinite thickness, it is seen from Appendix V, that if $\omega_p=\omega$, i.e., $\varepsilon_{rp}=0$, then g_{cp} vanishes, i.e., from (6) of Appendix V.

$$\lim_{\substack{\omega\to\omega_p \\ W\to\infty}} g_{cp}=0 \qquad (41)$$

although the susceptance does not vanish ($b_{c1}\to 0$ and $b_{c2}\to$constant).

This is perhaps an anticipated result, since for infinite thickness the external conductance should be directly proportional to the characteristic admittance of the infinite medium, $\sqrt{\varepsilon_{rp}}/\eta_v$ and, as such, should vanish with ε_{rp}. Thus, at plasma resonance ($\omega=\omega_p$), one can anticipate from this result a reduction in external conductance which, for the ideal case of no collisions and infinite thickness, will vanish. It can also be expected that if the collisions are finite, but small, and W is sufficiently large so that the outgoing wave is sufficiently attenuated at the radius ρ=b, then one can approximate this situation by the infinite coating case, but replace ε_{rp} with

$$\varepsilon_{rp}=1-\frac{\omega_p^2/\omega^2}{1-j\ \nu/\omega}\approx 1-(\omega_p^2/\omega^2)(1+j\ \nu/\omega) \text{ for } \nu/\omega<<1, \text{ which for } \omega=\omega_p$$

becomes $\sqrt{-j\nu/\omega_p} \approx \frac{(1-j)}{2}\sqrt{\nu/\omega_p}$; thus, one can anticipate that for this case g_{cp} will be proportional to $\sqrt{\nu/\omega_p}$, i.e.,

$$\lim_{\substack{\omega\to\omega_p \\ \nu/\omega_p<<1}} g_{cp} \sim \sqrt{\nu/\omega_p} \cdot \qquad (42)$$

W sufficiently large

Actual computations should be done to ascertain this anticipation, as well as to find the constant of proportionality.

As noted previously, [9], at plasma resonance the equatorial plane radiation patterns approach a circle for the limiting case of zero collisions. It appears, then, that these two observations taken together, and/or separately, may, perhaps, be useful in diagnosing the plasma layer.

VI. ANTENNA DESIGN AND CALIBRATION

a. Design Considerations

The parameters entering into the antenna design are C, ℓ, and w for the non-coated case and, additionally, ε_r and W for the coated case.

The choice of C is, in part, dictated by the previous observation [10] that too large a value of C (say, above 20) causes too critical a dependence of the external admittance on the coating parameters W and ε_r, since, in effect, one is then considering the input admittance of a transmission line which is many (C/2) wavelengths long, and a small change in its propagation factor or characteristic impedance (realized by a change in either ε_r or W) can result in a very large

change in the input admittance. For this reason, the lowest value of C that can be physically realized is preferred.

The lowest value of C is limited by the fact that a pure cosine field distribution must be produced along the length of the slot, so that the theory above is valid, and this means that the run of rectangular waveguide (of inner cross-section ℓ by w) must be long enough so that only the dominant TE_{10} mode remains after the excitation point. This length can be nominally taken as at least 3/4 of a guide wavelength, or approximately a free space wavelength; thus, $2a \approx \lambda_v$, i.e., $C \simeq \pi \approx 1.5$, is the minimum value of C that should be used. A lower value will make the higher order modes introduced at the excitation point too large to be neglected.

The length of the slot, ℓ, and the dielectric loading of the waveguide, are to be such that for a specified C near 1.5 the first higher order (TE_{20} and TE_{30}) modes are sufficiently attenuated at the slot location.

The width, w, of the slot must be made sufficiently small so that the assumption of circumferential and rectangular electric field equality across the slot width is valid.

All these factors are considered in detail in Appendix VI, which also describes the means of exciting the TE_{10} mode in the waveguide. The pertinent dimensions arrived at in the design are (with a Teflon loaded waveguide)

$$\begin{cases} a = 1.482 \text{ inches} \\ \ell = 3.540 \text{ inches} \\ w = 0.250 \text{ inches} \end{cases} \tag{43}$$

(The above value of outer cylinder radius, a, gives an approximate operating range of $1.40 \leq C \leq 1.60$ over a frequency range of $1.80 \leq f \leq 2.00$ gc. It was specified that f=1.90 gc (C=1.50) be the center frequency).

A sketch of the complete antenna waveguide feed assembly is shown in Fig. 6 (with a detailed drawing given in Fig. VI-7 of Appendix VI).

The coating parameters ε_r and W were chosen such that no axial surface waves could be excited. A Teflon coating was chosen for ease of machining and because its dielectric constant (ε_r=2.10) is representative of ablative materials. From Fig. 2, one then notes that for the operating frequency range of $1.40 \leq C \leq 1.60$, giving a maximum $C\sqrt{\varepsilon_r - 1} \approx 1.68$, that the choice of W must be chosen such that W<2.05. Thus, for W<2.05 and $C \leq 1.60$, no axial surface waves can exist.

The choices of W=1.00 (no coating), 1.20 and 1.50 were then made since, it was believed, that these thickness increments of ΔW=0.20, being about 20% of a quarter wavelength, would be sufficient to reveal the dependence of both admittance and pattern behavior versus coating thickness for the condition of no axial surface waves.

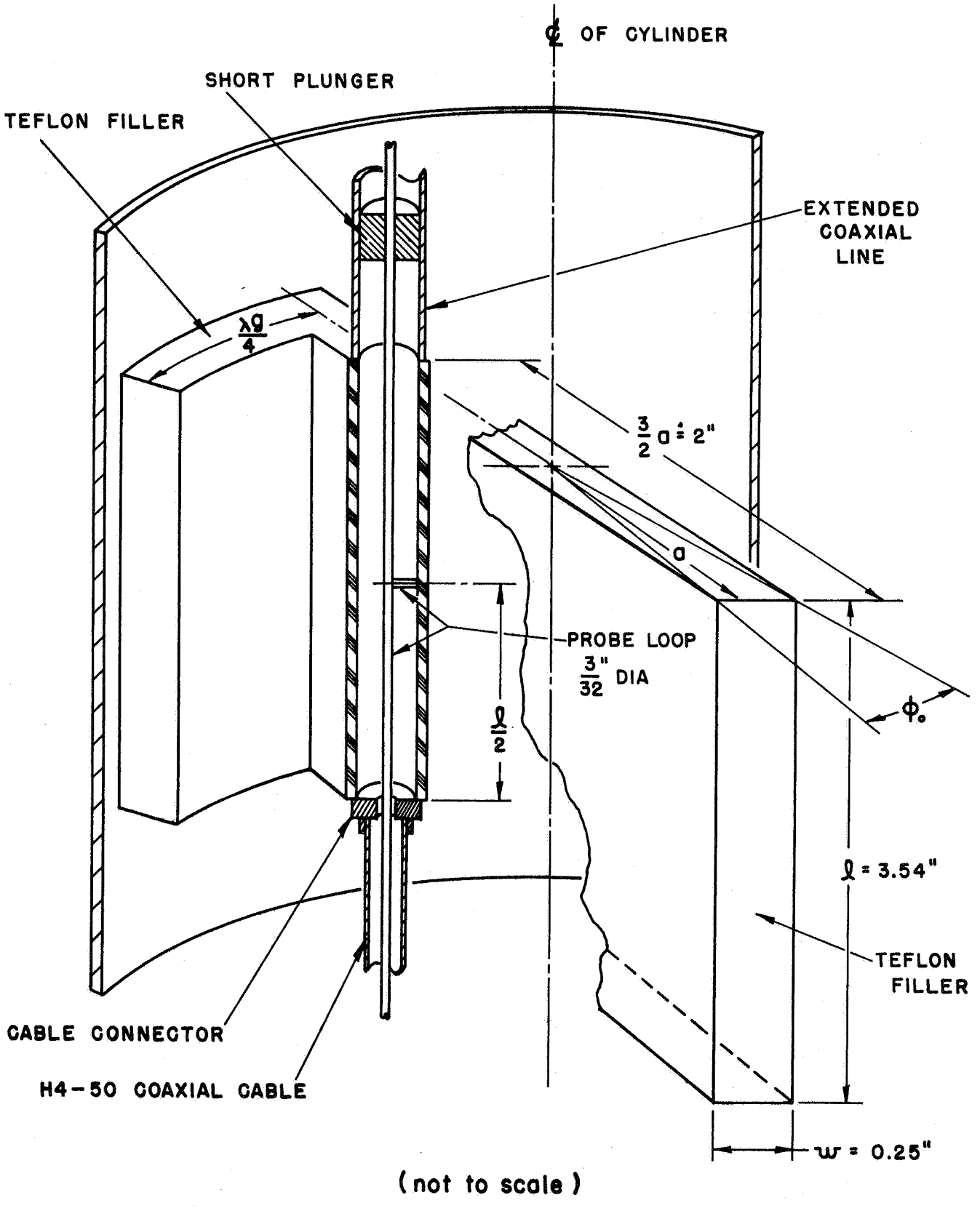

FIG. 6 SECTION OF ANTENNA-WAVEGUIDE FEED ASSEMBLY

b. Relationship between Coaxial Line Admittance and Waveguide Admittance

The coaxial feed-axial slot antenna can be characterized by a black box, as shown in Fig. 7, since both the input port (at its coaxial connector) and the output port (the rectangular waveguide termination at the slot location) carry only one propagating mode (the coaxial TEM mode and the TE_{10} mode, respectively). The reflection coefficients Γ_1 and Γ_2 existing at the input and output ports are related through the scattering matrix coefficients (S_{11}, S_{12} and S_{22}) through the relation [11]

$$\Gamma_1 = S_{11} + \frac{S_{12}^2 \Gamma_2}{1 - S_{22}\Gamma_2} \tag{44}$$

where

S_{11}, S_{12}, S_{22} = Complex scattering matrix coefficients of coax-waveguide network

Γ_1 = Complex reflection coefficient of TEM mode as measured at input of coaxial line.

Γ_2 = Complex reflection coefficient of TE_{10} mode as measured in waveguide at the slot location.

$$y_1 = \frac{1-\Gamma_1}{1+\Gamma_1} = \text{Normalized admittance (relative to 50 ohm coaxial line) at input of coaxial line.} \tag{45}$$

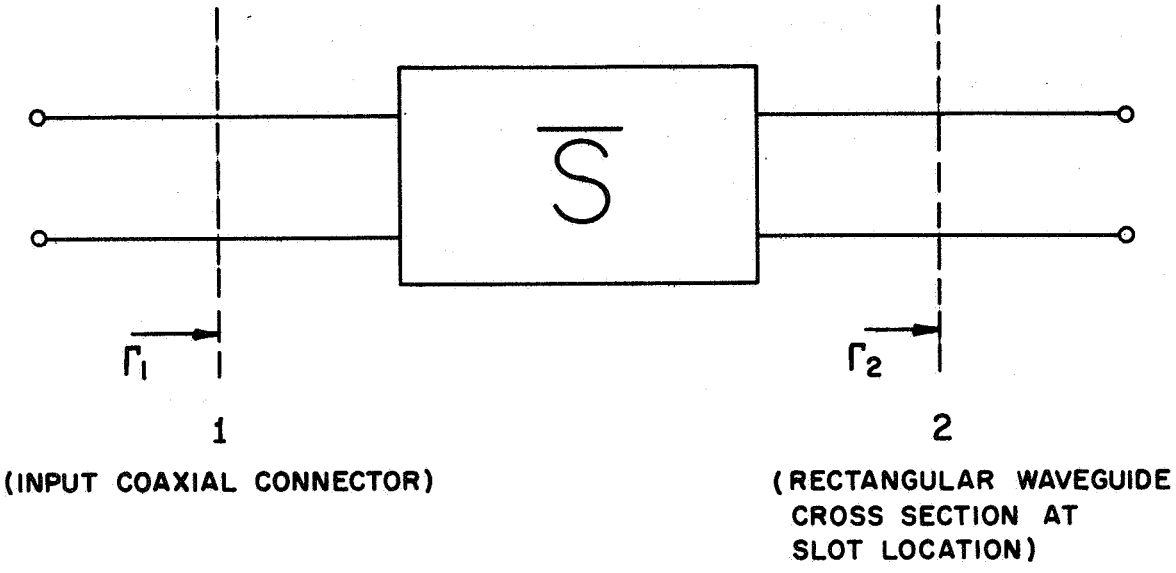

FIG. 7 TWO PORT EQUIVALENT NETWORK FOR ANTENNA

$$y_2 = y_{in} = \frac{1-\Gamma_2}{1+\Gamma_2} = \text{Normalized (relative to } Y_{10} \text{ of } TE_{10} \text{ mode) input waveguide admittance.} \quad (46)$$

Of course, y_2 is the same as y_{in}, as given by (18) and the relationship of y_{in} to the external normalized (with respect to the admittance of free space) admittance, y_c, is given by (22). Thus, once S_{11}, S_{12} and S_{22} are known, (44) can be used to determine Γ_1 from Γ_2, or vice versa.

c. Measurement of Scattering Matrix (Antenna Calibration)

To calibrate the antenna, the DesChamps method [12,13,14] was used. In this method at a given frequency, a moveable short circuit is placed at the Γ_2 location and the value of Γ_1 recorded. This is repeated for 8 successive sixteenth wavelength displacements of the short circuit, and then the values of S_{11}, S_{12} and S_{22} are determined via graphical constructions based on these measurements. The details are given in Appendix VIII. This procedure must be repeated at a sufficient number of frequencies in the frequency range of interest such that a smooth curve for each scattering matrix element is realized.

In the present application, an extension of the waveguide (but not filled with Teflon) was made in conjunction with an adjustable short circuit piston. This was attached to the slot-cylinder as shown in the photograph of Fig. 8, which also shows the coaxial feed line attached to a G.R. slotted line and associated conventional Klystron, frequency meter, and VSWR meter gear. The measurement of admittance in the slotted line was made in the conventional way

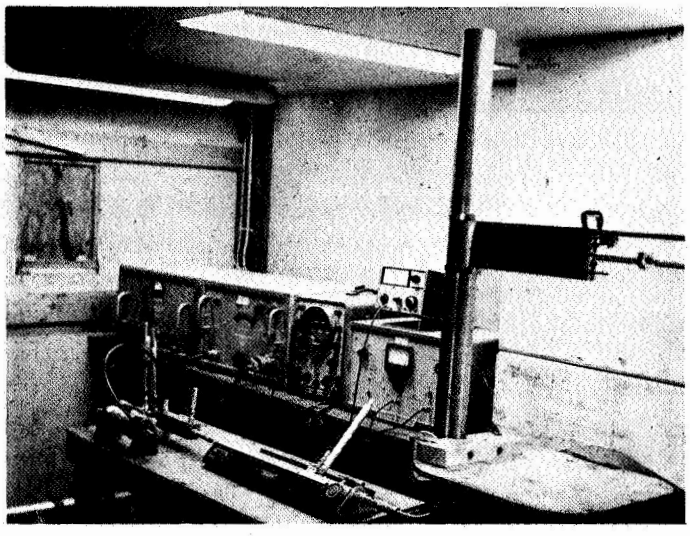

FIG. 8 PHOTO OF SCATTERING MATRIX CALIBRATION SET UP

(placing a short circuit on the slotted line, replacing it with the antenna, and noting the shift in minimum points, and reading the VSWR). However, since high VSWR's were to be measured, it was found necessary to calibrate the crystal-VSWR meter combination, since it departed from a square law curve. This was done by terminating the slotted line with a short circuit and recalling that the relative voltage distribution must then follow the law $\cos(2\pi X/\lambda_V)$. A new dial, based on this calibration was put on the VSWR meter scale. The calibration was done at 1.90 gc, and was assumed flat over the band of 1.80 to 2.00 gc, since the crystal law is probably not that frequency sensitive.

Following the procedure given in Appendix VIII gave the S_{11}, S_{12} and S_{22} curves shown in Figs. 9, 10 and 11, respectively. It is noted that these values of S_{11}, S_{12} and S_{22} are the same for both the non-coated and coated cases, since they relate Γ_1 (at the coaxial line input) to Γ_2 (at the waveguide-slot interface), i.e., the coating does not enter into the equivalent network of Fig. 7.

VII. EXPERIMENTAL RESULTS AND COMPARISON WITH THEORY

a. Input Admittance

The normalized input admittance was measured in the coaxial feed line referred to the plane of the input coaxial connector for both the no coating and coating cases. The measurement procedure was the standard one, as used to determine the scattering matrix coefficients above.

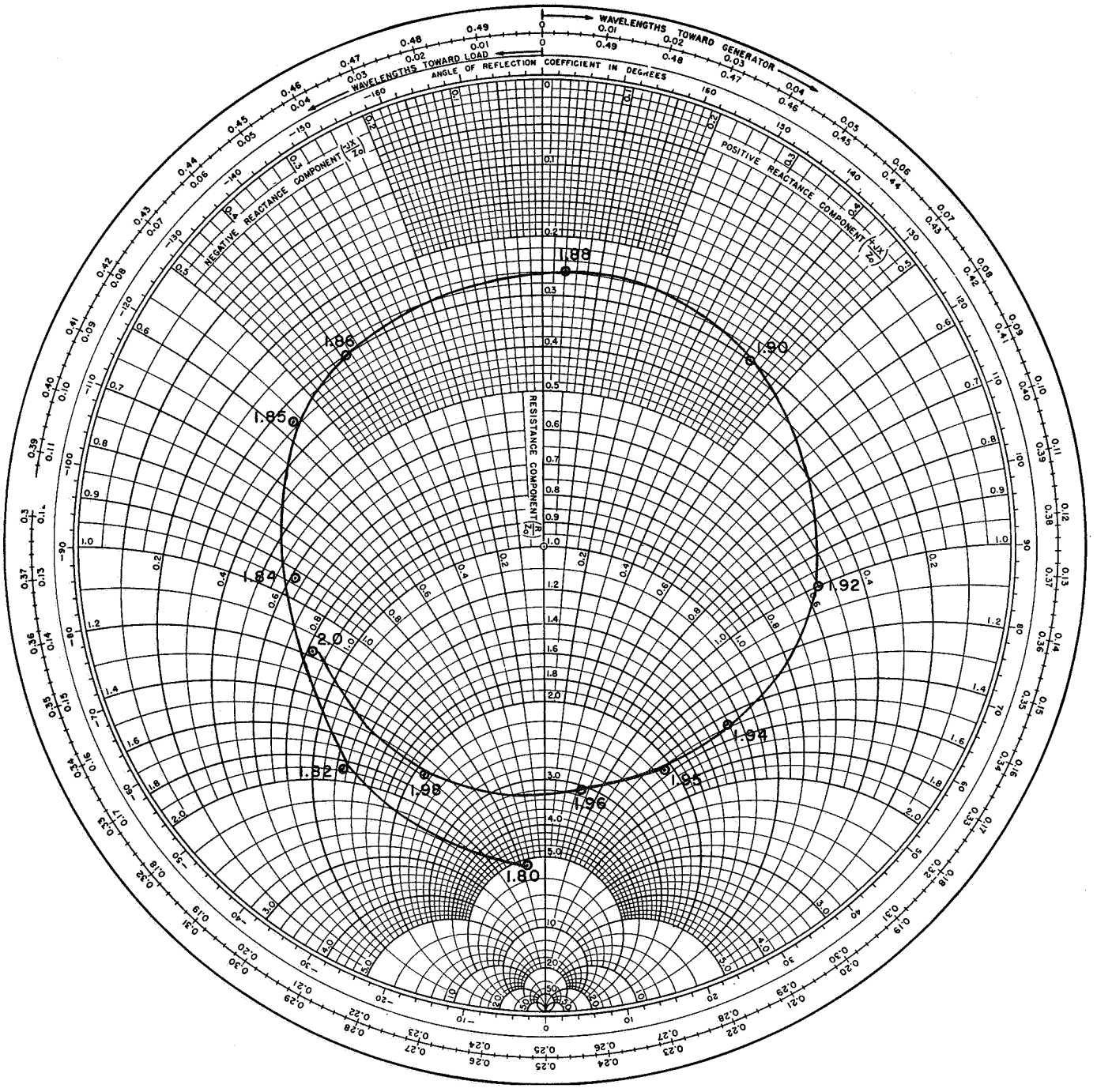

FIG. 9 MEASURED SCATTERING MATRIX ELEMENT, S_{11}

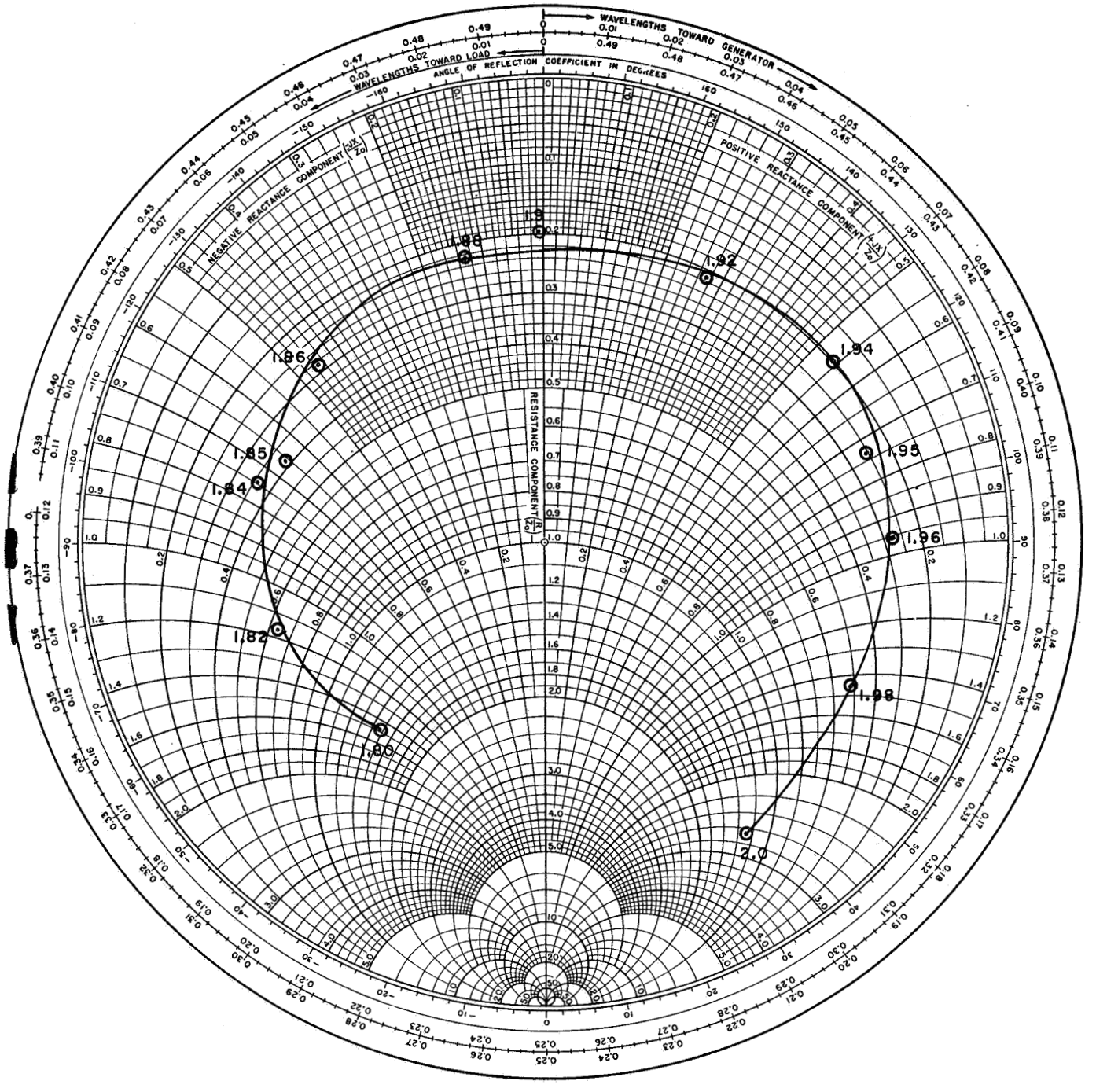

FIG. 10 MEASURED SCATTERING MATRIX ELEMENT, S_{12}

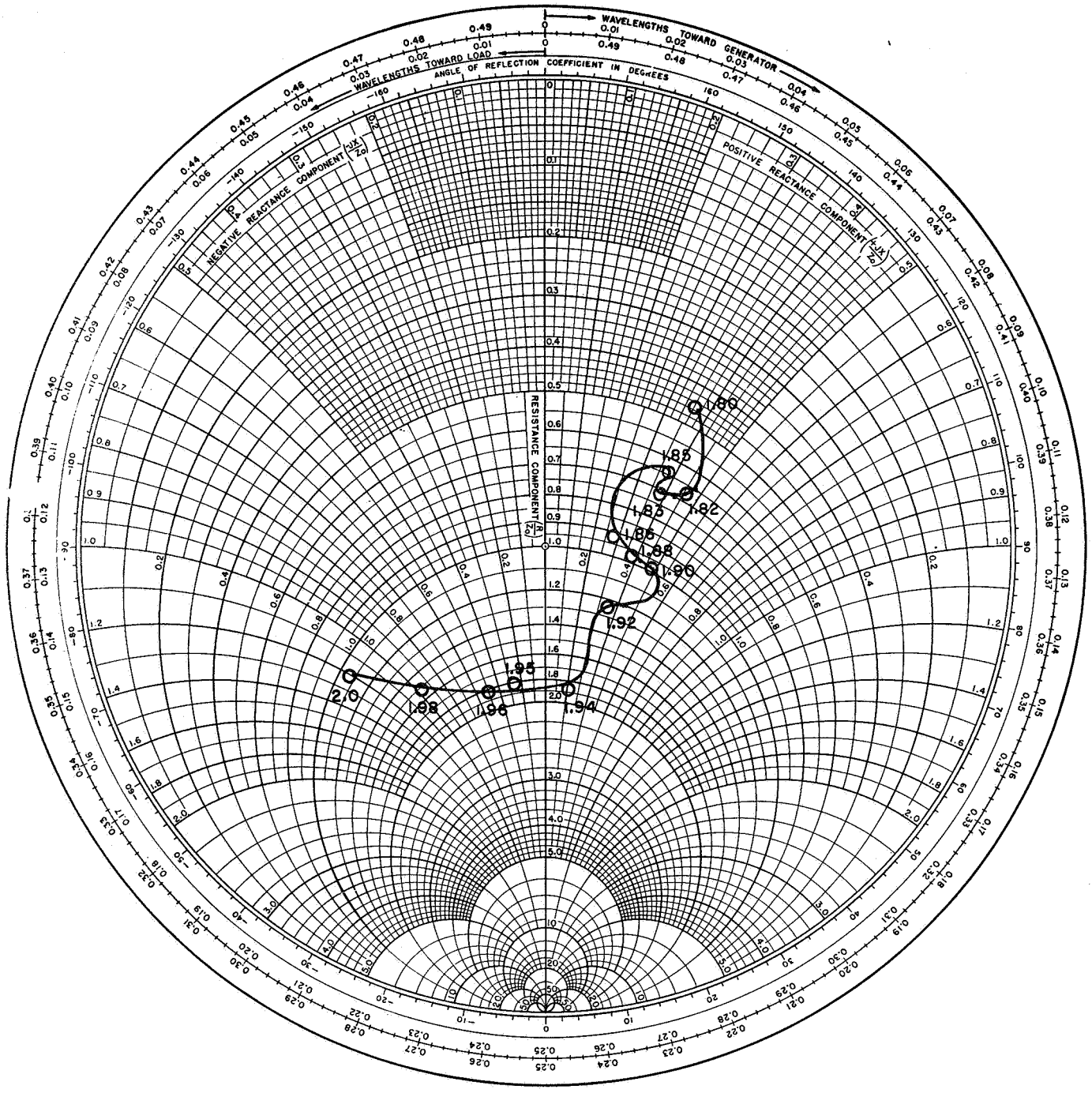

FIG. 11 MEASURED SCATTERING MATRIX ELEMENT, S_{22}

1. No Coating

The measured values of the normalized input coaxial line admittance, y_1, are shown as the dotted line in Fig. 12, on a Smith Chart, across the entire band from 1.80 to 2.00 gc. The corresponding theoretical value of this admittance was obtained from the computed values of g_{cv} and b_{cv} of Table IV to give y_{cv} and from (22) to compute $y_{in}=y_2$. Then, from (46), Γ_2 was computed from y_2, and finally using the measured values of S_{11}, S_{12} and S_{22} of Figs. 9, 10 and 11, (44)* and (45) were used to compute the theoretical value of y_1. These theoretical values are shown in Fig. 12 as the solid line. From the Smith Chart, the values of g_1 and b_1 are obtained and are plotted in Figs. 13 and 14, respectively, for ease of comparison of theory and experiment.

From Fig. 13, it is seen that the theoretical and experimental values of conductance agree within 10% over the entire band of 1.80 to 2.00 gc, i.e., over approximately a 10% bandwidth, whereas Fig. 14 shows that the theoretical and experimental values of susceptance agree within this same percentage only over the narrower bandwidth of 1.945 to 1.980 gc, i.e., over approximately a 2% bandwidth. It is suspected that the reason for this is that the scattering matrix element S_{22} was more accurately measured in the higher frequency range, since at the lower end of the band it (especially its angle) did not vary too smoothly, as

*Calculations of Γ_1 using (44) were made using the program described in Appendix XII.

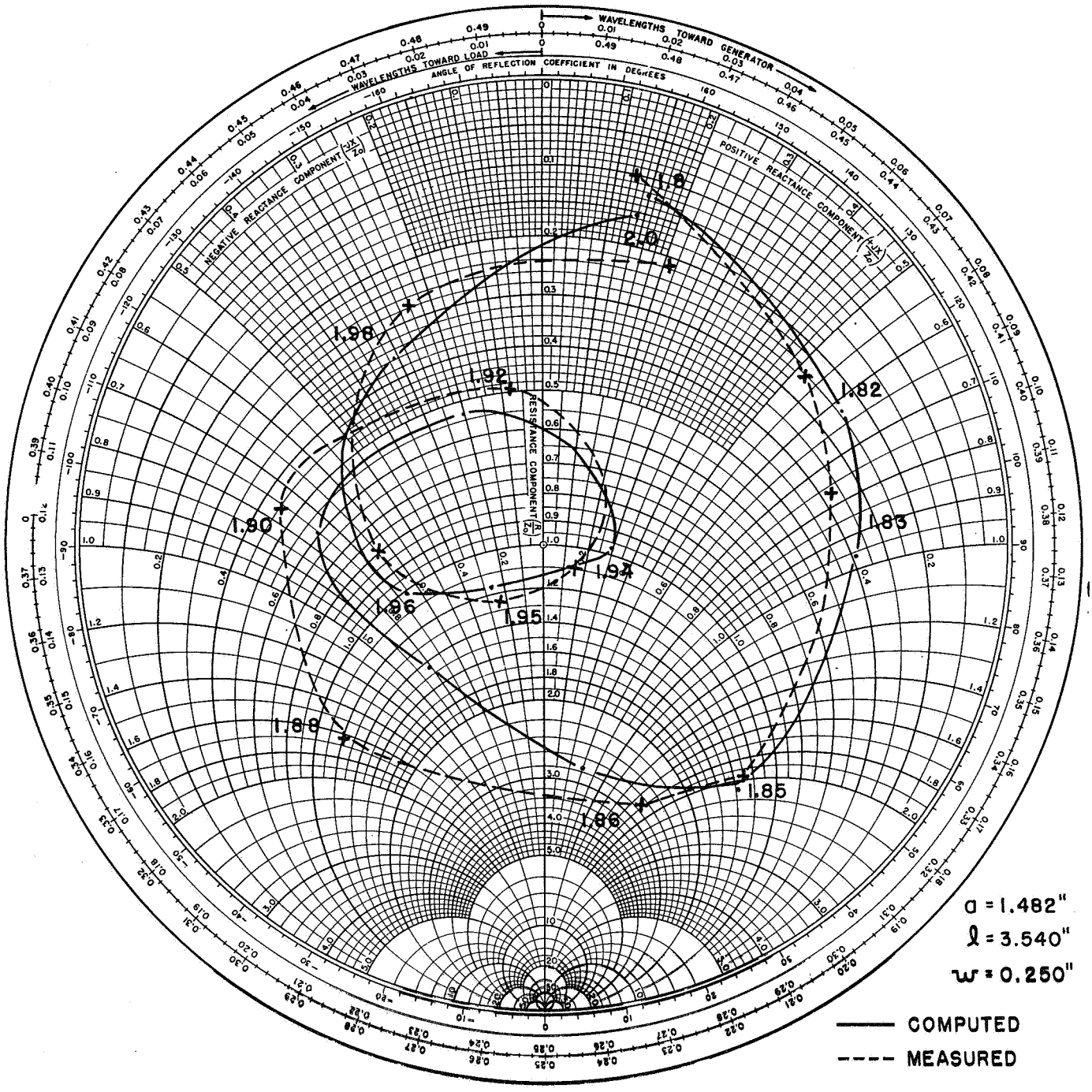

FIG. 12 MEASURED AND COMPUTED INPUT (COAXIAL LINE) ADMITTANCE – NO COATING

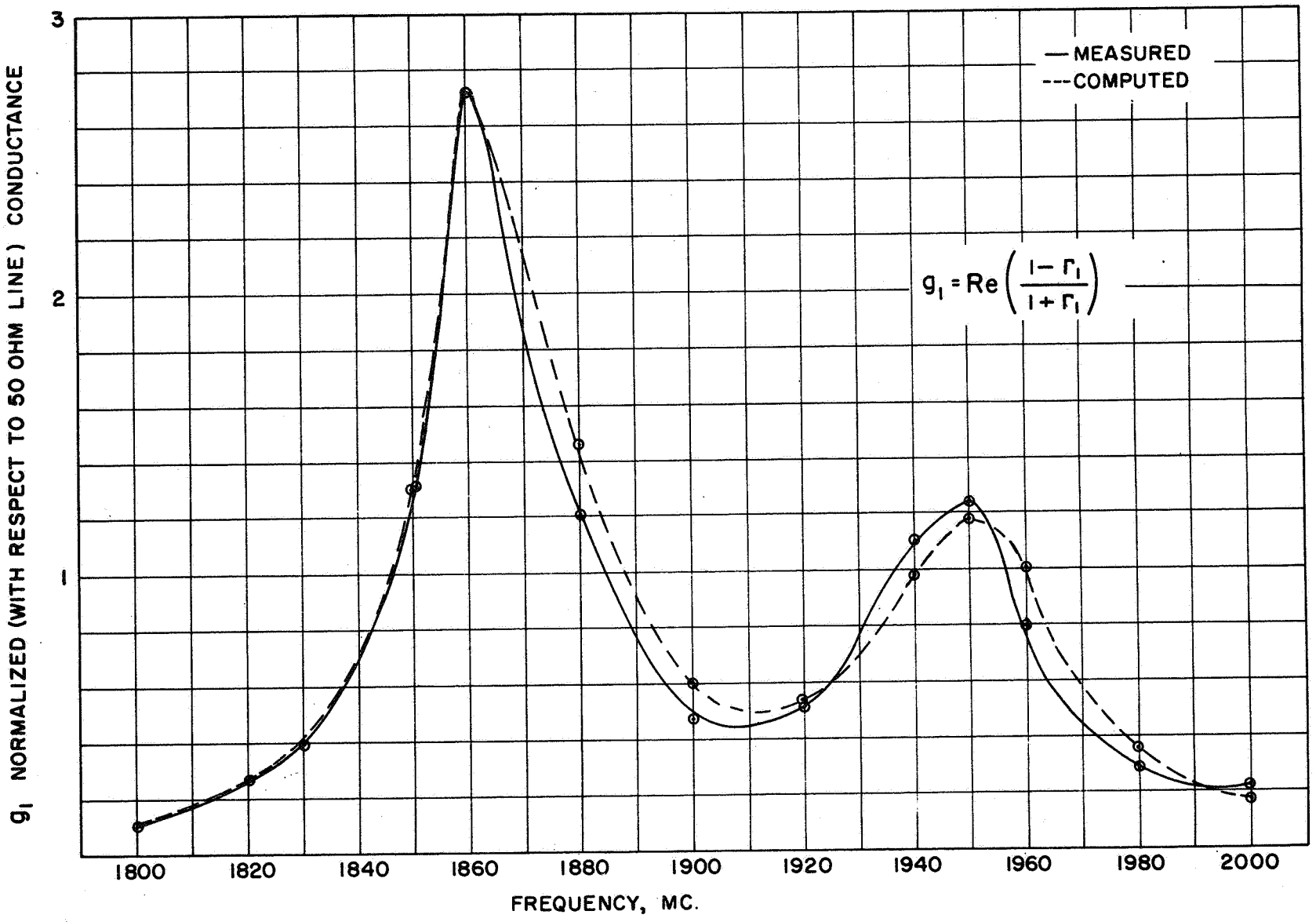

FIG. 13 MEASURED AND COMPUTED INPUT (COAXIAL LINE) CONDUCTANCE - NO COATING

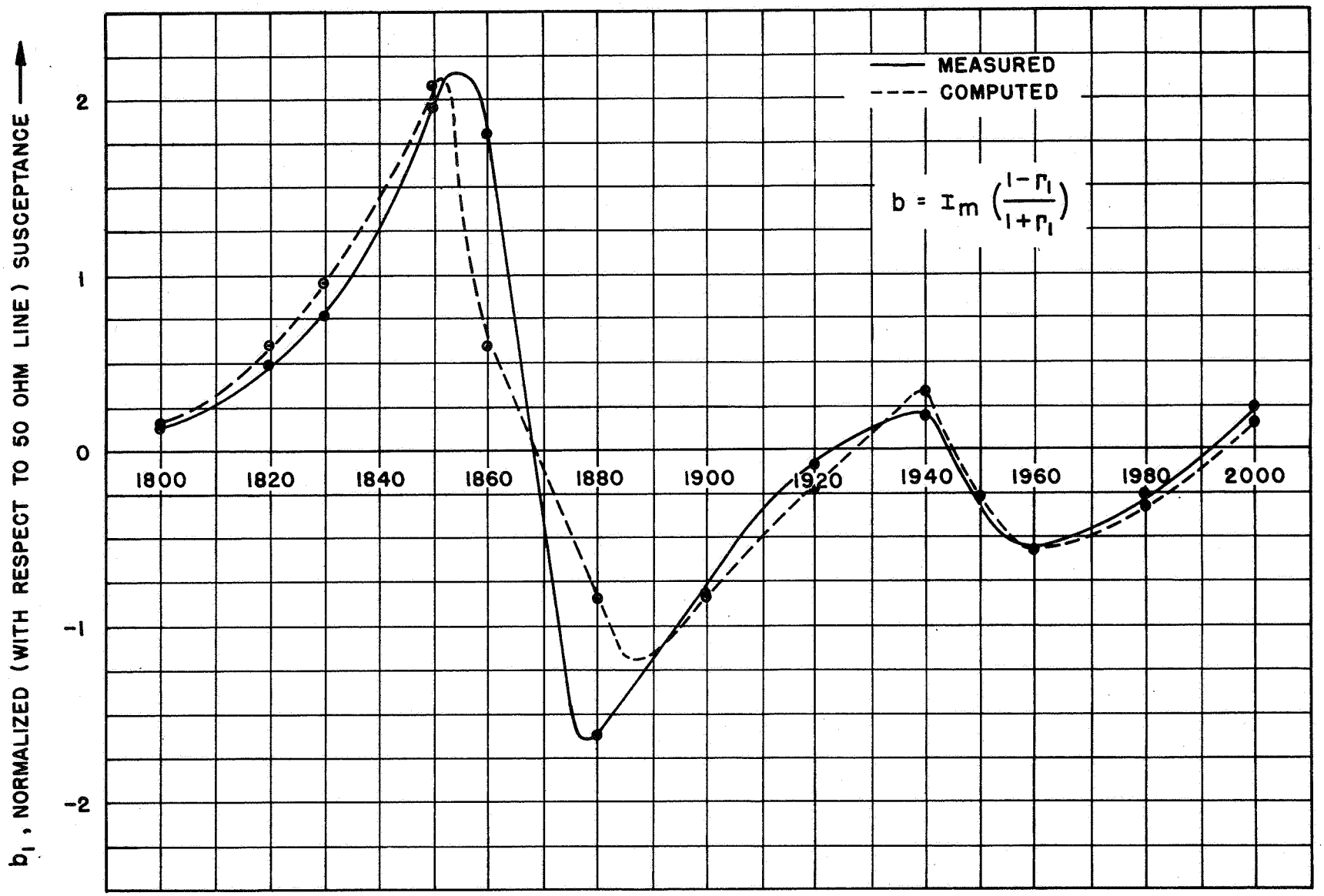

FIG. 14 MEASURED AND COMPUTED INPUT (COAXIAL LINE) SUSCEPTANCE, NO COATING

seen from Fig. 11. It is noted from Fig. 12 that, in going through the frequency range of 1.80 to 2.00 gc, a large loop around the origin of the Smith Chart is made by the admittance.

2. Teflon Coatings

The above measurements were repeated for two Teflon (ε_r=2.10) coatings of thickness 0.741" and 0.296", corresponding to W=1.50 and W=1.20, respectively. The set-up for all admittance measurements is shown in Fig. 15, which shows the Teflon coating in place. The coatings were machined to press fit on the metal cylinder, and were made in three pieces for ease of application. It was observed that no effect on input admittance was found if one placed metal foil or metal objects at the top or bottom ends of the Teflon coating, indicating that no axial surface waves were present, as should be, since, as was shown earlier, for these to exist for a Teflon coating in the frequency range of this antenna, one must have W>2.05.

The measured values of coaxial input admittance for these coating cases are shown in Figs. 16a and 16b, where it is seen, by comparison with Fig. 12, that the effect of adding a coating is to smooth out the admittance variation with frequency (for example, the loop traversed at roughly the center frequency becomes smaller with increasing coating thickness), as well as to improve the match over a wider bandwidth. This is more clearly seen by the cartesian plots of Figs. 17a and 17b for the conductance and susceptance,

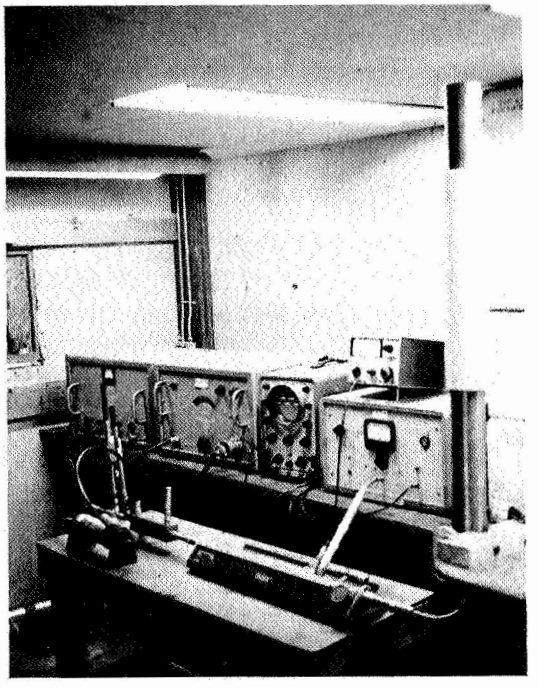

FIG. 15 PHOTOGRAPH OF COATED ANTENNA AND ADMITTANCE MEASUREMENT SET UP

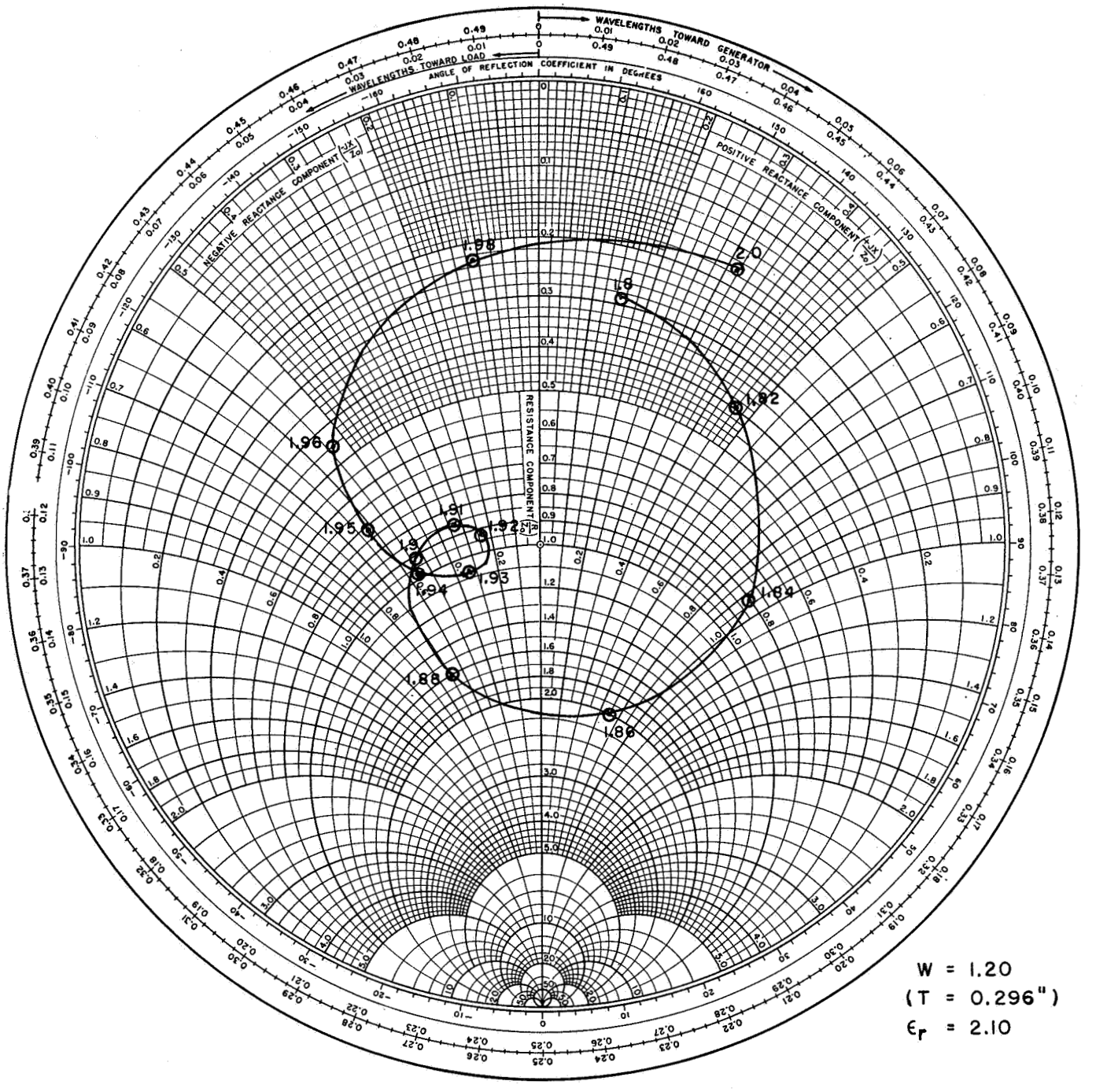

FIG. 16a MEASURED INPUT (COAXIAL LINE) ADMITTANCE – TEFLON COATING, W = 1.20

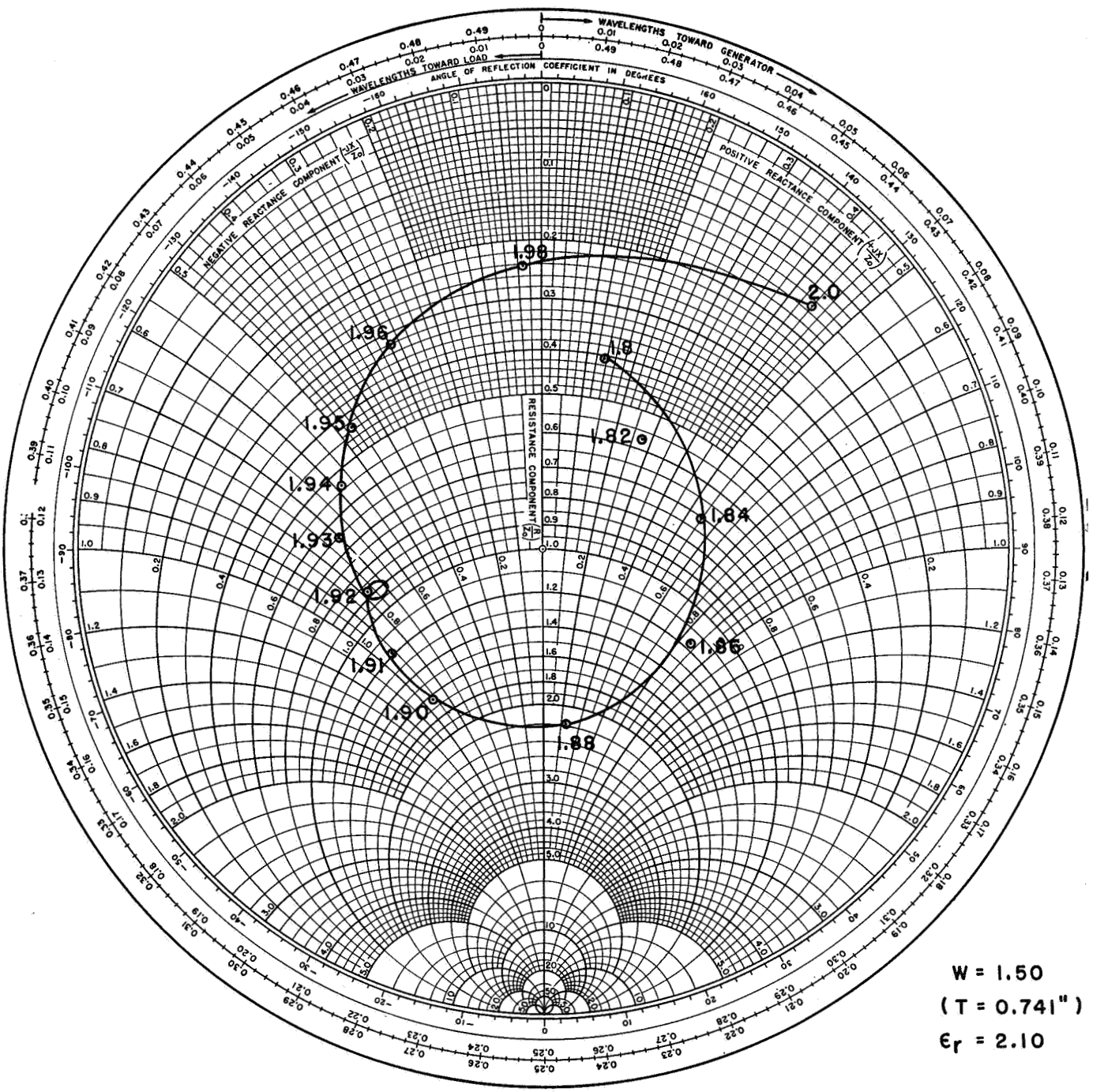

FIG. 16 b MEASURED INPUT (COAXIAL LINE) ADMITTANCE – TEFLON COATING , W = 1.50

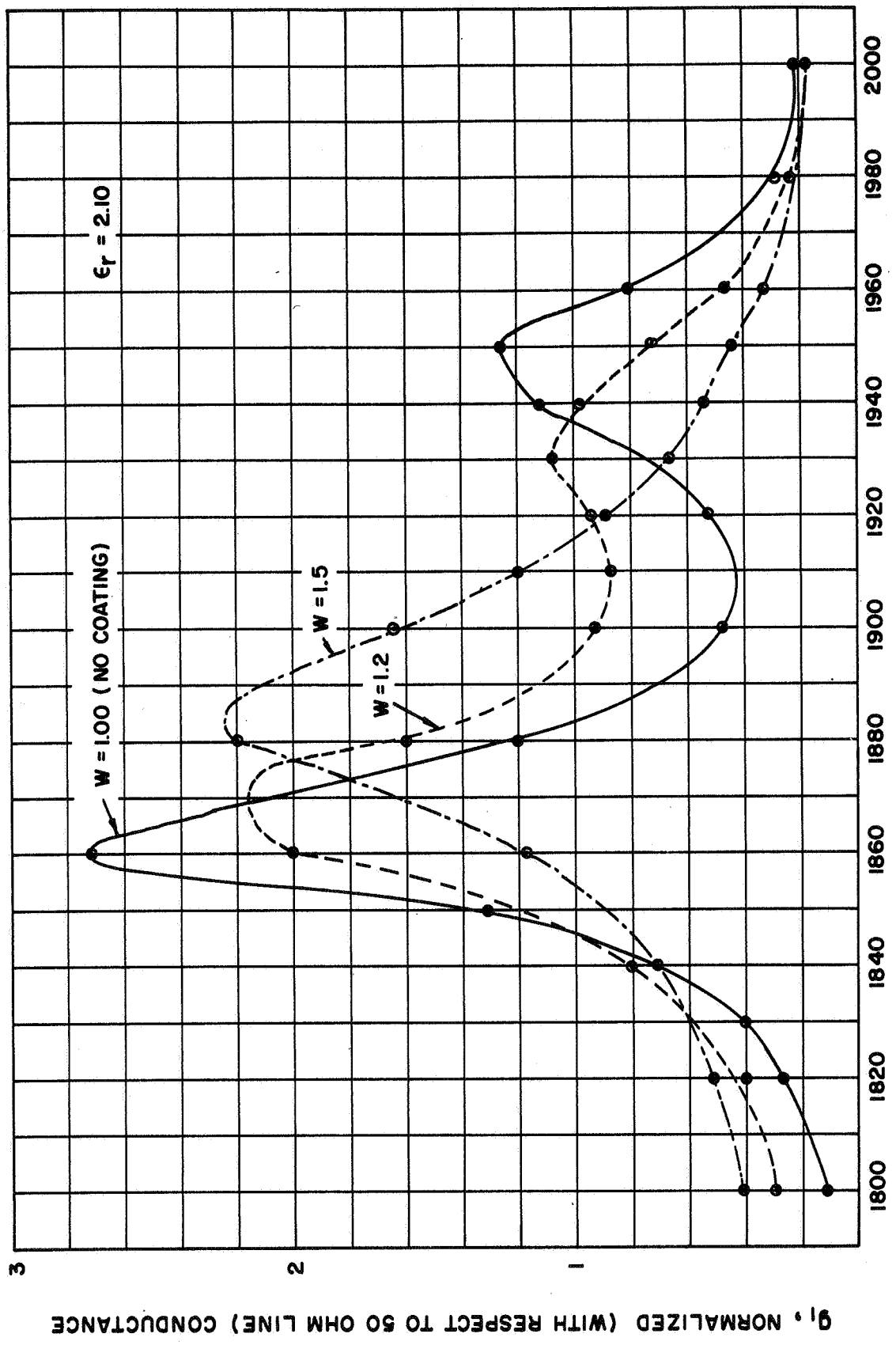

FIG. 17a MEASURED INPUT (COAXIAL LINE) CONDUCTANCE – TEFLON COATINGS

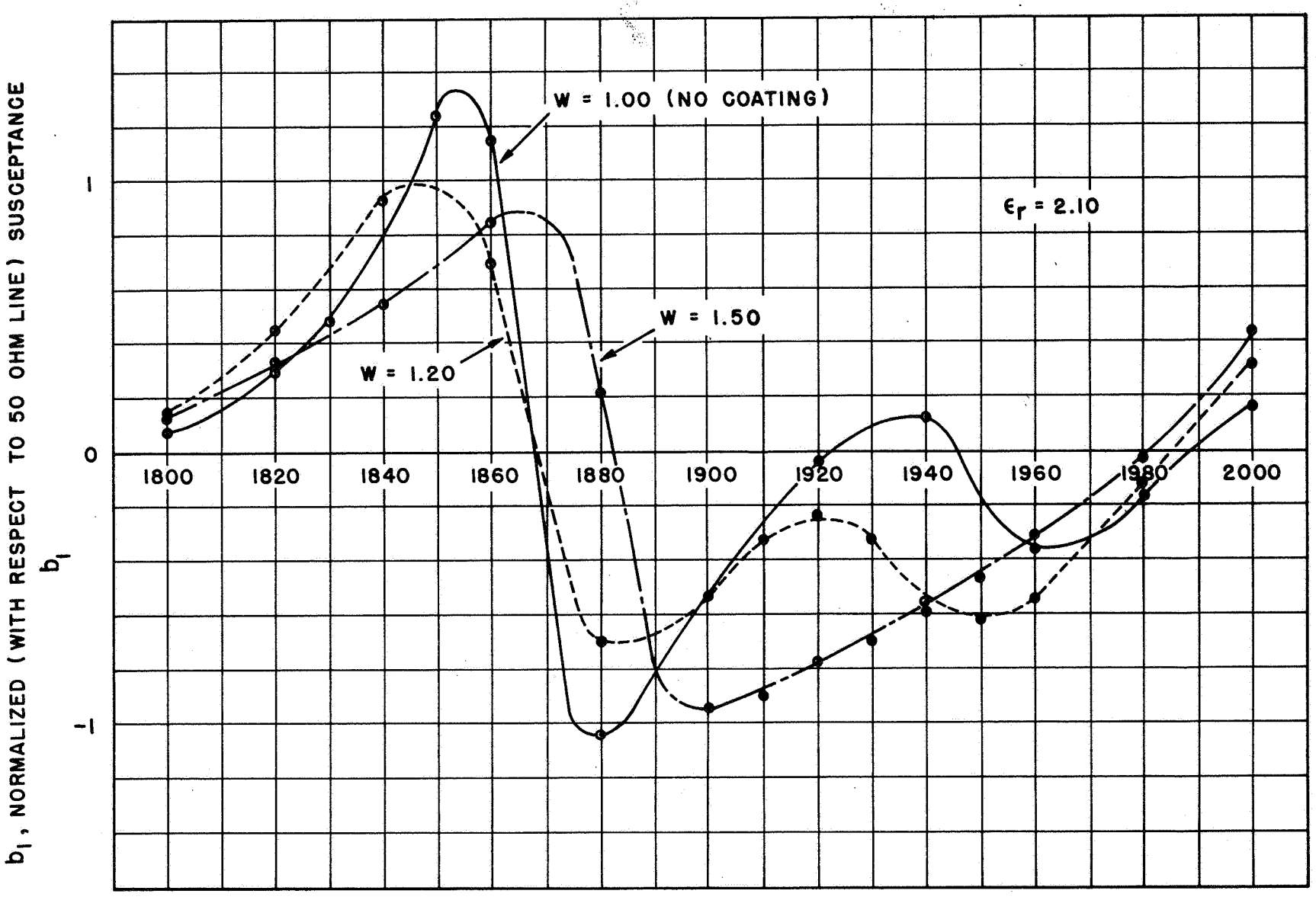

FIG. 17 b MEASURED INPUT (COAXIAL LINE) SUSCEPTANCE – TEFLON COATING

respectively. These plots also show the no coating case (W=1.00) for ease of comparison.

It was not possible to compare theory with experiment in the coaxial line, since both g_c and b_c computed values are required in going from y_2 to y_1 and only g_c has, thus far, been computed.

It is, of course, possible to go from y_1 to y_2 and compare y_2 measured with y_2 theoretical; however, as shown in Appendix IX, such a comparison can result in an amplification of the percent measurement error, and always results in a larger absolute error in y_2, because of the large value of $|\Gamma_2|$. This results in too much of a scattering of the measured values of y_2 about their theoretical values. For this reason, it is concluded that only comparisons of y_1 (theoretical and measured) are meaningful for the subject antenna.

b. Equatorial Plane Radiation Patterns

The equatorial plane ($\theta=\pi/2$) radiation field is given by (355) of Wait [1] and will not be rewritten here. It is known that the normalized equatorial plane radiation pattern for a thin finite length axial slot is the same as that for a thin infinite length axial slot. Recently, Swift [15] has considered the infinite axial slot antenna coated with an arbitrary non-homogeneous coating which includes, as a special case, the homogeneous coating.

Using his work, he has computed normalized power patterns,

$$(Db = 20 \log_{10} \left| \frac{E_\theta(o)}{E_\theta(\phi)} \right| \Bigg|_{\theta=\pi/2})$$

for the range of parameters in the range of C≈1.50, ε_r=2.10, W=1.00 (no coating), 1.20 and 1.50. The patterns for a given C were found to sharpen slightly with increasing coating thickness, and all have a null at approximately $\phi=\pm 130°$, the severity of which increases with coating thickness. Representative computed patterns are shown in Figs. 18a, b and c, for the cases of C=1.405, 1.500 and 1.635, respectively.

Measured patterns for the representative case of C=1.50 are shown in Figs. 19a and b for the no coating condition (W=1.00) and for the coating condition of ε_r=2.10 and W=1.20, respectively. The agreement with theory is seen to be excellent (within $\pm$0.10 db); the effect of the coating for this case being to increase the back lobe by about 1.0 db, and to increase the null at approximately 142° by slightly more than 1.0 db.

This pattern agreement is typical of others taken and, as such, these others will not be reported here. All patterns were taken at NASA, Langley Field, Hampton, Virginia.

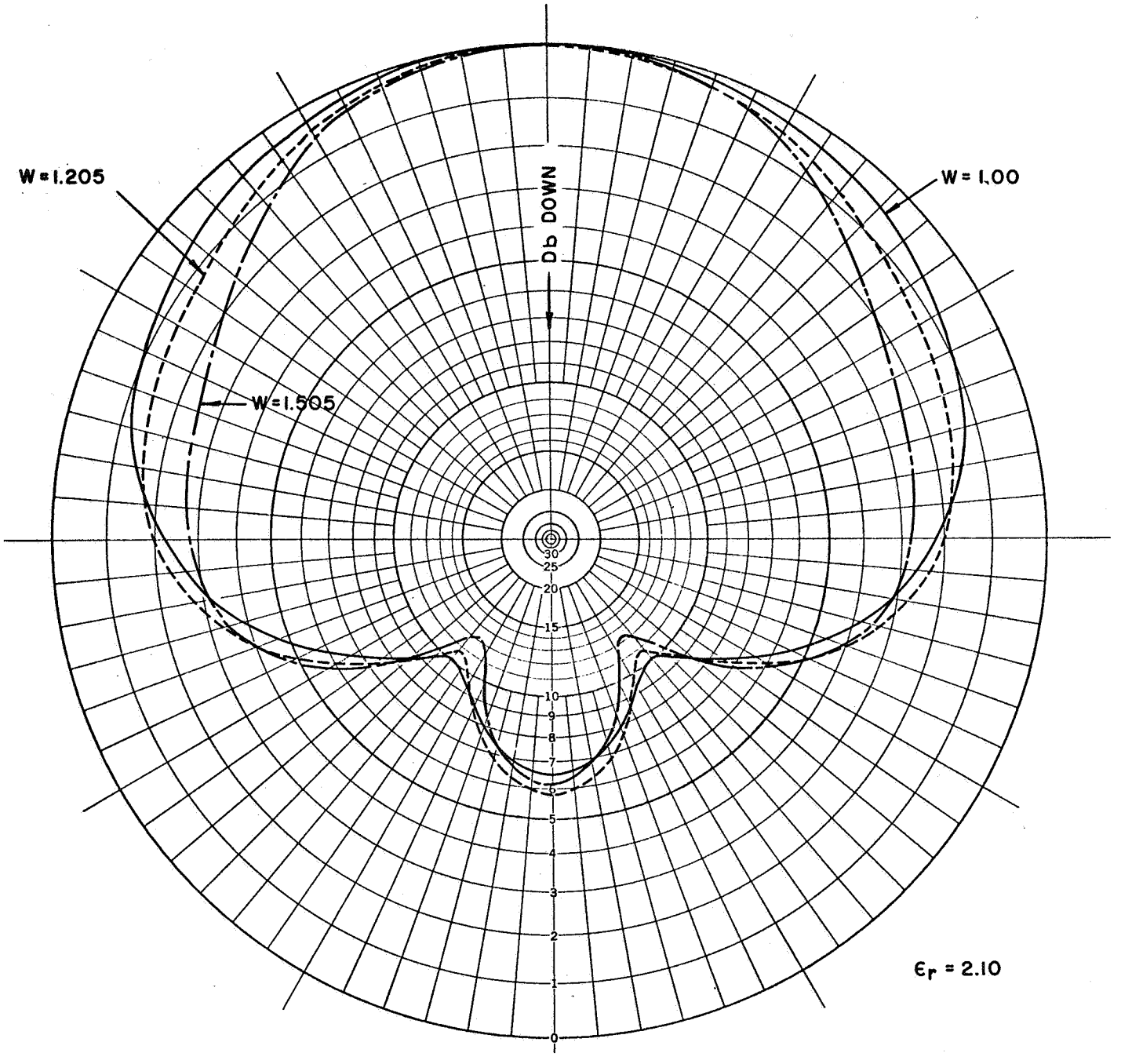

FIG. 18a COMPUTED EQUATORIAL PLANE RADIATION PATTERNS, C=1.405

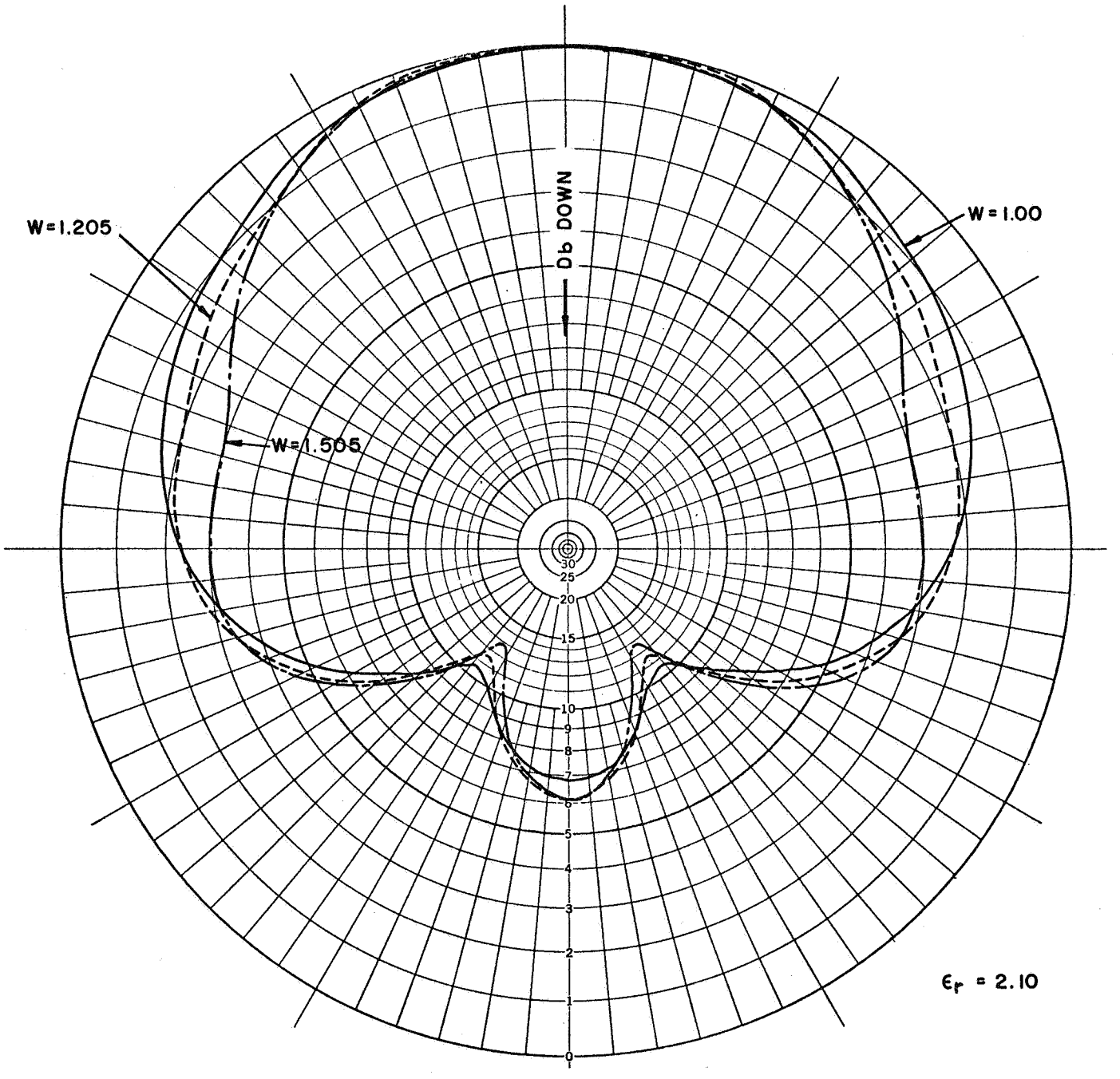

FIG. 18b COMPUTED EQUATORIAL PLANE RADITION PATTERNS, C= 1.50

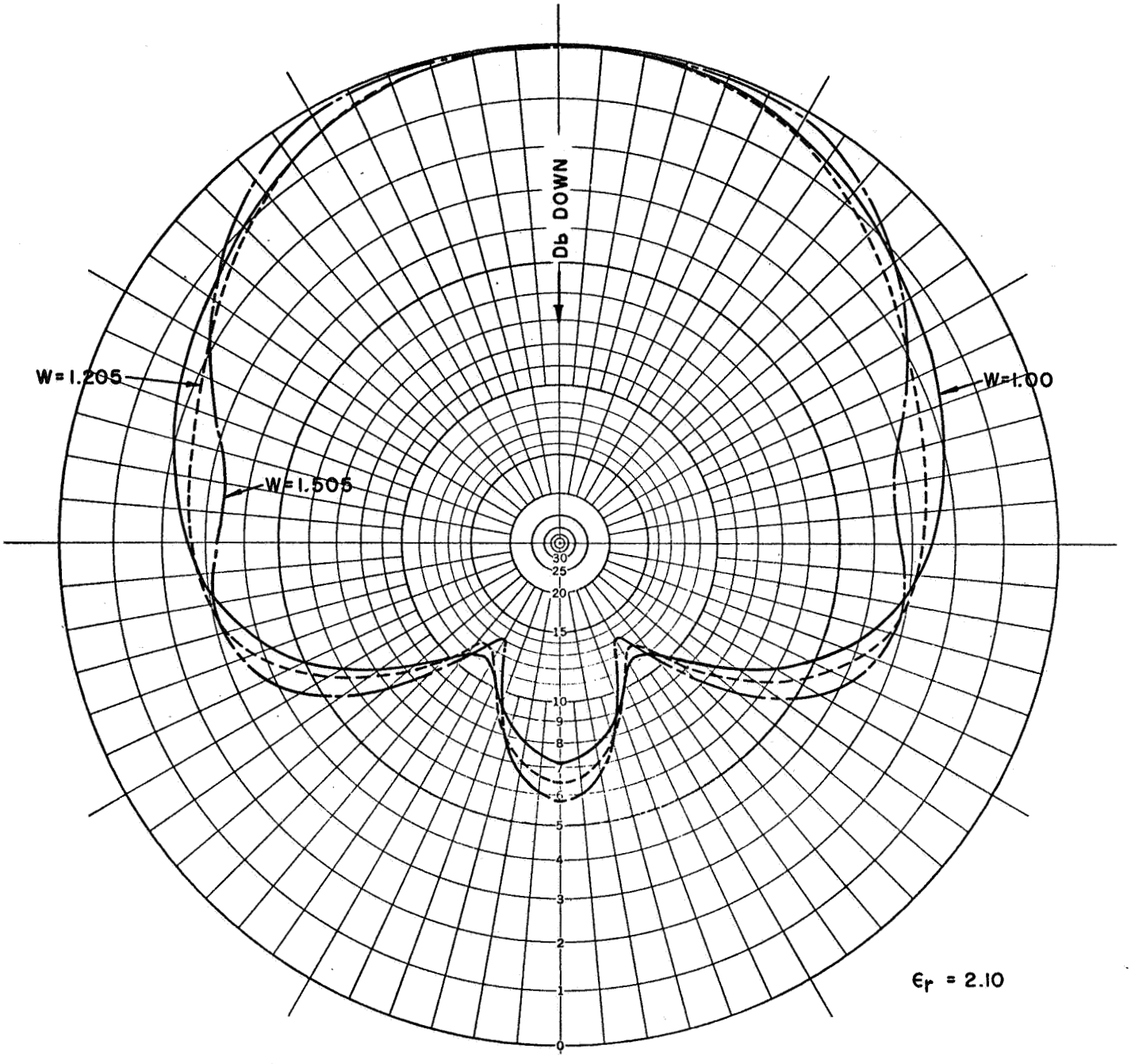

FIG. 18c COMPUTED EQUATORIAL PLANE RADIATION PATTERNS, C=1.635

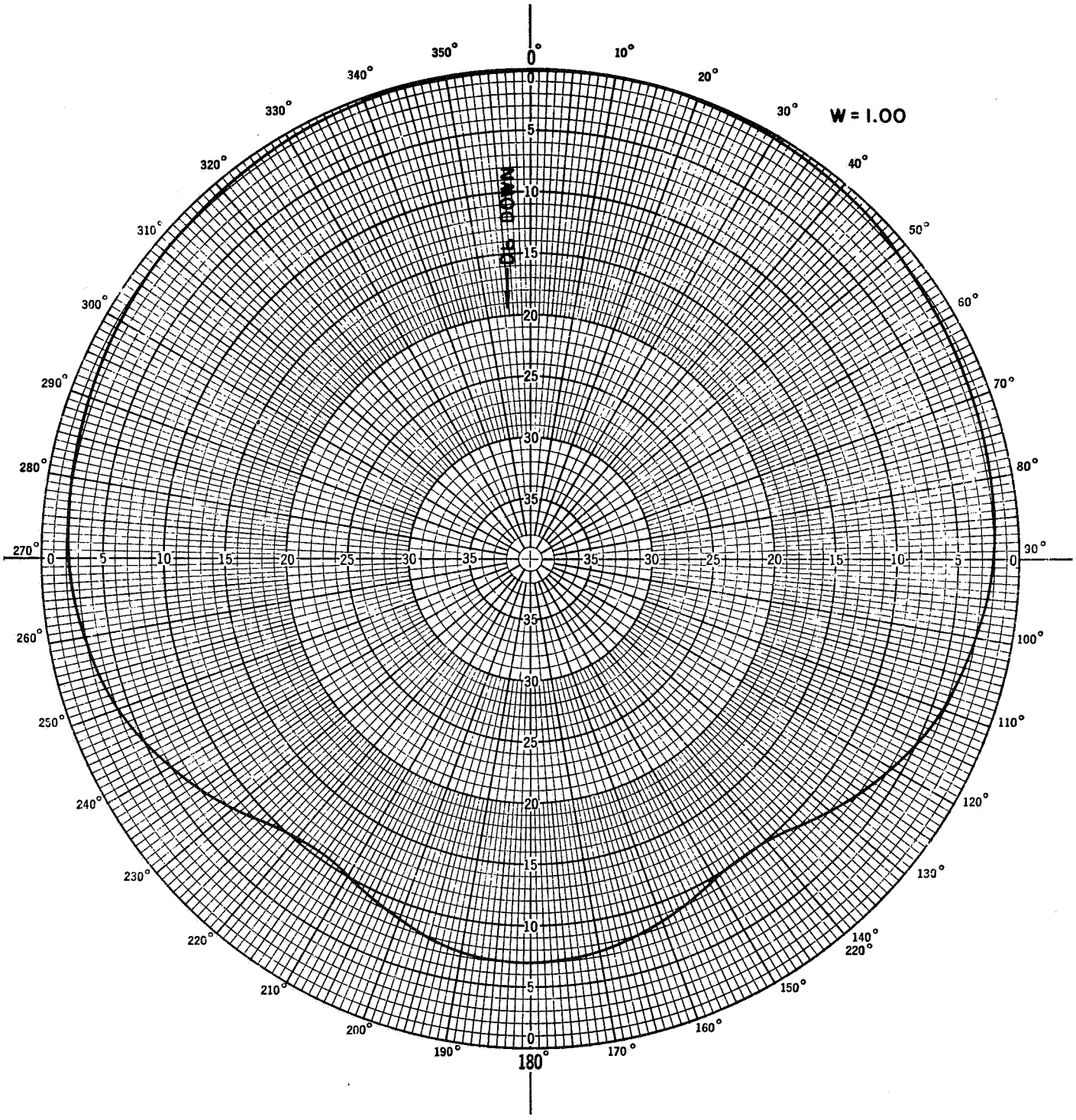

FIG. 19a MEASURED EQUATORIAL PLANE RADIATION PATTERN, C=1.50
NO COATING

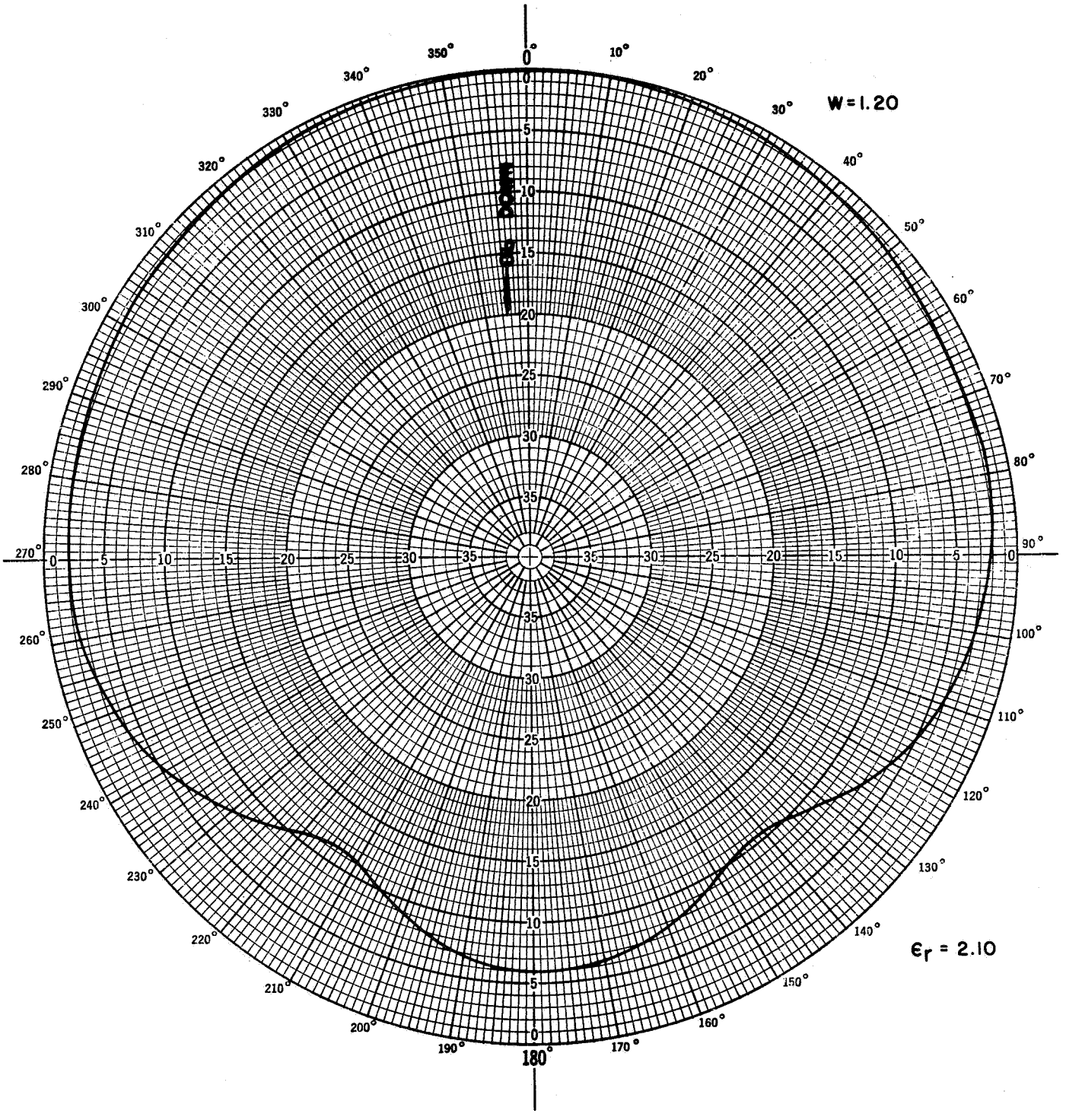

FIG. 19b MEASURED EQUATORIAL PLANE RADIATION PATTERN, C=1.50 TEFLON COATING

VIII. APPLICATION TO PLASMA DIAGNOSTICS

The basic idea for the pursuit of this work is to use the calibrated antenna as a diagnostic tool by measuring, essentially, the dielectric constant of the material coating the antenna. Thus, the antenna is to be used as a dielectrometer. In reentry plasma work, the dielectric coating is the plasma layer. For a homogeneous coating, using the theory and scattering matrix measurement scheme described above, one can prepare theoretical curves of both g_1 and/or b_1 (normalized values of coaxial line input conductance and susceptance, respectively) as a function of frequency with W and ε_r as parameters, as suggested in Fig. 20 for g_1. Here, for a specified known coating thickness (i.e., a known value of W, say W=1.20) theoretical curves of g_1 versus frequency for a given set of values of ε_r are prepared as in Fig. 20a. The increments taken in ε_r must be sufficiently small, so that one can then prepare a smooth curve of ε_r versus g_1 for a given frequency (say f=1.90 gc), as suggested in Fig. 20b. Thus, at a given frequency from a measured value of g_1, one can determine ε_r. This should be repeated for several frequencies to insure uniqueness. Thus, the axial slot-cylinder antenna can be used as a diagnostic tool. A photograph of the subject antenna shown in a carrying case with its associated calibrating moveable short circuit and Teflon rings is shown in Fig. 21.

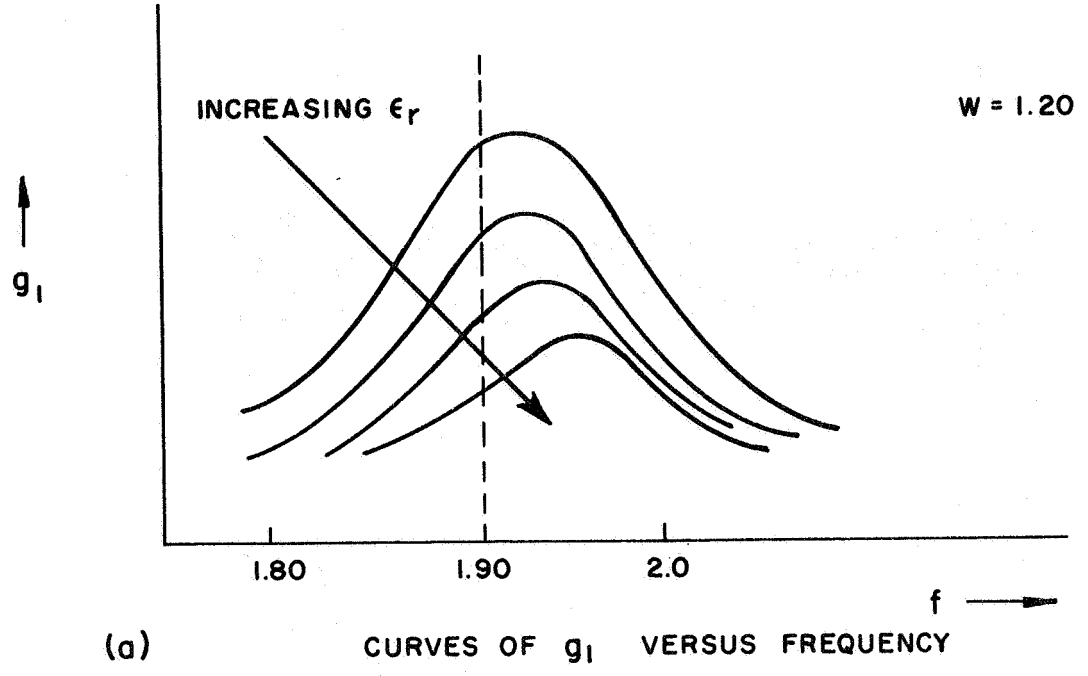

(a) CURVES OF g_1 VERSUS FREQUENCY

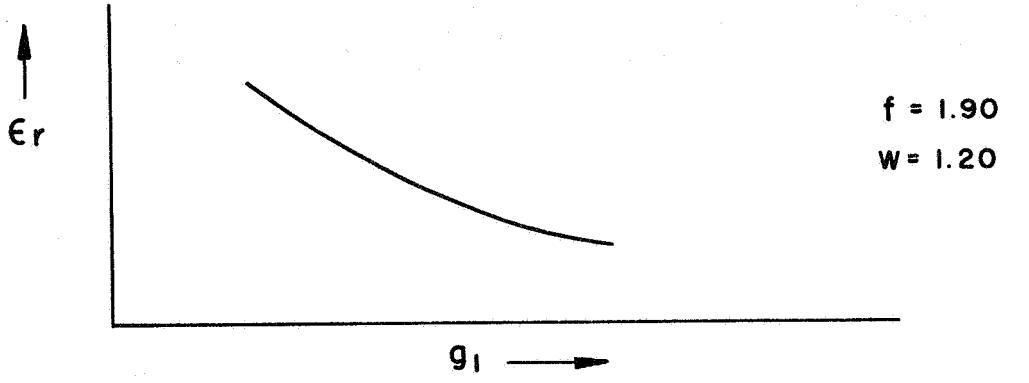

(b) CURVE OF ϵ_r VERSUS g_1

FIG. 20 SUGGESTED CURVES FOR DIELECTROMETER USE

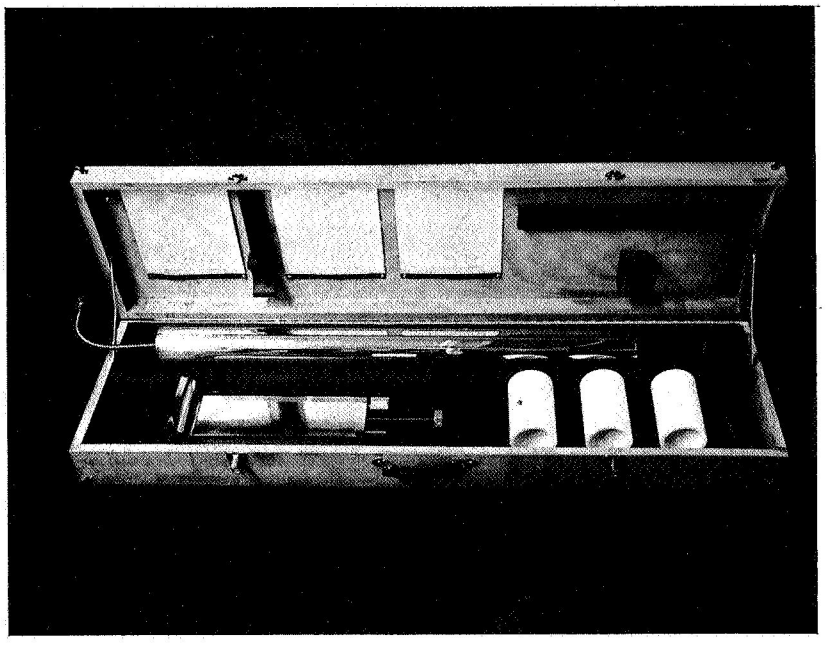

FIG. 21 - PHOTO OF DIAGNOSTIC AXIAL SLOT-CYLINDER ANTENNA AND CARRYING CASE

Of course, more realistic models of the plasma sheath should be used, but these, too, can, in principle, be diagnosed as above, since once the antenna is calibrated (i.e., the relation between y_1 and y_2 is known) one can use the work of Swift to obtain y_2 for a variety of non-homogeneous plasma distributions typifying reentry plasmas to obtain the corresponding value of y_1.

However, the basic first step in this work is to ascertain that the antenna is, indeed, properly calibrated. This could be done by preparing curves like that of Fig. 20 for, say a Teflon coating range of dielectric material, to see if the measurements would give $\varepsilon_r = 2.10$. Secondly, the next step would be to measure a homogeneous laboratory plasma sheath.

IX. CONCLUSIONS AND RECOMMENDATIONS

From the preceeding, the following conclusions and recommendations are made:

(1) The input admittance of a thin axial slot cylinder antenna, as measured in the coaxial line feeding the waveguide whose end forms this slot, can be predicted using the theory outlined in conjunction with the measured scattering matrix elements of the coaxial-slot network.

In particular, for any given frequency, the normalized input admittance in the coaxial line, y_1, can be predicted using (44) with (45) and the measured values of S_{11}, S_{12} and S_{22}, along with the theoretical value of Γ_2, as obtained from (46) using (22) to obtain y_{in} in terms of the normalized

external admittance, y_c, as given by Table I.

(2) Theoretical and measured values of this y_1 input admittance for the case of no coating agreed within 10 percent in conductance over approximately a 10 percent bandwidth (1.80 to 2.00 gc) and within 10 percent in susceptance over approximately a 2 percent bandwidth (1.945 to 1.980 gc), as shown in Figs. 12, 13 and 14.

(3) Measured values of this input admittance with a Teflon coating show that the frequency sensitivity of this admittance decreases with increasing coating thickness, as seen from Figs. 16 and 17. This suggests that perhaps such a coating be used between the cylinder and a plasma layer to be diagnosed to control the frequency dependence of the admittance.

(4) Due to the nature of the network (S_{11}, S_{12} and S_{22}) and the high value of reflection in the waveguide ($|\Gamma_2| \approx 1$) it is not meaningful to compare theoretical and measured values of admittance in the waveguide, since the errors are too large (as discussed in Appendix IX). It is, therefore, recommended that only measurements in the coaxial feed line (i.e., of y_1) be used to compare with theory. This observation is, in part, due to the desire to make the cylinder electrically small ($C \approx 1.5$). If a larger cylinder (say, $C \approx 6$) can be used, this problem could be overlooked, since then measurements of admittance could be made directly in the waveguide. However, as the cylinder becomes larger (C increasing), the previously noted problem, [10],

of extreme critical dependence of external admittance on the coating parameters exists.

(5) Computations of the normalized external conductance of the axial slot, g_c, with a Teflon (ε_r=2.10) coating indicate that it increases with coating thickness in the manner shown by Fig. 5.

(6) Since only computations of external conductance were made for the Teflon coating case, a comparison with theory could not be made, due to conclusion (4) above, and since a knowledge of external susceptance is also required to determine the coaxial line input admittance.

(7) Equatorial plane radiation patterns were measured and computed for both the non-coated and Teflon coated cases, and are in excellent agreement (Figs. 18 and 19).

(8) From the established ability to predict the antenna input admittance, suggestions for application to plasma diagnostics using the antenna as a dielectrometer are made in Section V-c and Section VIII. This could be supplemented by radiation pattern diagnostics.

(9) It is emphasized that the critical factor relating theoretical to measured values of coaxial line input admittance is the ability to measure the scattering matrix elements S_{11}, S_{12} and S_{22} accurately throughout the frequency range of interest. A smooth curve for these elements as a function of frequency should be obtained (see Figs. 9, 10 and 11).

(10) Throughout this work, the coating conditions were selected so that no axial surface waves could be excited. It is shown that no TM_o or EH modes can be excited on a dielectric coated metal cylinder by a thin axial slot, and that the dominant axial surface wave mode for such a slotted cylinder is the TE_o mode. The cutoff condition for this mode is given in Fig. 2.

If this mode or higher axial surface wave modes are excited, their contribution to the external conductance appears as a singularity contribution (since they only carry power down the axis of the cylinder), as can be evaluated by the method discussed in Appendix III.

(11) Azimuthal surface waves can and do exist on the axial slotted dielectric coated cylinder. The dominant azimuthal surface wave is a TM_o wave having a zero cutoff frequency, or, i.e., which for a finite frequency can exist even for an arbitrarily small coating thickness. However, the contribution these azimuthal surface waves make to the external conductance is automatically included in the integration, i.e., they do not appear as singularities, since the power associated with them ultimately appears as radiation.

(12) It is suggested that perhaps axial surface wave launching conditions also be examined as to suitability for plasma diagnostics and/or related antenna applications.

APPENDIX I

THE DIELECTRIC COATED METAL CYLINDER SURFACE WAVEGUIDE

Consider a metal cylinder (with no slots) concentrically coated with a homogeneous dielectric material of relative dielectric constant ε_r, as depicted in Fig. 1 of the text.

From Maxwell's equations, it follows that the pertinent field components which can exist are of the form (Region 1 $a \leq \rho \leq b$)

$$
\begin{aligned}
&(a)\ H_{z1} = A_m[J_m(u\rho)Y_m'(ua) - J_m'(ua)Y_m(u\rho)] \\
&(b)\ E_{z1} = C_m[J_m(u\rho)Y_m(ua) - J_m(ua)Y_m(u\rho)] \\
&(c)\ E_{\phi 1} = \frac{1}{u^2}\left\{ j\omega\mu_v u A_m[J_m'(u\rho)Y_m'(ua) - J_m'(ua)Y_m'(u\rho)] \right. \\
&\qquad \left. - \frac{mh}{\rho} C_m[J_m(u\rho)Y_m(ua) - J_m(ua)Y_m(u\rho)] \right\} \\
&(d)\ H_{\phi 1} = -\frac{1}{u^2}\left\{ \frac{mh}{\rho} A_m[J_m(u\rho)Y_m'(ua) - J_m'(ua)Y_m(u\rho)] \right. \\
&\qquad \left. + j\omega\varepsilon_v\varepsilon_r u\, C_m[J_m'(u\rho)Y_m(ua) - J_m(ua)Y_m'(u\rho)] \right\}
\end{aligned}
\tag{1}
$$

and Region 2, $b \leq \rho \leq \infty$

$$
\begin{aligned}
&(a)\ H_{z2} = A_m\bar{L}_m \frac{K_m(p\rho)}{K_m(pb)} \\
&(b)\ E_{z2} = -C_m\bar{V}_m \frac{K_m(p\rho)}{K_m(pb)} \\
&(c)\ E_{\phi 2} = -\frac{1}{p^2}\left\{ j\omega\mu_v p\bar{L}_m A_m \frac{K_m'(p\rho)}{K_m(pb)} + \frac{mh}{\rho} C_m\bar{V}_m \frac{K_m(p\rho)}{K_m(pb)} \right\} \\
&(d)\ H_{\phi 2} = \frac{1}{p^2}\left\{ \frac{mh}{\rho} A_m\bar{L}_m \frac{K_m(p\rho)}{K_m(pb)} - j\omega\varepsilon_v p C_m\bar{V}_m \frac{K_m'(p\rho)}{K_m(pb)} \right\}
\end{aligned}
\tag{2}
$$

where the factor $e^{j\omega t}e^{-jhz}e^{-jm\phi}$ is understood, and

$$u^2 = \beta_v{}^2\varepsilon_r - h^2, \quad u = +\beta_v\sqrt{\varepsilon_r - h^2/\beta_v{}^2}, \tag{3}$$

$$p^2 = h^2 - \beta_v{}^2, \quad p = +\sqrt{h^2-\beta_v{}^2}, \quad \beta_v \leq h \leq \beta_v\sqrt{\varepsilon_r} \tag{4}$$

$$\bar{L}_m = J_m(ub)Y_m'(ua) - J_m'(ua)Y_m(ub) \tag{5}$$

$$\bar{V}_m = J_m(ua)Y_m(ub) - J_m(ub)Y_m(ua) \tag{6}$$

and where A_m and C_m are arbitrary non-zero source constants, and prime denotes differentiation with respect to the entire argument, e.g., $K_m'(pb) = \left.\frac{dK_m(X)}{dx}\right|_{x=pb}$.

The above equations describe the axial and tangential fields of a particular (m^{th} mode) surface wave propagating down the z axis with a phase velocity, $v_p = \frac{\omega}{h}$, which falls in the range of $\frac{c}{\varepsilon_r} \leq v_p \leq c$, i.e., is a slow wave. At cutoff (p=0) the phase velocity becomes equal to c. The relationship which exists between the wave numbers p, h, and u is obtained by insisting that the circumferential boundary conditions at ρ=b be satisfied, i.e.,

$$\begin{cases} \text{(a)} \quad E_{\phi 1} = E_{\phi 2} \\ \\ \text{(b)} \quad H_{\phi 1} = H_{\phi 2} \end{cases} \qquad \text{at } \rho = b \tag{7}$$

since the other two tangential boundary conditions ($E_{z1}=E_{z2}$ and $H_{z1}=H_{z2}$ at ρ=b) are already satisfied by (1) and (2).

Using the two equations of (7) to eliminate A_m and C_m gives the transcendental equation

$$0 = p^2u^2\beta_v^2\left[\varepsilon_r p\bar{U}_m \frac{K_m}{K_m'} + u\bar{V}_m\right]\left[p\bar{T}_m \frac{K_m}{K_m'} + u\bar{L}_m\right] \qquad (8)$$

$$- \left(\frac{mh}{b}\right)^2 \beta_v^4 (\varepsilon_r - 1)^2 \bar{V}_m \bar{L}_m \left(\frac{K_m}{K_m'}\right)^2$$

as the equation relating p, u and h, which is seen to be equal to $d_m(y)$ of the text. It is this equation which must be satisfied to have fields of the form (1) and (2).

Cutoff Conditions

At cutoff (p=0) the factor $h \to \beta_v$ and $u \to \beta_v\sqrt{\varepsilon_r - 1}$, and

$$\lim_{p\to 0} \frac{K_m(pb)}{K_m'(pb)} \approx \left(-\frac{pb}{m}\right) + \Delta_m \qquad (9)$$

where Δ_m goes to zero faster than $(pb)^1$. Substitution of this relation into (8) and taking the limit gives the identity 0=0, which is true (since at cutoff the transcendental equation must be satisfied), but is not helpful for the general case of $m \geq 1$. However, for the case of m=0, one obtains:

Case of m=0

If one considers first the special case of m=0, the second term of (8) drops out, and (8) can then be satisfied by either, or both, of the following equations:

$$\frac{K_1(pb)}{(pb)K_0(pb)} = \frac{\varepsilon_r \bar{U}_0}{(ub)\bar{V}_0} \quad (TM_0 \text{ modes}) \qquad (10)$$

$$\frac{K_1(pb)}{(pb)K_0(pb)} = \frac{\bar{T}_0}{(ub)\bar{L}_0} \quad (TE_0 \text{ modes}) \qquad (11)$$

which are recognized [16] as the transcendental equations for the relatively well-known TM_o ($H_z=0$, m=0) and TE_o ($E_z=0$, m=0) axial surface wave modes, respectively. It is noted that, since each individually satisfy (8), that these modes can exist independently, i.e., alone, or together, which is not the case for $m\neq 0$, where both E_z and H_z must, in general, be finite and (8) for $m\neq 0$ must be satisfied.

Cutoff Conditions for the m=0 Modes

By letting p=0 in (10) and (11), one can obtain the cutoff conditions for the TM_o and TE_o modes, respectively. (Only the first (lowest order) mode for a given m will be found here and, hence, no second subscript after the first subscript will be used.)

First TM_o Mode Cutoff Condition

For p=0, the L.H.S. of (10) becomes positively infinite; inspection of the R.H.S. of (10) shows that (using small argument approximations, for the Bessel and Neumann functions, as given in Appendix II),

$$\lim_{C\sqrt{\varepsilon_r-1}\to 0} \left.\frac{\varepsilon_r \bar{U}_o}{(ub)\bar{V}_o}\right|_{p=0} = \frac{\varepsilon_r}{(CW)^2(\varepsilon_r-1)\log W} \qquad (12)$$

which also approaches positive infinity; hence, the first root of (10) occurs for C=0, $\varepsilon_r=1$, or W=1. That is, the cutoff condition for the dominant TM_o mode is zero cutoff

frequency for a specified W and ε_r; zero thickness (W=1) for a specified frequency and ε_r, or a dielectric constant of ϵ_r=1 for a specified frequency and coating thickness. This is the well known result for this Goubau line mode [16].

Cutoff Conditions for the First TE_o Mode

If p=0, the L.H.S. of (11) becomes positively infinite; inspection of the R.H.S. of (11) shows that

$$\lim_{CW\sqrt{\varepsilon_r-1} \to 0} \left. \frac{\bar{T}_o}{(ub)\bar{L}_o} \right|_{p=0} = -\frac{1}{2}\left(1 - \frac{1}{W^2}\right) \tag{13}$$

Hence, it is bounded for all W and thus the TE_o mode does not have a zero cutoff frequency. Inspection of $\bar{T}_o/ub$ shows that it is bounded for finite $C\sqrt{\varepsilon_r-1}$ and, hence, the only way the R.H.S. of (11) can become infinite is for the $\bar{L}_o$ term to vanish at p=0, i.e., the cutoff condition for the TE_o modes are

$$\left. \bar{L}_o \right|_{p=0} = 0 = J_o(CW\sqrt{\varepsilon_r-1})\,Y_o'(C\sqrt{\varepsilon_r-1}) - J_o'(C\sqrt{\varepsilon_r-1})\,Y_o(CW\sqrt{\varepsilon_r-1}) \tag{14}$$

The first root of (14) has been found in the text, and is plotted in Fig. 2 of the text.

Cutoff Condition for Hybrid Modes

For $m \geq 1$ the modes that can exist are hybrid modes; i.e., both E_z and H_z will be finite and dependent on one another. This dependence comes about becuase for $m \geq 1$, C_m and A_m are related by (via (1d) and (2d) with (6b))

$$C_m = \frac{A_m \left(\frac{mh}{b}\right) \bar{L}_m \, \omega\mu_v(\epsilon_r - 1)}{jpu \left[p\epsilon_r \bar{U}_m + u\bar{V}_m \frac{K_m'}{K_m} \right]} \tag{15}$$

and, hence, if A_m is finite, C_m, too, will, in general, be finite. Thus, from (1) and (2), both H_z and E_z will be finite. (It is noted that if m=0, C_m and A_m are not dependent; allowing m=0 in (15) would give $C_o=0$ for $A_o \neq 0$ only if the denominator were finite, but the denominator must vanish, since the term $p\epsilon_r \bar{U}_m + u\bar{V}_m \frac{K_o'}{K_o} = 0$ is the TM_o mode equation. Thus, both A_o and C_o can be finite and are independent for m=0.)

As mentioned earlier, the substitution of p=0 into the transcendental equation (8) for $m \geq 1$ leads to the identity of 0=0. To obtain the cutoff roots for the hybrid modes is, apparently, somewhat more involved. Recently, Savard [17] has obtained the cutoff equations as (using the notation of this report)

$$\begin{cases} EH & \bar{V}_m \Big|_{p=0} = 0 \\ HE & \bar{L}_m \Big|_{p=0} = 0 \end{cases} \tag{16}$$

and additionally, has shown that the first hybrid EH_1 mode, like the TM_o, has, for a given ε_r and W a cutoff frequency of zero, or a coating thickness of zero (W=1) for a given C and ε_r, or an ε_r=1 for a given C and W (i.e., $C\sqrt{\varepsilon_r-1}=0$ and/or a W=1).

His method will not be given here, but an appeal to physical intuition will be given to support his results, as follows:

EH Mode Cutoff Condition

It is known that for TM (and similarly for the TM portion of a hybrid mode) modes the surface impedance looking down into the dielectric surface must be inductive, and at cutoff (p=0) it vanishes. This impedance for an EH mode is $E_{z1}/H_{\phi 1}\Big|_{\substack{\rho=b\\p=0}}$. This can vanish only if $E_{z1}\Big|_{\substack{\rho=b\\p=0}}$ vanishes, since H_{ϕ_1} is always bounded. From either (1b) or (2b), since $C_m\neq 0$, it then follows that the hybrid EH mode cutoff condition must be:

$$\bar{V}_m\Big|_{p=0}=0=J_m(C\sqrt{\varepsilon_r-1})Y_m(CW\sqrt{\varepsilon_r-1})-J_m(CW\sqrt{\varepsilon_r-1})Y_m(C\sqrt{\varepsilon_r-1}). \quad (17)$$

HE Mode Cutoff

In a similar way, at cutoff the surface impedance presented by the surface to the TE component of a hybrid HE mode must be an infinite capacitive reactance, i.e.,

$$\left.\frac{E_{\phi 1}}{H_{z1}}\right|_{\substack{\rho=b\\p=0}} = -j\infty \quad (18)$$

Since $E_{\phi 1}$ must be bounded, it follows that H_{z1} must vanish; from (1a) or (2a) one then obtains, since $A_m \neq 0$, the hybrid EH mode cutoff condition as

$$\bar{L}_m \Big|_{p=0} = 0 = J_m(CW\sqrt{\varepsilon_r - 1})\, Y_m'(C\sqrt{\varepsilon_r - 1}) - J_m'(C\sqrt{\varepsilon_r - 1})\, Y_m(CW\sqrt{\varepsilon_r - 1}), \quad (19)$$

which agree with Savard [17].

The cutoff conditions for the EH modes (i.e., (17)) were not found in this report, since, like the TM modes, these modes cannot be excited, despite their cutoff frequency, by a thin axial slot, as shown in the text.

It is interesting to note that Savard correctly points out that numerical errors were made by Hersch [18] in obtaining the cutoff conditions for the hybrid surface wave modes, and the statement made in Barlow and Brown [19] concerning his work is also incorrect. The correct conditions are as given above.

APPENDIX II

SMALL ARGUMENT APPROXIMATIONS FOR BESSEL-NEUMANN TYPE FUNCTIONS

Using the small argument approximations [20] for the Bessel and Neumann functions of (for $m \geq 1$)

$$J_m(X) \approx \frac{1}{2^m m!} X^m \tag{1}$$

$$J_m'(X) \approx \frac{1}{2^m (m-1)!} X^{m-1} \tag{2}$$

$$Y_m(X) \approx -\frac{2^m (m-1)!\ X^{-m}}{\pi} \tag{3}$$

$$Y_m'(X) \approx \frac{2^m m!\ X^{-(m+1)}}{\pi} \tag{4}$$

and (for m=0) of

$$J_o(X) \approx 1 - \frac{X^2}{4} \approx 1 \tag{5}$$

$$J_o'(X) \approx \frac{-X}{2} \tag{6}$$

$$Y_o(X) \approx \frac{2}{\pi} \log X \tag{7}$$

$$Y_o'(X) \approx \frac{2}{\pi X} \tag{8}$$

cause the $\bar{V}_m$, $\bar{U}_m$, $\bar{T}_m$, and $\bar{L}_m$ functions to become for $C\sqrt{\epsilon_r - 1} \to 0$ and p=0 for m=0:

$$\bar{V}_o = \frac{2}{\pi} \log W \tag{9}$$

$$\bar{U}_o = \frac{2}{\pi C W \sqrt{\varepsilon_r - 1}} \tag{10}$$

$$\bar{T}_o = -\frac{1}{\pi}\left(W - \frac{1}{W}\right) \tag{11}$$

$$\bar{L}_o = \frac{2}{\pi C \sqrt{\varepsilon_r - 1}} \tag{12}$$

and for $m \geq 1$

$$\bar{V}_m = \frac{1}{m\pi}\left(W^m - \frac{1}{W^m}\right) \tag{13}$$

$$\bar{U}_m = \frac{1}{\pi C \sqrt{\varepsilon_r - 1}}\left(\frac{1}{W^{m+1}} + W^{m-1}\right) \tag{14}$$

$$\bar{T}_m = \frac{m}{\pi C^2 (\varepsilon_r - 1)}\left(W^{m-1} - \frac{1}{W^{m+1}}\right) \tag{15}$$

$$\bar{L}_m = \frac{1}{\pi C \sqrt{\varepsilon_r - 1}}\left(W^m + \frac{1}{W^m}\right) \tag{16}$$

APPENDIX III

CONTRIBUTION TO CONDUCTANCE DUE TO AXIAL SURFACE WAVES

Equation (10) of the text gives the total external conductance, as seen at the cylinder-slot interface, as an integration over real normalized mode space, y, from $0 \leq y \leq \infty$. The possibility exists that a singularity (or singularities) exist in this region of integration. In particular, in the region $1 \leq y \leq \sqrt{\epsilon_r}$, corresponding to axially slow waves, singularities may exist; if they do, they correspond to axial surface waves of discrete mode numbers, u, h, in the dielectric and p, h, in the air region, respectively, where the first wave number is that in the radial direction and the second that in the axial direction, with $\beta_v \leq h \leq \beta_v \sqrt{\epsilon_r}$. Whether or not such a wave can exist has been found in the text by determining the singularity points, i.e., the cutoff conditions. Even though the coating-frequency conditions in this work were chosen such as to operate below cutoff of the dominant TE_o mode of the axially slotted dielectric coated cylinder so that no surface waves were excited, this appendix will outline a method to obtain the surface wave conductance contribution to the total conductance of a surface wave, if excited, for future use.

Consider the case where a single (say, for the dominant TE_o mode, i.e., m=0 - first root) singularity, y_o, exists, somewhere between $1 \leq y_o \leq \sqrt{\epsilon_r}$, as shown in Fig. III-1. In this event, the path of integration can be indented in the form

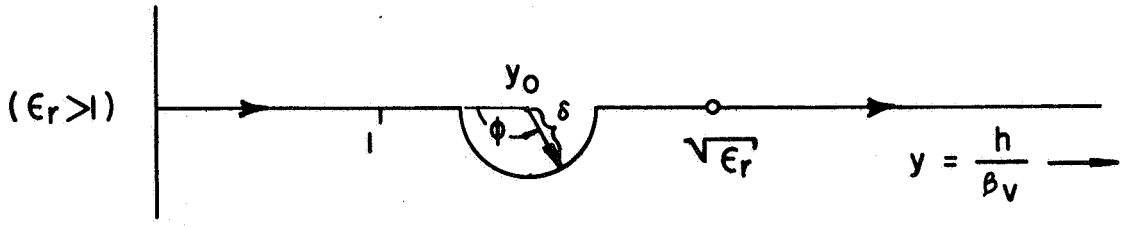

FIG. III – 1 PATH OF INTEGRATION IN COMPLEX y PLANE

of a small circle of radius δ about y_o (on the negative imaginary side so as to preserve the bounded outgoing wave criteria) then (10) of the text can be written (symbolically) as

$$y_c = \int_o^\infty = \lim_{\delta \to 0}\left[\int_o^1 + \int_1^{y_o-\delta} + \int_{y_o+\delta}^\infty + \oint\right] \tag{1}$$

where the last integration is that over the semi-circle about y_o. Now, if the integrand of (10) of the text (call it $f_o(y)$, has a simple pole at y_o, i.e., is of the form

$$f_o(y) = \frac{R_o(y_o)}{(y-y_o)} + \phi(y) \tag{2}$$

where $R_o(y_o)$ is the residue at y_o, and $\phi(y)$ is analytic and bounded in the neighborhood of y_o; then, since on the semi-circle $y=y_o+\delta e^{j\phi}$, $o \leq \phi \leq \pi$, so that

$$\lim_{\delta \to 0} \oint = \lim_{\delta \to 0} \int_{-o}^{\pi} f_o(y) j\delta e^{j\phi} d\phi = jR_o\pi \tag{3}$$

Thus, (1) becomes

$$y_c = \int_o^\infty + jR_o\pi \tag{4}$$

But, for a simple pole, the residue R_o is given by [21]

$$R_o = \left. \frac{\text{numerator of } f_o(y)}{\text{derivative of denominator of } f_o(y) \text{ with respect to } y} \right|_{y=y_o} \tag{5}$$

Here, $f_o(y)$ is given by (10) of the text with m=0; hence,

$$R_o = \left. \frac{j2(\beta_v \ell)^{-2} C^{-1} \cos^2\left(\frac{\beta_v \ell}{2} y\right) \left[p\bar{U}_o \frac{K_o}{K_o'} + u\bar{V}_o\right] \left[y^2 - \left(\frac{\pi}{\beta_v \ell}\right)^2\right]^{-2} \sqrt{N^2 - y^2}}{\frac{d}{dy}\left[p\,\bar{T}_o \frac{K_o}{K_o'} + u\bar{L}_o\right]} \right|_{y=y_o} \tag{6}$$

Thus, from (4),

$$y_c = g_{swo} + \int_o^\infty \tag{7}$$

where g_{swo} is the contribution to y_c due to the residue at y_o (we note this contribution is purely real) given by

$$g_{swo} = \frac{2\pi\sqrt{\varepsilon_r - y_o^2}\left\{\cos^2\left[\frac{C}{2}\left(\frac{\ell}{a}\right) y_o\right]\right\}}{C^3\left(\frac{\ell}{a}\right)^2\left[y_o^2 - \frac{\pi^2}{C^2\left(\frac{\ell}{a}\right)^2}\right]^2} \cdot \tag{8}$$

$$\cdot \frac{\left[\sqrt{y_o^2 - 1}\,\bar{U}_o \frac{K_o}{K_1} - \sqrt{\varepsilon_r - y_o^2}\,\bar{V}_o\right]\Big|_{y=y_o}}{d_o'(y_o)}$$

where

$$d_o'(y_o) = \frac{d}{dy}\left[-p\,\bar{T}_o \frac{K_o}{K_1} + u\bar{L}_o\right]\Bigg|_{y=y_o} \tag{9}$$

Equation (8) is ready to be computed once y_o is found. It is noted that a plot of $d_o(y)$ versus y in the range $1 \leq y \leq \varepsilon_r$ could be used to determine y_o and would look something like Fig. III-2. If drawin sufficiently accurate, the term $d_o'(y_o)$ could be obtained directly from the plot.

Thus, g_{swo} can be found. If more than one axial surface wave can exist (as can be determined from the cutoff conditions given in the text), then the above procedure would have to be repeated for each such wave (assuming each pole wave a simple pole).

As noted earlier, throughout this work the coating conditions and frequency were chosen such that no axial surface waves could exist, i.e., here no y_o exists and, therefore, here

$$g_{swo} = 0. \tag{10}$$

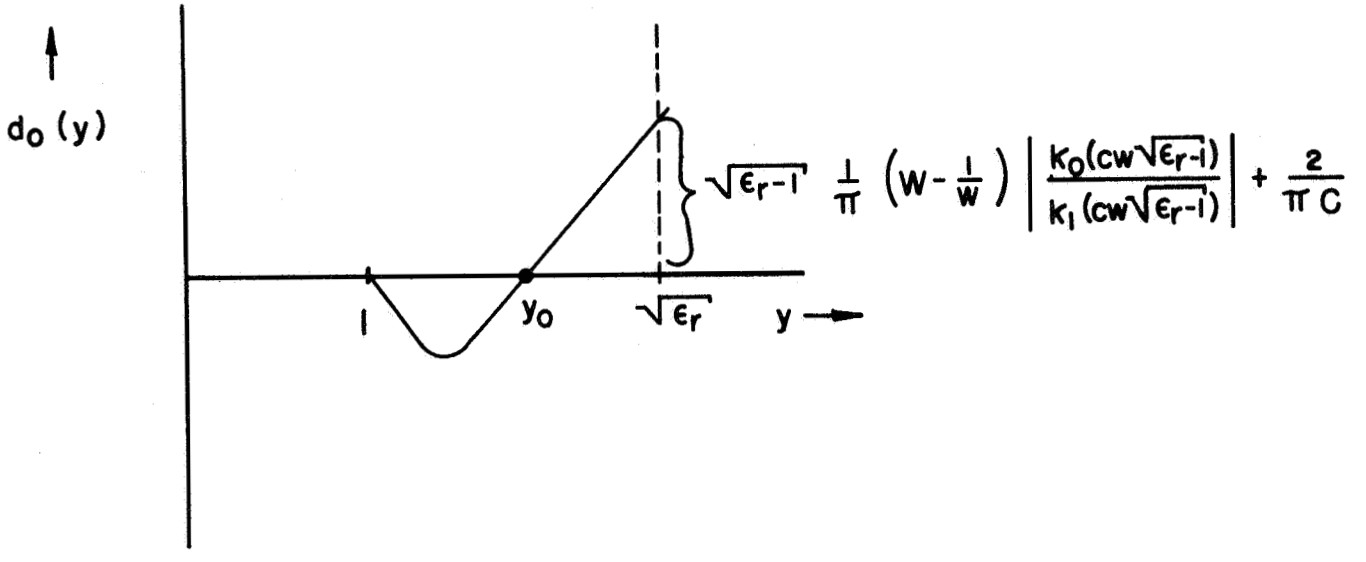

FIG. III-2 ROUGH PLOT OF $d_o(y)$

APPENDIX IV

MANUAL COMPUTATION OF EXTERNAL ADMITTANCE - NO COATING

The external admittance, denoted by y_{cv}, is given by

$$y_{cv} = g_{cv} + j\, b_{cv} \tag{1}$$

where g_{cv}, the external conductance, and b_{cv}, the external susceptance, are given by (XIX) and (XXI) of Table I of the text, respectively.

To serve as a check on the computer results, the case for C=1.50 was manually computed* using Tables [5,22].

The resulting manually computed integrals of equations (XX), (XXII) and (XXIII) of Table I, i.e., the integrands of I_{mg}, I_{1m} and I_{2m} are plotted in Figs. IV-1, IV-3 and IV-5, respectively. The integrations (i.e., the computation of the area under a given value of m curve) of I_{mg}, I_{1m} and I_{2m} were performed using these plots with a planometer and are tabulated in Table IV-1 and plotted in Figs. IV-2, IV-4, IV-6, respectively. It is noted from either the plots or Table IV-1, that the convergence of the conductance integral-summation is much faster than that for the susceptance integral-summation; the conductance computation required only four terms in the sum (m=0,1,2,3), whereas the susceptance computations required 36 terms (although 36 were actually

*In this computation, the values of Bessel functions required were obtained using a computer, and the references sited were used to check these values.

TABLE IV-1

CALCULATED VALUES OF

I_{mg}, I_{1m} AND I_{2m} INTEGRANDS

m	$a_m/(1+\delta_o^m)$	$+I_{mg}$	$\frac{a_m I_{mg}}{(1+\delta_o^m)}$	I_{1m}	I_{2m}	$I_{1m}-I_{2m}$	$\frac{a_m(I_{1m}-I_{2m})}{(1+\delta_o^m)}$
0	0.5	2.305	1.152	-0.303	+0.3258	0.6288	-0.3144
1	0.9888	2.342	2.316	-0.271	-0.566	0.2950	+0.2917
2	0.9901	1.039	1.029	-0.220	-0.984	0.7640	0.7564
3	0.9786	0.059	0.058	-0.184	-0.616	0.432	0.4227
4	0.9627			-0.153	-0.409	0.256	0.2464
5	0.9172			-0.133	-0.3195	0.1865	0.1711
6	0.9174			-0.116	-0.262	0.146	0.1339
7	0.8887			-0.102	-0.2215	0.1195	0.1062
8	0.8571			-0.092	-0.1945	0.1025	0.0875
9	0.8219			-0.087	-0.1711	0.0841	0.06912
10	0.7840			-0.089	-0.1565	0.0675	0.05292
11	0.74394			-0.073	-0.1371	0.0641	0.04768
12	0.7019			-0.0685	-0.1273	0.0588	0.04127
13	0.6581			-0.065	-0.1203	0.0553	0.03639
14	0.61332			-0.060	-0.1101	0.0501	0.03073
15	0.5679			-0.056	-0.1023	0.0463	0.02629
16	0.5224			-0.053	-0.0956	0.0426	0.02225
17	0.4471			-0.050	-0.0900	0.0400	0.01788
18	0.4324			-0.048	-0.0832	0.0352	0.01522
19	0.3887			-0.046	-0.0803	0.0343	0.01333
20	0.3464			-0.0432	-0.0750	0.0318	0.01105
21	0.3058			-0.041	-0.072	0.0310	0.009479
22	0.2672			-0.0383	-0.0692	0.0309	0.008256
23	0.2309			-0.037	-0.065	0.028	0.006465
24	0.1970			-0.035	-0.063	0.028	0.005516
25	0.1657			-0.034	-0.060	0.026	0.004308
26	0.1371			-0.032	-0.059	0.027	0.003701
27	0.1114			-0.031	-0.0506	0.0196	0.002183
28	0.0885			-0.029	-0.0504	0.0214	0.00189
29	0.0685			-0.028	-0.0502	0.0222	0.00152
30	0.0513			-0.027	-0.0500	0.0230	0.00118
31	0.0369			-0.0255	-0.049	0.0235	0.000867
32	0.0251			-0.024	-0.048	0.024	0.000602
33	0.0196			-0.0215	-0.047	0.0255	0.0004998
34	0.0040			-0.02	-0.0465	0.0265	0.000106
35	0.0012			-0.019	-0.046	0.027	0.0000324
SUM			4.5555				+2.652

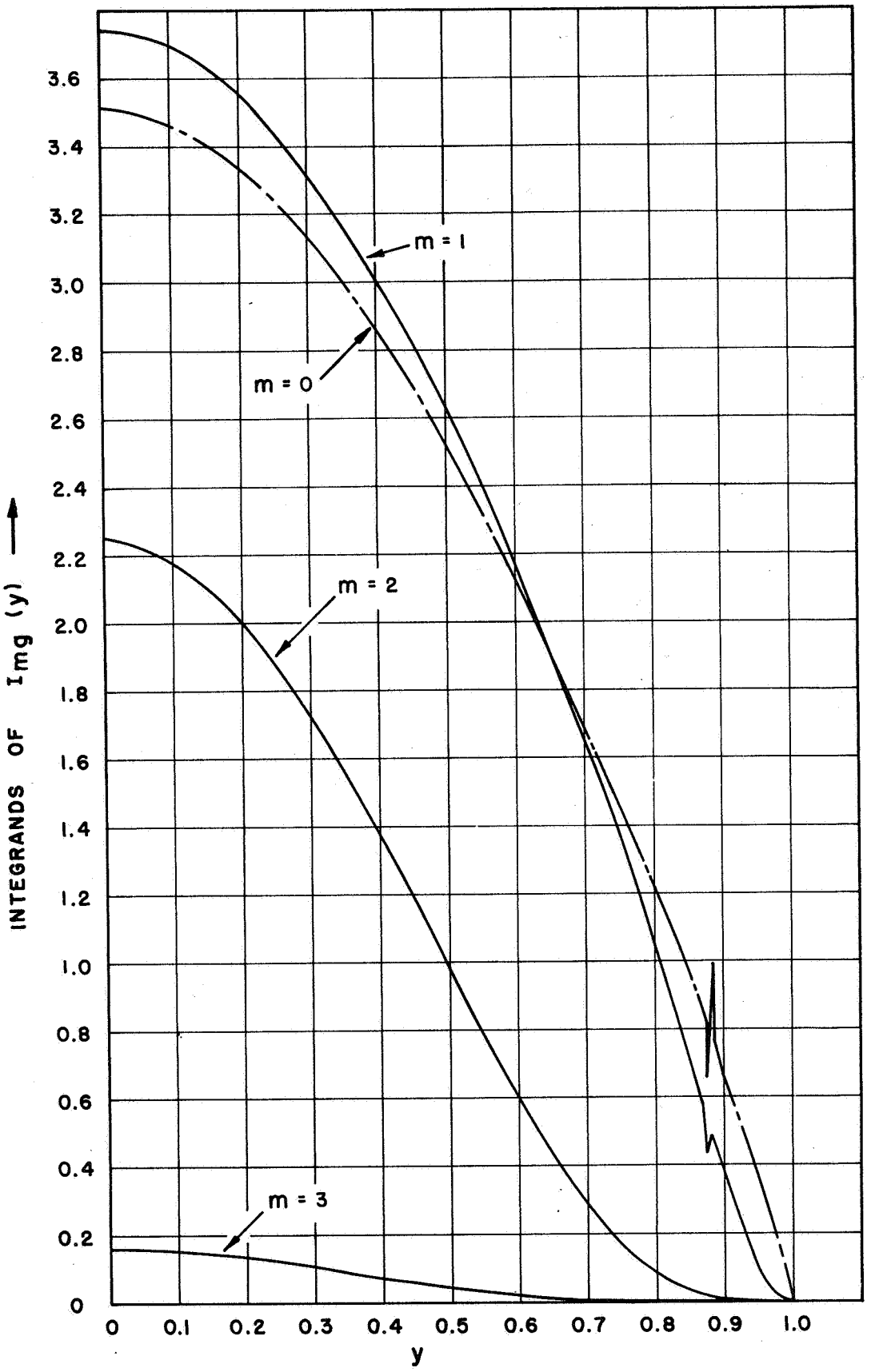

FIG. IV-1 CONDUCTANCE INTEGRANDS OF I_{mg}

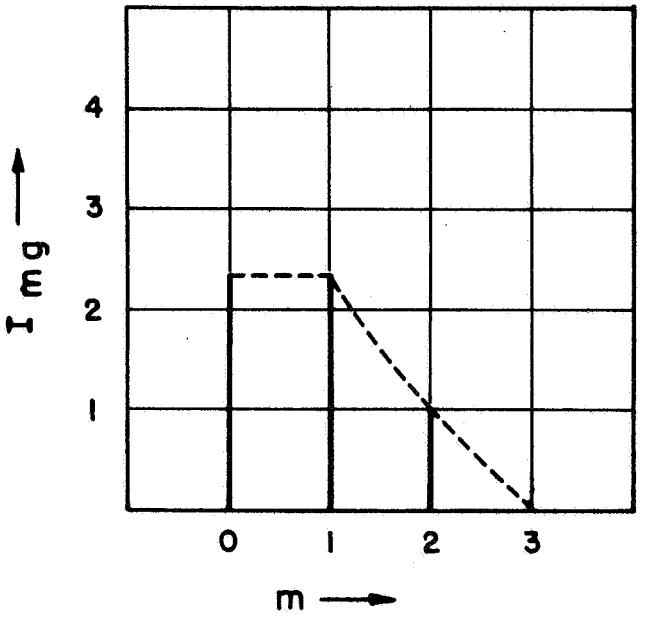

FIG. IV-2 DEPENDENCE OF I_{mg} ON m

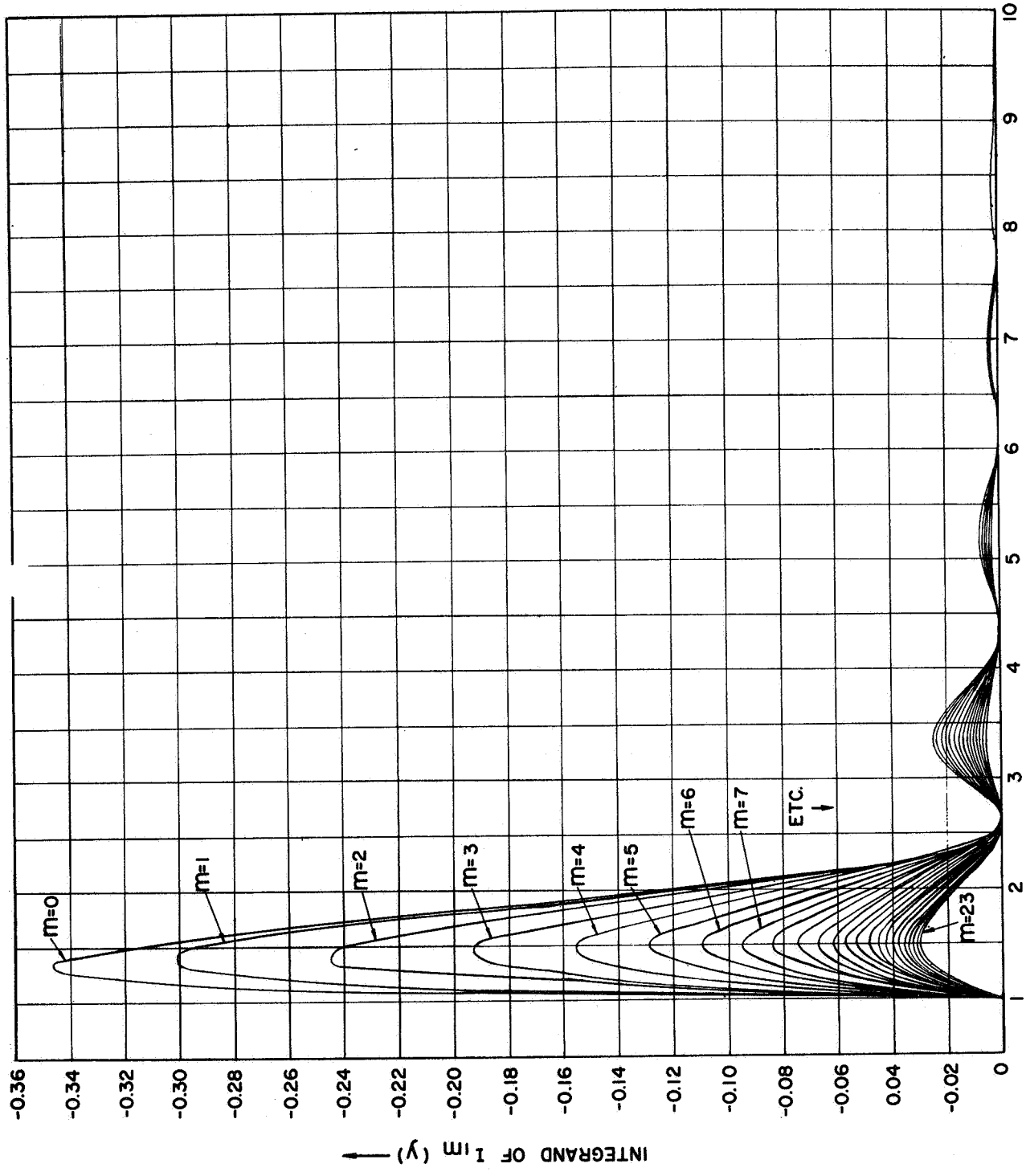

FIG. IV-3 SUCEPTANCE INTEGRANDS OF I_{1m}

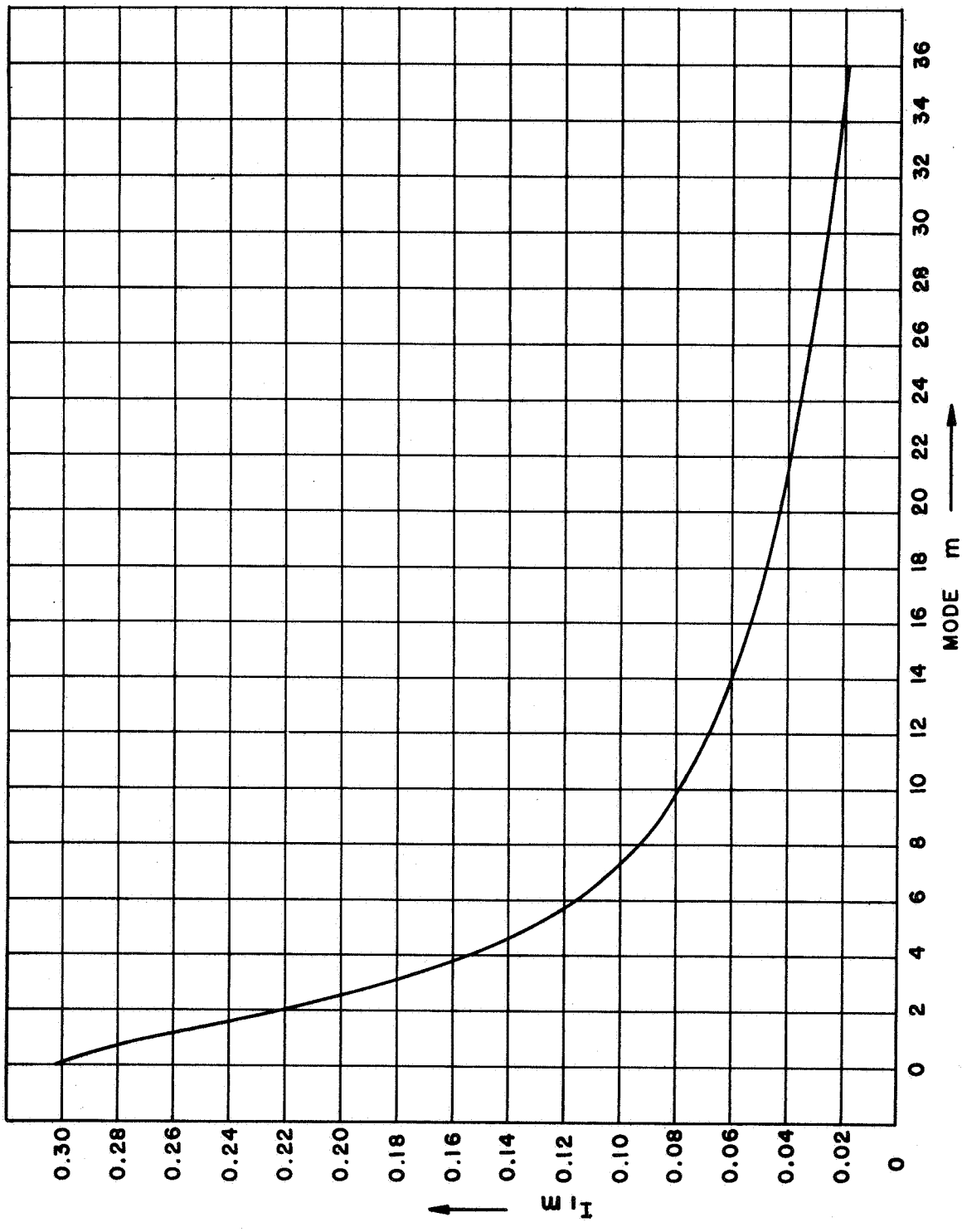

FIG. IV-4 DEPENDANCE OF I_{1m} ON m

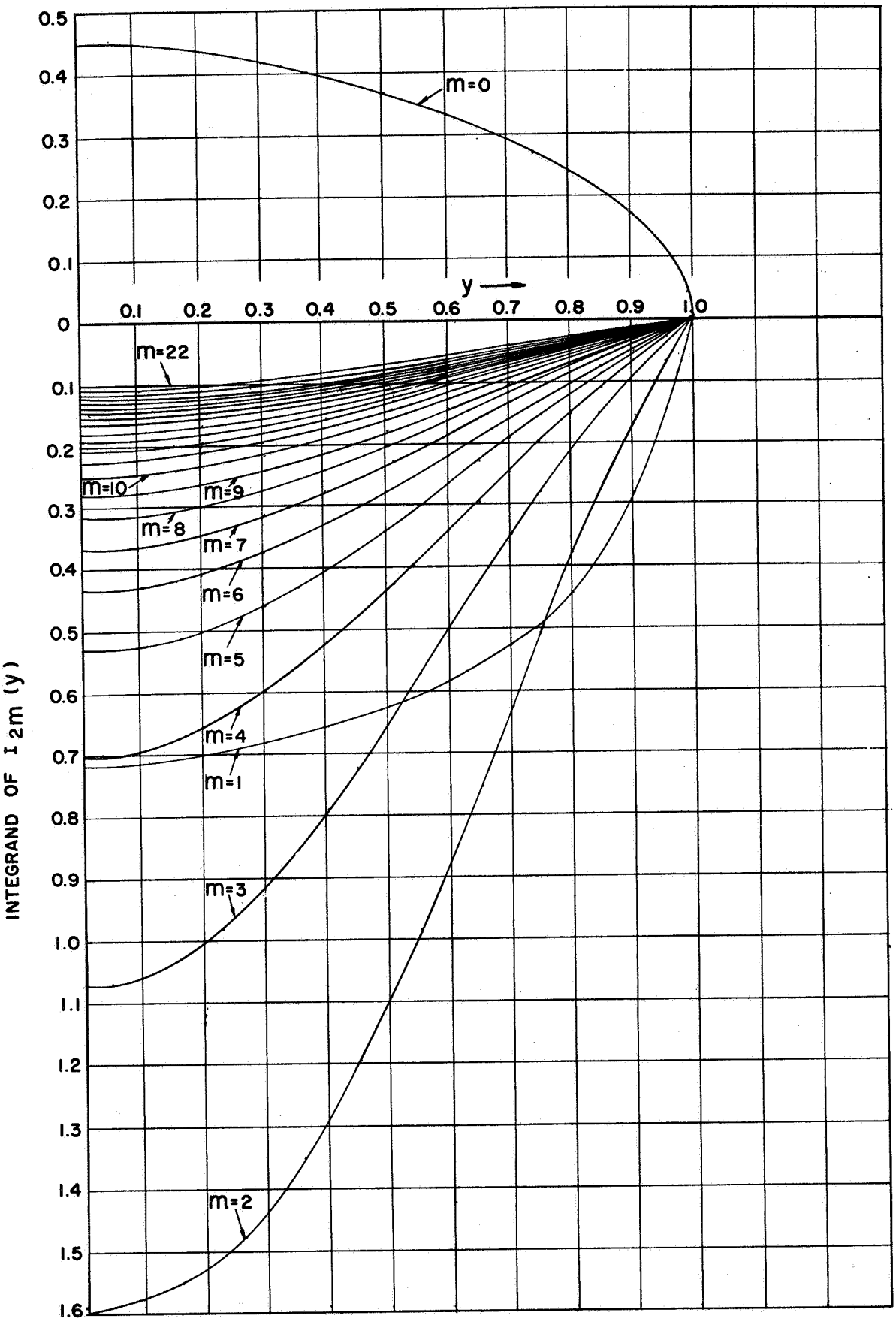

FIG. Ⅳ-5 SUCEPTANCE INTEGRANDS OF I_{2m}

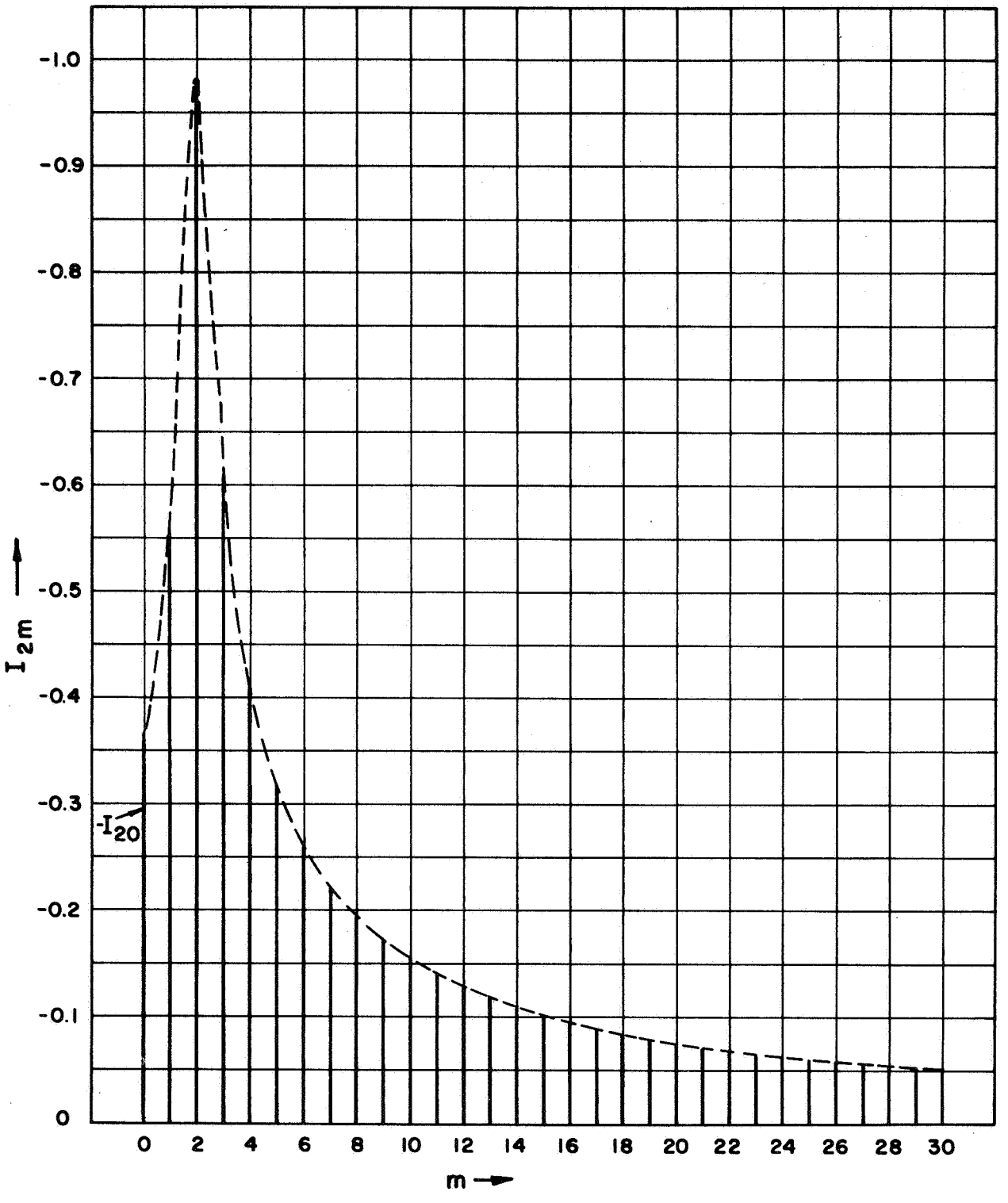

FIG. IV-6 DEPENDENCE OF I_{2m} ON m

computed, as indicated in Table IV-1, not all the plots are shown, for clarity, since, as seen from Table IV-1, all the terms beyond 24 only change b_{cv} by approximately 2 parts in 265) for three significant figure accuracy in each.

The summing of all terms to give g_{cv} and b_{cv} then give (also indicated in Table IV-1)

$$g_{cv}\Big|_{\substack{C=1.50\\(\text{four terms})}} = \frac{8}{\pi C^4 \left(\frac{\ell}{a}\right)^2}\,(4.555) = (0.0882)(4.555) = 0.4017 \quad (1)$$

$$b_{cv}\Big|_{\substack{C=1.50\\(36\ \text{terms})}} = \frac{4}{\pi C^4 \left(\frac{\ell}{a}\right)^2}\,(2.652) = (0.21869)(2.652) = 0.5799 \quad (2)$$

These manually computed results agree reasonably well with the machine computed results of $g_{cv} = 0.4034$ and $b_{cv} = 0.5492$ (C=1.50), and hence serve as a partial check on the latter's computer programming.

APPENDIX V

EXTERNAL ADMITTANCE FOR CASE OF INFINITE COATING THICKNESS

Considering the case of an infinite coating thickness causes the problem to become one of a single region. For the same assumed slot distribution of (3) and (4) of the text, one obtains, directly, (5) and instead of (6), the result

$$\bar{H}_z = \frac{u\,\bar{E}_\phi}{j\omega\mu_v\, H_m^{(2)'}(u\rho)} \tag{1}$$

where

$$u = \begin{cases} \beta_v\sqrt{\varepsilon_r - y^2} & \varepsilon_r > y^2 \\ -j\beta_v\sqrt{y^2-\varepsilon_r} & \varepsilon_r < y^2 \end{cases} \tag{2}$$

Use of (1) above and (5) of the text then causes (9a) of the text to become, realizing that for $y^2>\varepsilon_r$,

$$H_m^{(2)}(ua) = \frac{2}{\pi}\, j^{m+1} K_m(C\sqrt{y^2-\varepsilon_r}) \tag{3}$$

$$H_m^{(2)'}(ua) = j\,\frac{2}{\pi}\, j^{m+1} K_m'(C\sqrt{y^2-\varepsilon_r}) \tag{4}$$

$$Y_c \Big|_{\substack{W=\infty \\ \varepsilon_r \text{ real}}} = g_c + jb_c \tag{5}$$

where

$$g_c = \frac{8}{C^4 \left(\frac{\ell}{a}\right)^2 \pi} \sum_{m=0}^{\infty} \frac{a_m}{(1+\delta_o^m)} \quad I_g \tag{6}$$

with

$$I_g = \int_0^{\sqrt{\epsilon_r}} \frac{\cos^2\left(\frac{\beta_v \ell}{2} y\right) dy}{\left[y^2 - \frac{\pi^2}{(\beta_v \ell)^2}\right]^2 \left| H'\left(C\sqrt{\epsilon_r - y^2}\right)\right|^2}$$

$$b_c = b_{c1} + b_{c2} \tag{7}$$

$$b_{c1} = \frac{-4}{C^3 \left(\frac{\ell}{a}\right)^2} \sum_{m=0}^{\infty} \frac{a_m}{(1+\delta_o^m)} \quad I_{1m} \tag{8}$$

with

$$I_{1m} = \int_0^{\sqrt{\epsilon_r}} \frac{\sqrt{\epsilon_r - y^2}\,[JJ' + YY']\cos^2\left(\frac{\beta_v \ell}{2} y\right) dy}{\left[y^2 - \frac{\pi^2}{(\beta_v \ell)^2}\right]^2 \left| H'\left(C\sqrt{\epsilon_r - y^2}\right)\right|^2}$$

with the arguments of J, J', Y and Y' being $C\sqrt{\epsilon_r - y^2}$, and

$$b_{c2} = \frac{4}{C^3 \left(\frac{\ell}{a}\right)^2} \sum_{m=0}^{\infty} \frac{a_m}{(1+\delta_o^m)} \quad I_{2m} \tag{9}$$

with

$$I_{2m} = \int_{\sqrt{\epsilon_r}}^{\infty} \frac{\sqrt{y^2 - \epsilon_r}\,\cos^2\left(\frac{\beta_v \ell}{2} y\right) K_m\left(C\sqrt{y^2 - \epsilon_r}\right) dy}{\left[y^2 - \frac{\pi^2}{(\beta_v \ell)^2}\right]^2 K_m'\left(C\sqrt{y^2 - \epsilon_r}\right)}$$

As a partial check, it is noted that for no coating,(i.e., free space ε_r=1), that (5) through (9) give the results of (XIX) and (XXI) of Table I of the text, as should be.

APPENDIX VI

DETAILS OF ANTENNA DESIGN

(a) Determination of Slot Length and Dielectric Loading

For design purposes, two parameters C and k are defined as,

$$C = \frac{2\pi a}{\lambda_v} \tag{1}$$

$$k = \frac{2a}{\lambda_g} \tag{2}$$

where C = Electrical circumference of cylinder in free space wavelengths.

a = Outer radius of the cylinder.

λ_v = Free space wavelength at operating frequency.

λ_g = Waveguide wavelength, given by

$$\lambda_g = \frac{\lambda_v}{\sqrt{\varepsilon_r - \left(\frac{\lambda_v}{\lambda_c}\right)^2}} \tag{3}$$

with ε_r = Dielectric constant of the material filling waveguide.

$\lambda_c = 2\ell$ = Cutoff wavelength of the dominant $TE_{1,0}$ mode.

ℓ = Internal width of waveguide = slot length.

Then, from (1) and (2) it follows that

$$C = \frac{\pi k}{\sqrt{\varepsilon_r - \left(\frac{\lambda_v}{\lambda_c}\right)^2}} \tag{4}$$

For the purpose of operation of this antenna, the first higher mode ($TE_{2,0}$) above the principal $TE_{1,0}$ mode should be sufficiently attenuated at the slot location. This requires that the dielectric constant, ε_r, be such that this mode (and hence all other higher modes) be below cutoff.

The phase constant, β_1, of the dominant TE_{10} mode may be expressed in terms of λ_v and λ_c as,

$$\beta_1 = \beta_v \sqrt{\varepsilon_r - \left(\frac{\lambda_v}{\lambda_c}\right)^2} \tag{5}$$

For $TE_{1,0}$ mode to propagate down the guide, it is required that

$$\varepsilon_r - \left(\frac{\lambda_v}{2\ell}\right)^2 > 0$$

i.e.,

$$\varepsilon_r > \frac{1}{4}\left(\frac{\lambda_v}{\ell}\right)^2 \tag{6}$$

whereas for $TE_{2,0}$ not to propagate down the guide, it is required that

$$\varepsilon_r - \left(\frac{\lambda_v}{\ell}\right)^2 < 0$$

i.e.,

$$\varepsilon_r < \left(\frac{\lambda_v}{\ell}\right)^2 \tag{7}$$

Therefore, the restriction of ε_r is

$$\frac{1}{4}\left(\frac{\lambda_v}{\ell}\right)^2 < \varepsilon_r < \left(\frac{\lambda_v}{\ell}\right)^2$$

or,

$$\varepsilon_r < \left(\frac{\lambda_v}{\ell}\right)^2 < 4\,\varepsilon_r \tag{8}$$

Fig. VI-1 shows the relation (8) of the allowable ε_r to the size of the squared slot length normalized with respect to free space wavelength, $(\ell/\lambda_v)^2$.

The parameters ℓ and ε_r are determined by insisting that the $TE_{2,0}$ mode be attenuated by at least 20 db over the guide length from the excitation point (probe location) to the slot, which is taken as (3/4)(2a). The attenuation, A, of the $TE_{2,0}$ mode at (3/4)(2a) is

$$A = 20 \log_{10} e^{(3/4)(2a)\alpha} \text{ db} \tag{9}$$

where

$$\alpha = \beta_v \sqrt{\left(\frac{\lambda_v}{\lambda_c}\right)^2 - \varepsilon_r} \quad \text{nepers/meter} \tag{10}$$

i.e.,

$$A_2 = 30C \sqrt{\left(\frac{\lambda_v}{\ell}\right)^2 - \varepsilon_r} \, (\log_{10} e) \text{ db} \tag{11}$$

Setting A = 20 db and solving (11) for $\left(\frac{\lambda_v}{\ell}\right)^2$ gives,

$$\left(\frac{\lambda_v}{\ell}\right)^2 = \varepsilon_r + \frac{2.35644}{C^2} \tag{12}$$

From (4)

$$\varepsilon_r = \frac{1}{4} \left(\frac{\lambda_v}{\ell}\right)^2 + \left(\frac{k\pi}{C}\right)^2 \tag{13}$$

From (12) and (13)

$$\varepsilon_r = \frac{0.78548}{C^2} + (4/3)\left(\frac{k\pi}{C}\right)^2 \tag{14}$$

As discussed in the text, a value of C = 1.5 is desirable, hence (12) and (14) give,

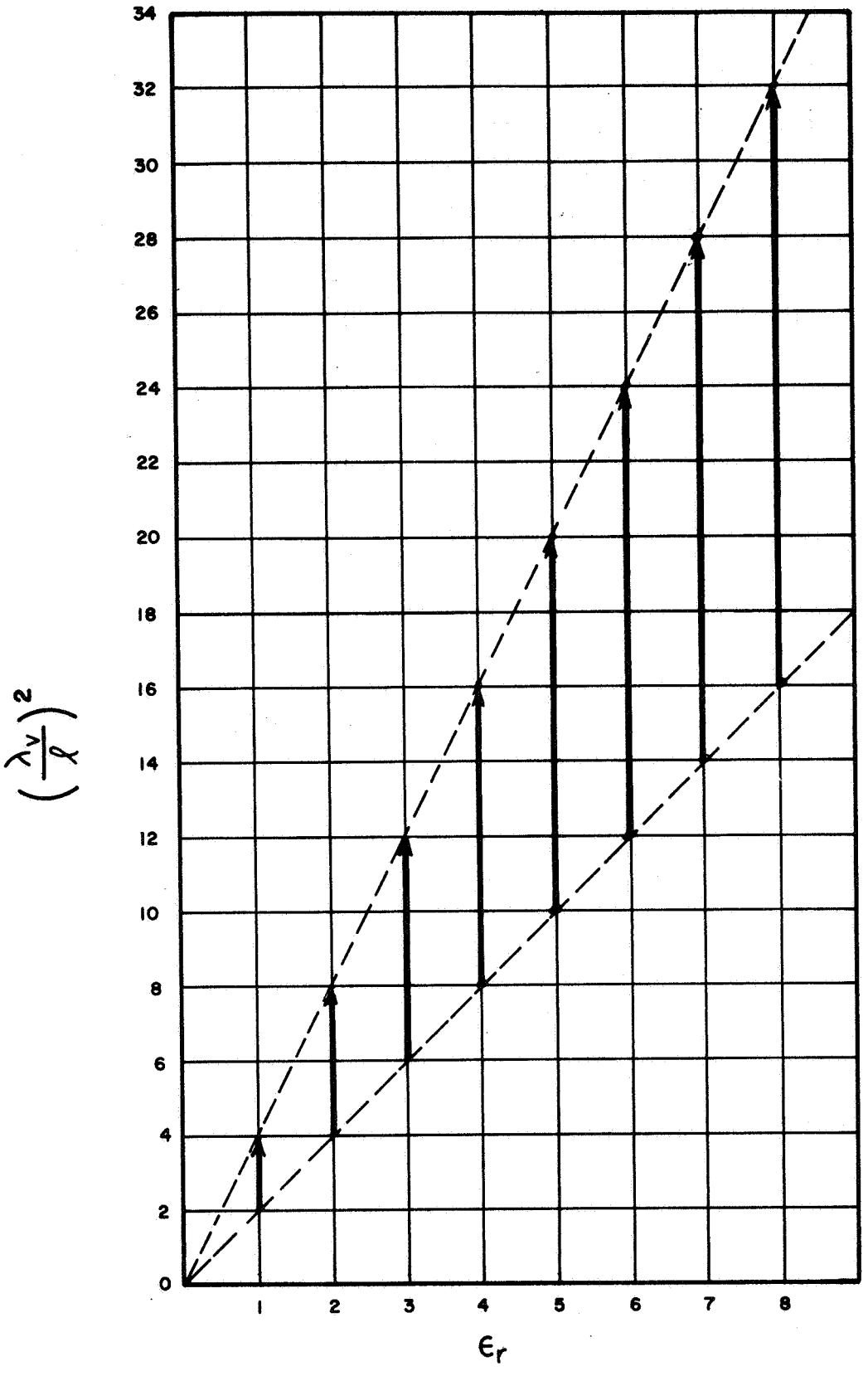

FIG. VI -1 ALLOWABLE RANGE OF ϵ_r

$$\left(\frac{\lambda_v}{\ell}\right)^2 = \varepsilon_r + 1.04731 \tag{15}$$

$$\varepsilon_r = 5.84272\ k^2 + 0.3491 \tag{16}$$

respectively.

The parameters $\left(\frac{\lambda_v}{\ell}\right)^2$ and ε_r (as well as $\ell/a = \frac{2\pi(\ell/\lambda_v)}{C}$) are plotted in Fig. VI-2 as a function of $2a/\lambda_g$. These plots give the values of the parameters for C = 1.5 and 20 db attenuation of the $TE_{2,0}$ mode over the guide length 2a(3/4).

From these curves, one can determine k for a specified value of ε_r, and from this k, determine ℓ/a. In this antenna, it is desirable to use Teflon filler, since this material has very low loss and also eventually the cylinder will be coated with this material and the use of the same material for the filler may result in superior matching properties.

Hence, from Fig. VI-2, one obtains for Teflon* (ε_r = 2.028 at the frequency of f=1,902 MHz, corresponding to C = 1.5 for 2a = 2.964 in.),

$$\varepsilon_r = 2.028$$

$$k = 0.536$$

$$\ell/a = 2.388$$

For 2a = 2.964",

$$\ell = 3.54"$$

Having determined the parameters ℓ and ε_r at the center design frequency corresponding to C = 1.50, it remains to

*The dielectric constant of the Teflon material used in the waveguide was measured over the frequency range of interest, as discussed in Appendix VII.

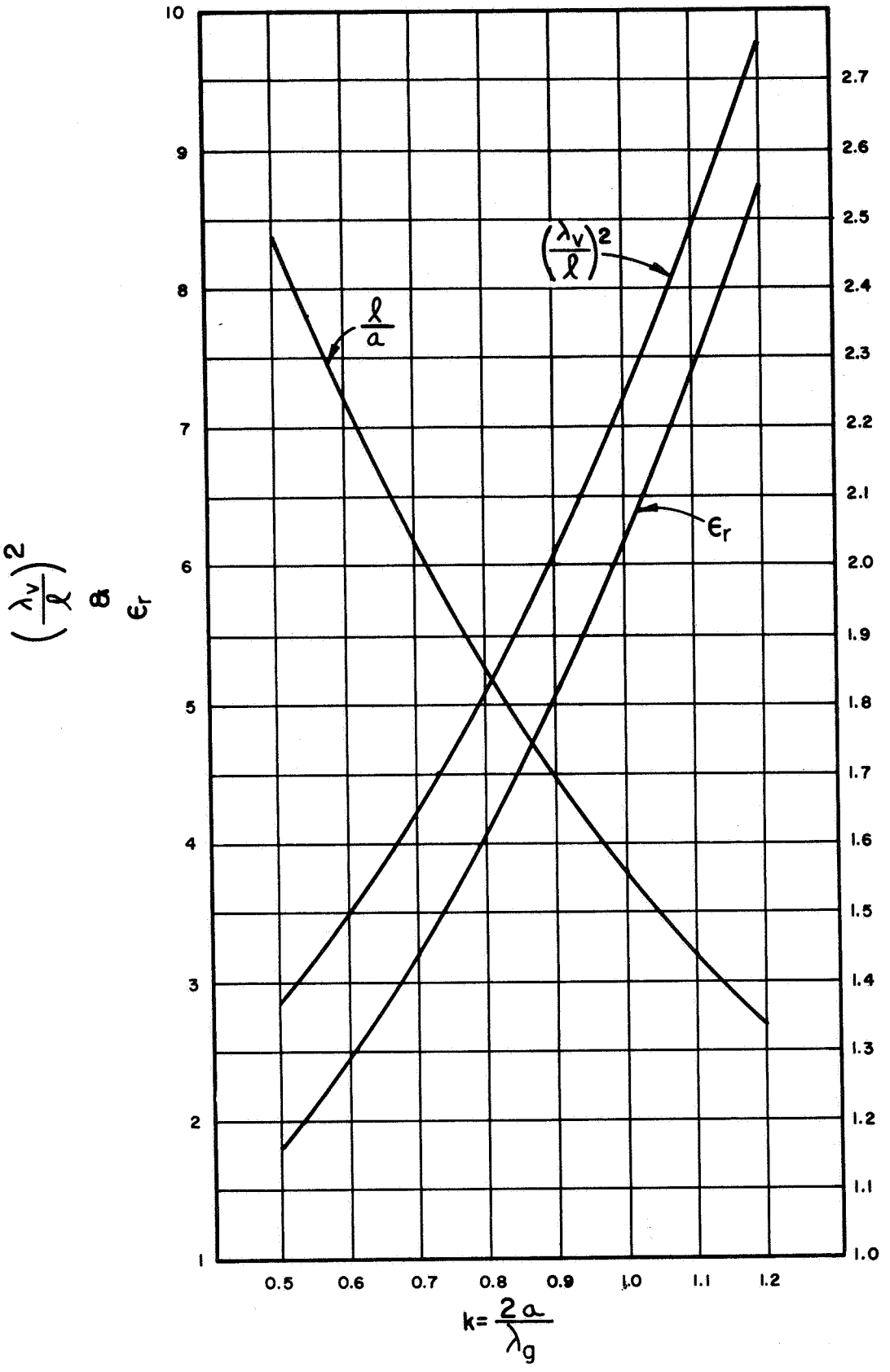

FIG. VI-2 SLOT ANTENNA LENGTH AS FUNCTION OF DIELECTRIC LOADING

determine the change in higher order mode attenuation over the specified operating bandwidth (about ±10%).

Using (9) and (10), the attenuation A_3 for $TE_{3,0}$ mode is given as

$$A_3 = 30C\sqrt{9/4\ (\frac{\lambda_v}{\ell})^2 - \varepsilon_r}\ (\log_{10}e)\ \text{db}. \qquad (17)$$

The attenuations A_2 and A_3 for ε_r=2.028, ℓ=3.54" are plotted in Fig. VI-3. The plots show that these attenuation levels are ±2 db about 20 db for $TE_{2,0}$ mode and ±1 db about 43.2 db for $TE_{3,0}$ mode. These levels are sufficient to justify the neglection of these modes at the slot.

(b) Slot Width Determination

The slot width, w, is chosen as small as possible to validate the assumption of circumferential and rectangular equality of field components, as discussed in the text. Essentially, this is equivalent to insisting that the electrical distance Δ/λ_g, as depicted in Fig. VI-4, be sufficiently small so that the impedance transformation over this distance is negligible.

From Fig. VI-4, it is seen that

$$\Delta \approx \frac{w^2}{8a} \qquad (18)$$

For a choice of w = 0.25 inches (which is the minimum practical choice of w for conventional fabrication processes) the ratio Δ/λ_g over the operating bandwidth has a maximum value of 0.00106, as shown in Fig. VI-5. Thus, the resulting impedance transformation over the gap length, Δ, is negligible, as seen from a Smith Chart.

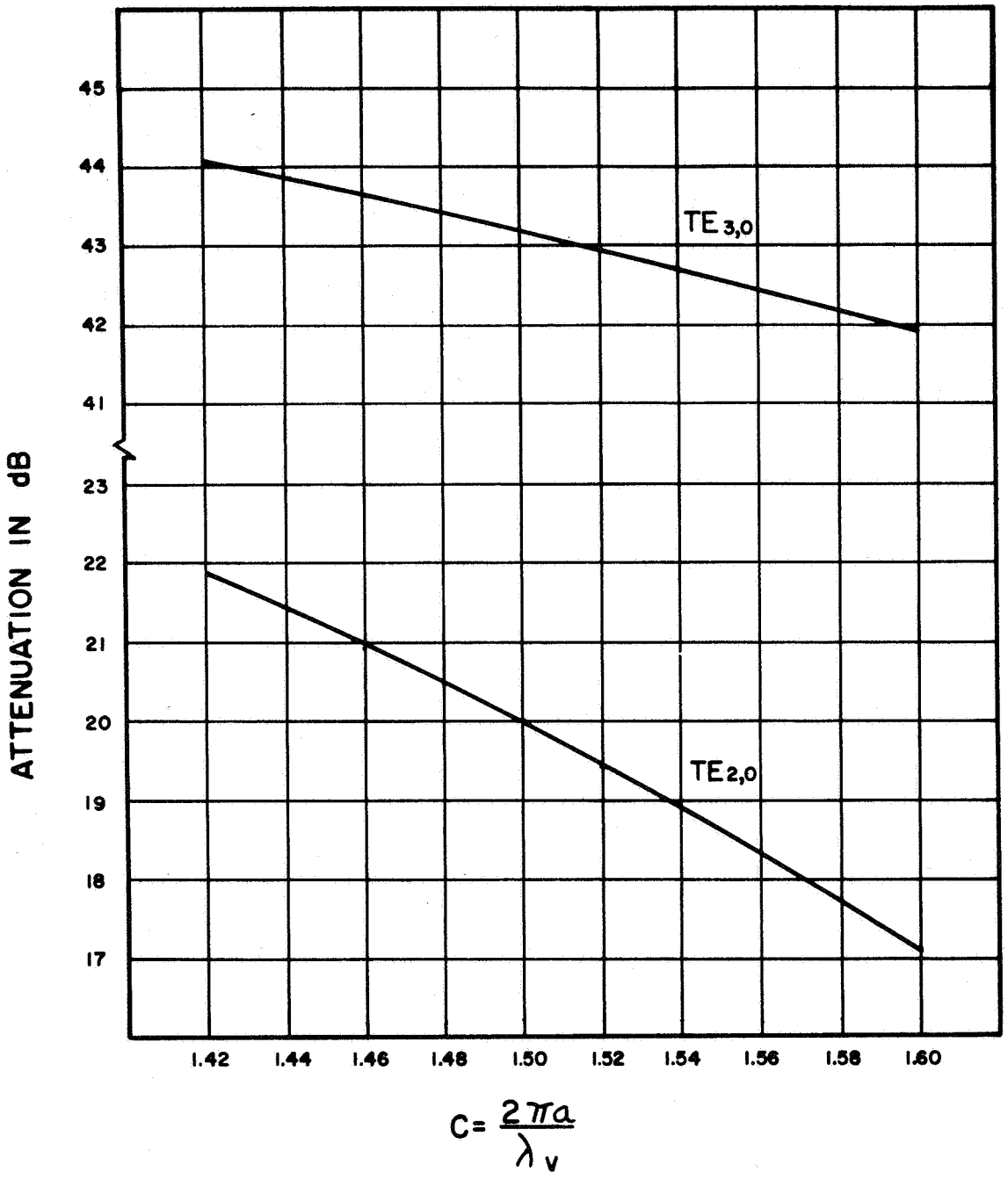

FIG. VI-3 ATTENUATION OF HIGHER ORDER TE 2,0 and TE 3,0 MODES

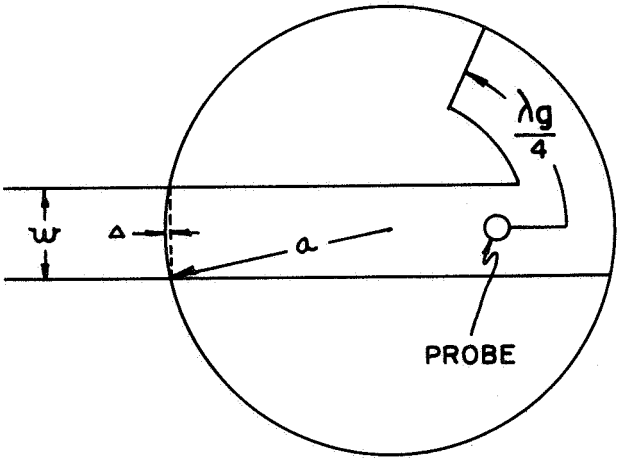

w = 0.25"

a = 1.482"

NOT TO SCALE

FIG. VI-4 CROSS SECTION OF CYLINDER-SLOT INTERSECTION

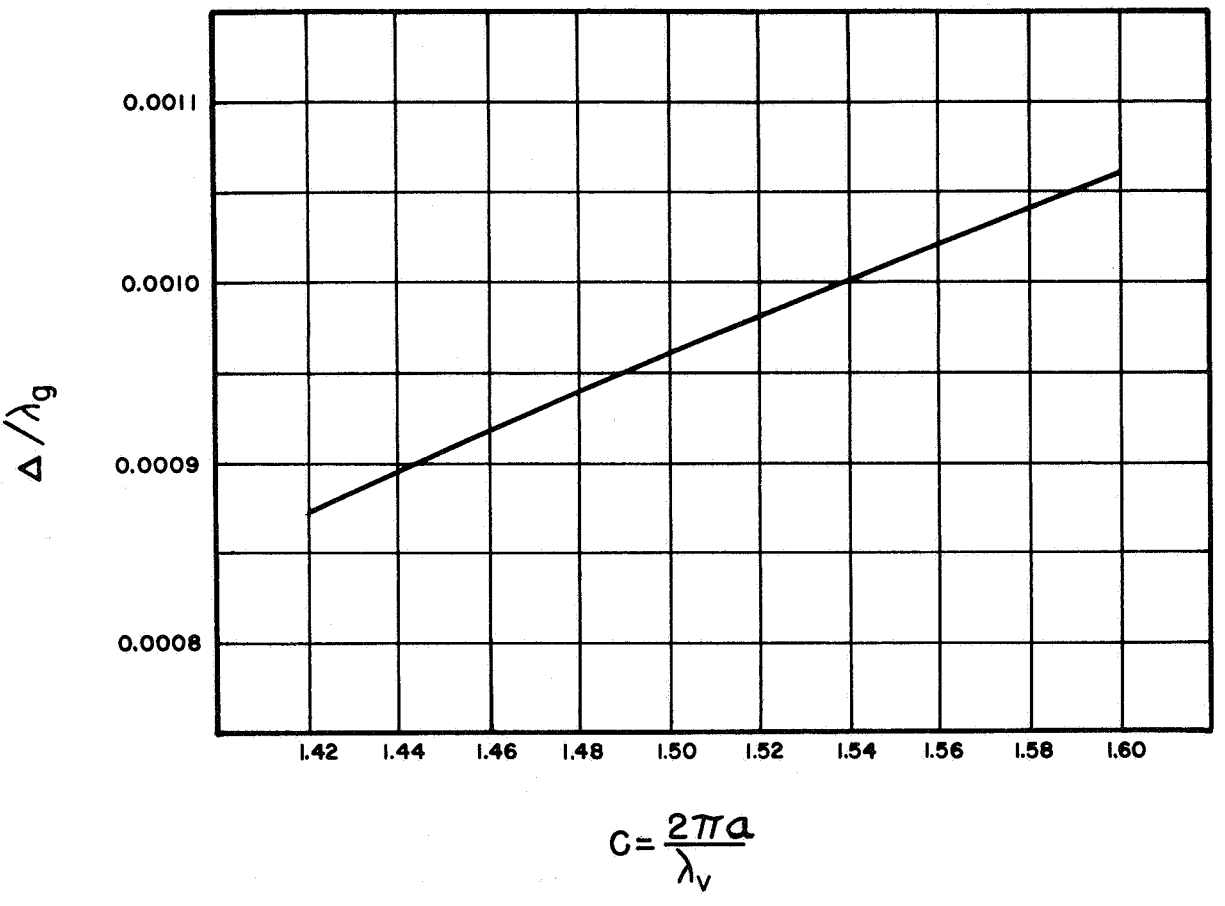

FIG. VI-5 GAP LENGTH NORMALIZED WITH RESPECT TO WAVEGUIDE WAVELENGTH

c. Loop-Feed Design

To guide the principal TE_{10} mode to the slot opening, a straight run of rectangular waveguide (with internal cross-section of 0.25" x 3.54") extends from the slot to the rear of the cylinder, where it is curved along the inner wall of the cylinder (see Fig. 6 of the text). This curved section of waveguide extends approximately a quarter of a guide wave length back from the probe position at the center frequency, so as to insure that all the incident power to the probe goes toward the slot.

To excite the TE_{10} wave in the waveguide, a combined type of E plane loop coupling and cross-bar transition [23] was used. This combination was found to have good matching properties for the narrow height ($w/\lambda_v \approx \frac{1}{24}$)waveguide used.

The probe was fed through the narrow wall and part was tapped off in a bend to the wide wall to form a loop, while the main probe was extended to a coaxial short plunger (1/4" inner diameter) at the opposite narrow wall for tuning purposes, as shown in Fig. VI-6.

The probe position, S,was determined approximately by neglecting the probe thickness and assuming that the waveguide is matched in both directions at the probe. Assuming that the current on the wire varies as $\cos\beta_v \ell$ where ℓ is a length of the loop and β_v is the phase constant along the wire, the input circuit resistance was determined as, following Harrington [24],

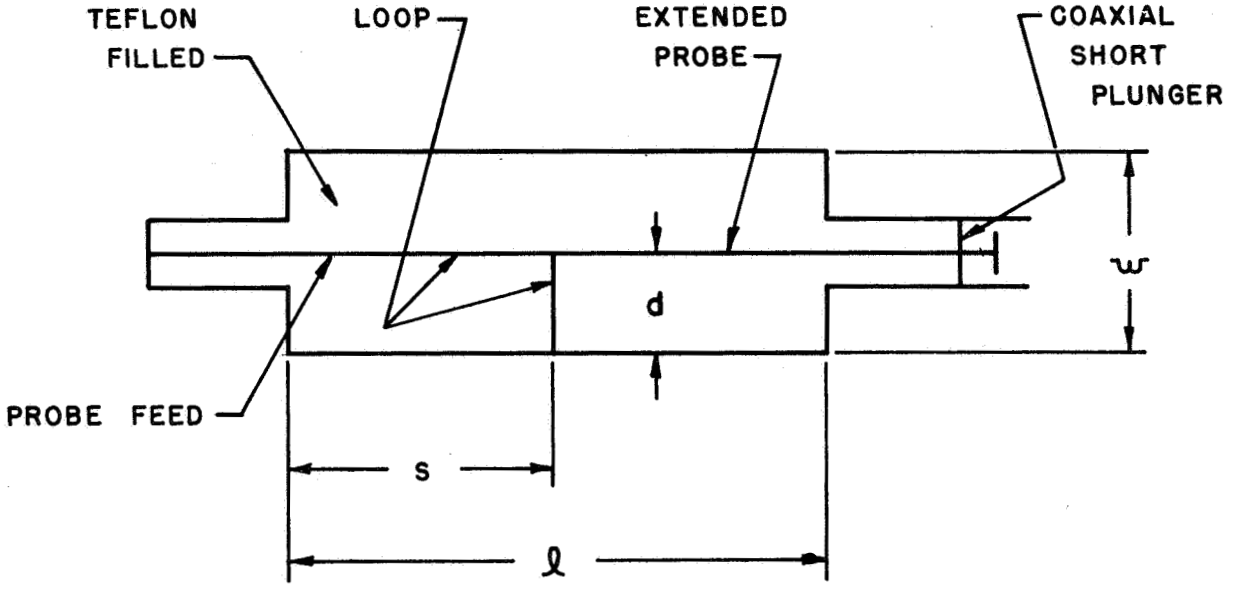

FIG. VI-6 COMBINATION E PLANE LOOP - CROSS BAR FEED

$$R_i = \left(\frac{\ell}{w}\right)\left(Z_{TE_{10}}\right)\left[\frac{\sin\frac{\pi S}{\ell}\sin\beta_v d}{\beta_v w\cos\beta_v(S+d)}\right]^2 \qquad (19)$$

where:

R_i = input circuit resistance

$Z_{TE_{10}}$ = characteristic wave impedance = $\eta_v \frac{\lambda_g}{\lambda_v}$

$\lambda_g = \lambda_v\sqrt{\varepsilon_r-(\lambda_v/2\ell)^2}$

ℓ = waveguide width

w = waveguide height

S = loop probe position

Setting $d = \frac{w}{2}$ and $R_i = 50\Omega$ (the impedance of the coaxial line), the probe position, S, was found to be 4.5 cm.

The actual input impedance may differ from 50Ω because the probe has a finite thickness. To determine that probe thickness which gives a smooth transition from the coaxial line to the waveguide, the guide was assumed to behave like a slab line in the region of the feed. This assumption holds, since the width of the guide, w, is much smaller than the distance from the end of the guide to the probe position.

From the work of Chrisholm [25], the characteristic impedance of the slab line is determined approximately as

$$Z_o \triangleq Z_{TE}\left[\frac{1}{2\pi}\ln\left(\frac{2w}{\pi p}\right) - \frac{.2153\ (\frac{P}{w})^4}{1-5.682(\frac{P}{w})^4}\right] \qquad (20)$$

where w = guide height

P = probe radius

Setting $Z_o = 50\Omega$ in (20), the probe diameter (2P) was determined to be approximately $\frac{3}{32}$". Using the above design parameters, a position of the adjustable short circuit coaxial plunger was found to match the antenna fairly well near the center frequency. The match over the band of 1.80 to 2.00 GHz is as shown in Fig. 12 of the text.

d. Final Antenna Assembly

The final antenna was constructed using the above dimensions on a cylindrical section of about a six inch length with threaded ends, so as to add a 16 inch length on each end. It was found necessary to connect the coaxial line feed directly into the waveguide as shown, rather than using a conventional type N connector, to reduce insertion loss. For this reason also, a low loss flexible Andrew Type H4-50 air dielectric coaxial line feed was used. The complete antenna assembly is shown in Fig. VI-7.

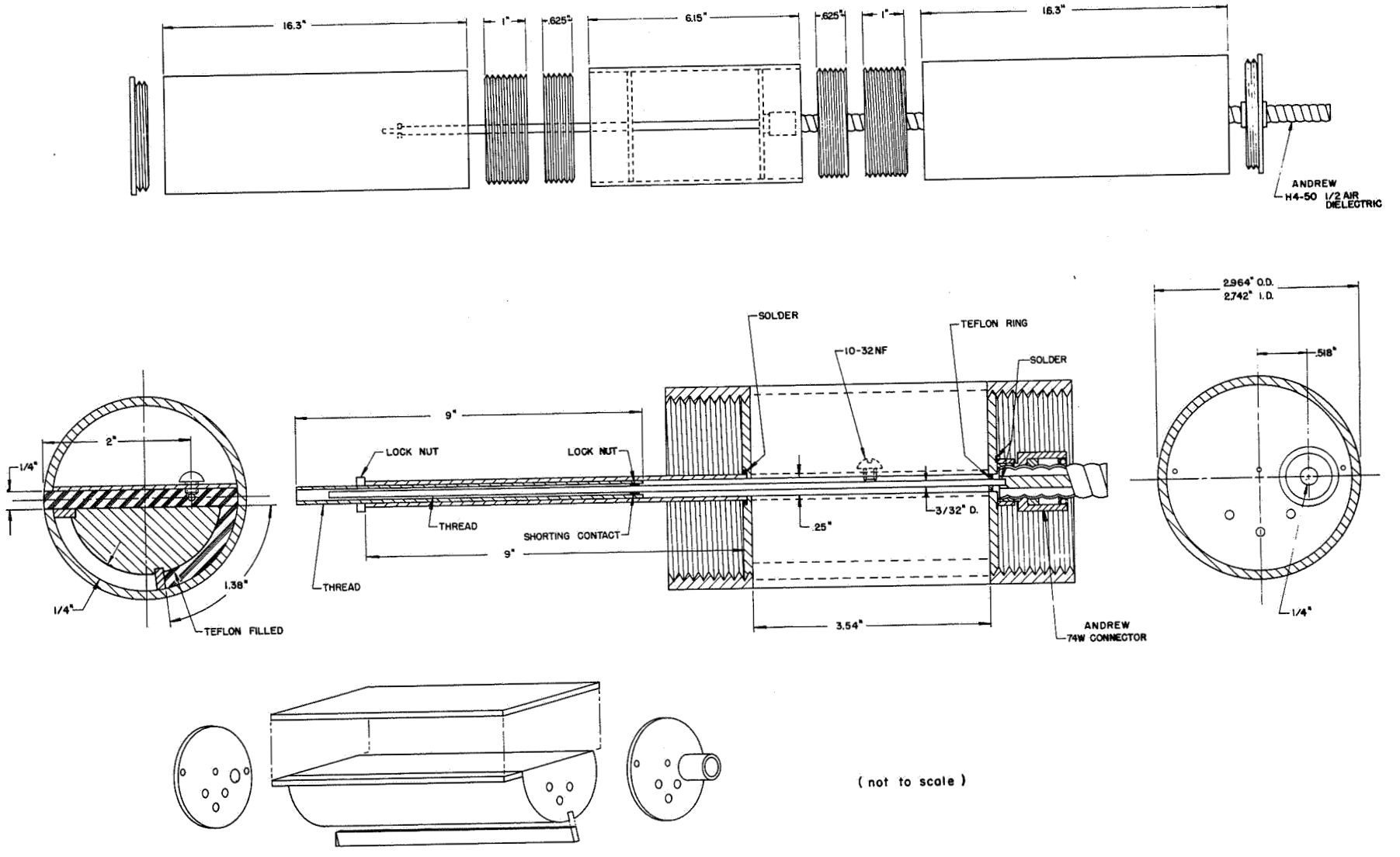

Fig. VI-7 ANTENNA ASSEMBLY

APPENDIX VII

MEASUREMENT OF DIELECTRIC CONSTANT OF TEFLON

There are a variety of methods of measuring the dielectric constant of a solid material. These include transmission line or waveguide methods, cavity measurements or cavity perturbation technkques. Among these various techniques, a relatively simple transmission line method (Von Hipple), involving the solution of a transcendental equation, was used to measure the dielectric constant, ε_r, of Teflon.

The Teflon sample was fabricated into a coaxial cylindrical shape, as shown in Fig. VII-1, to fit in the General Radio Type 900-L2 Reference Air Line as the sample holder. The sample was held tight to prevent air gaps between the sample material and the inner and outer conductors, and one end of the holder was accurately terminated by a short circuit.

Since the loss tangent of Teflon is around 0.0001, the measurements and analysis were performed using the justifiable assumption of a lossless material. The method consists of measuring the input impedance, Z_{in}, of the short circuited sample in the holder and solving a transcendental equation. The analysis follows:

$$Z_{in} = Z_T \tanh \gamma L \qquad (1)$$

where

Z_{in} = Input impedance looking into the input reference plane of the sample.

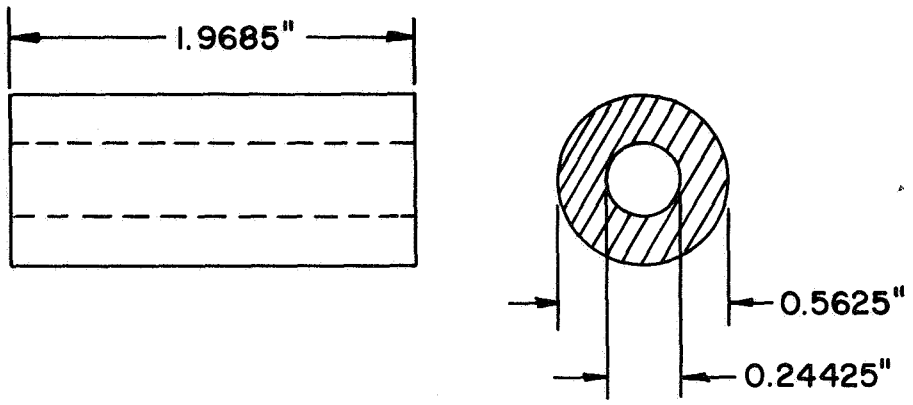

FIG. VII-1 DIELECTRIC SAMPLE GEOMETRY

$Z_T = Z_o \frac{\beta_v}{\beta}$ = Characteristic wave impedance of the coaxial line containing the sample.

$\gamma = \alpha + j\beta$ = Complex propagation constant of the coaxial line containing the sample.

α = Attenuation constant of the coaxial line containing the sample.

$\beta = \beta_v\sqrt{\varepsilon_r}$ = Phase constant of the coaxial line containing the sample.

ε_r = Dielectric constant of non-permeable sample.

Z_o = Characteristic impedance of the air-filled slotted line having the same inner and outer conductor sizes as the coaxial line containing the sample.

λ_v = Free space wavelength of excitation = $2\pi/\beta_v$.

L = Length of sample.

Assuming a lossless line ($\alpha \approx 0$), (1) gives,

$$Z_{in} = j\, Z_T \tan \beta L$$

$$= j \frac{2\pi Z_o L}{\lambda_v} \frac{\tan \beta L}{\beta L} \qquad (2)$$

The normalized input impedance with respect to the air-filled slotted line, z_{in}, is then given by,

$$z_{in} = \frac{Z_{in}}{Z_o} = j \frac{2\pi L}{\lambda_v} \frac{\tan X}{X} \qquad (3)$$

where

$$X = \beta L = \frac{2\pi L\sqrt{\varepsilon_r}}{\lambda_v} . \qquad (4)$$

z_{in} was measured by a conventional method for impedance measurement by finding the precise minimum (null) positions on the slotted line and the VSWR, for the load conditions of the slotted line terminated with (1) a short circuit and (2) with the short circuited sample. The null positions for each load were read to three significant figures by using a micrometer, and VSWR's for the sample only were read in db.

Obtaining the normalized input impedance on a Smith Chart from the measured values of the minimum locations and VSWR, the next step is to solve the transcendental equation (3) for X. Then, from (4),

$$\varepsilon_r = \left(\frac{\lambda_v X}{2\pi \ell}\right)^2 \tag{5}$$

It is noted that the solution to (4) has multiple roots of X; the correct root is selected here by using (5) and taking into account that $\varepsilon_r \approx 2$. The roots, X, of (4) obtained from tabulated values [26] of tan X/X. In this case, the first root was the correct root.

The measured values of ε_r are tabulated in Table VII-1 and are plotted in Fig. VII-2. As shown in this figure, the dielectric constant of Teflon is essentially 2.028 over the bandwidth from 1,800 MHz to 2,000 MHz, where the Teflon will be used. This value (2,028) is within, approximately, three and a half percent of the nominal published value of 2.10.

TABLE VII-1

MEASURED VALUES OF DIELECTRIC CONSTANT FOR TEFLON

f MHz	λ_v cm	Minimum Pos. Slotted Line Short cm	Load cm	VSWR db	z_{in}	X	ε_r
1500.5	19.993	20.0507	22.3527	50	-j 0.88	2.24314	2.0379
1596.98	18.7854	18.8627	20.6177	50	-j 0.665	2.38307	2.0306
1642.93	18.260	18.330	19.865	50	-j 0.58	2.45107	2.0297
1690.52	17.746	17.8165	19.1245	45	-j 0.50	2.52262	2.0306
1744.28	17.199	17.253	18.347	45	-j 0.421	2.60151	2.0285
1803.75	16.632	16.701	17.570	50	-j 0.341	2.68956	2.0275
1852.3	16.617	16.269	16.978	50	-j 0.28	2.68887	2.0276
1897.29	15.812	15.866	16.4245	50	-j 0.226	2.83001	2.0289
1956.05	15.337	15.410	15.795	50	-j 0.16	2.91753	2.0286
1988.99	15.083	15.1525	15.446	50	-j 0.122	2.96939	2.033
2004.27	14.968	15.046	15.3105	48	-j 0.11	2.98634	2.0246
2058.82	14.5714	14.679	14.8057	48	-j 0.056	3.06252	2.0178
2113.42	14.195	14.2635	14.2605	48	+j 0.0001	3.14159	2.0149

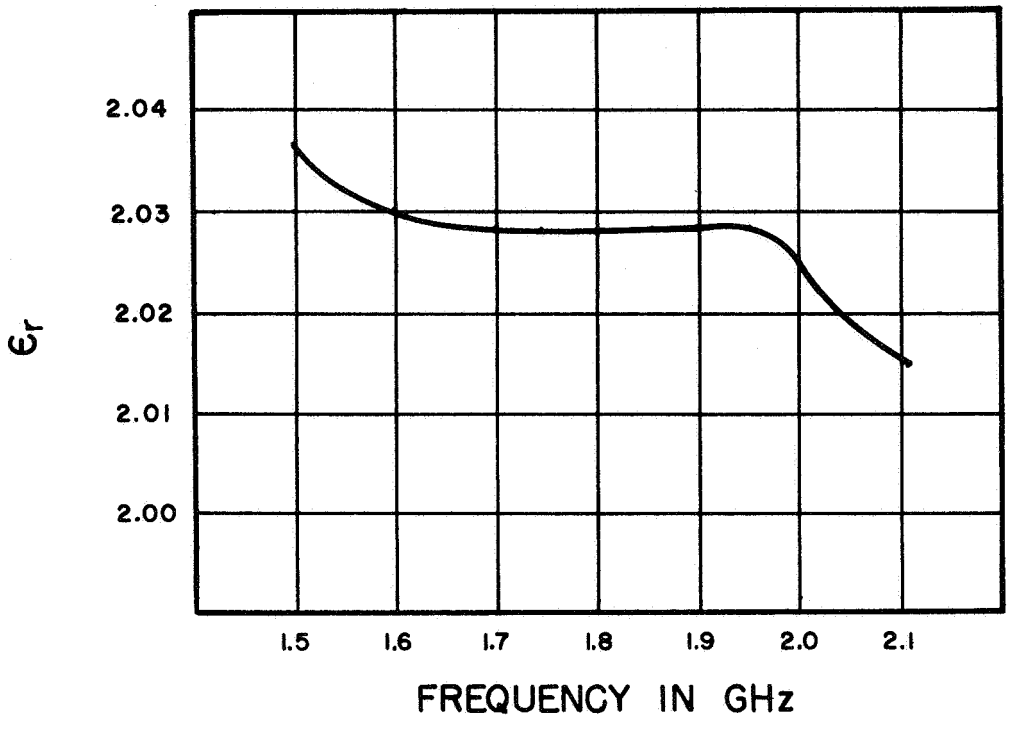

FIG. VII-2 MEASURED DIELECTRIC CONSTANT OF TEFLON

APPENDIX VIII

SCATTERING MATRIX MEASUREMENT METHOD

The scattering coefficients, S_{ij}, were determined using a graphical technique conceived by Deschamps and applied by Storer, et al [14]. A concise outline of this procedure is discussed below.

The output port (here the open end of the slot) of the two port junction was connected to an additional section of waveguide terminated by a shorted plunger. The complex reflection coefficient at the input port (here the coaxial line) was then measured for each of a set of eight plunger positions spaced $\frac{\lambda_{gp}}{16}$ apart, where λ_{gp} is the guide wavelength in the shorted plunger, $\lambda_{gp} = \lambda_v/\sqrt{1-(\frac{\lambda_v}{2\ell})^2}$. The first plunger position was chosen such that it corresponded to a short at the surface of the cylinder and, hence, the fifth position (a quarter wavelength away) corresponds to an open circuit at the surface of the cylinder.

The measured points fall on a circle of radius r, Fig. VIII-1. Although it is not necessary, a Smith Chart was used in the constructions that follow.

After fitting a circle to the measured points and determining the center, c, the pairs of points corresponding to plunger positions $\frac{\lambda_{gp}}{4}$ apart are connected with straight lines. The chords thus determined intersect at some point, a. It should be noted that in constructing the circle, the measured data points $(\Gamma_1)_1$, $\ldots(\Gamma_1)_8$ are smoothed to reduce

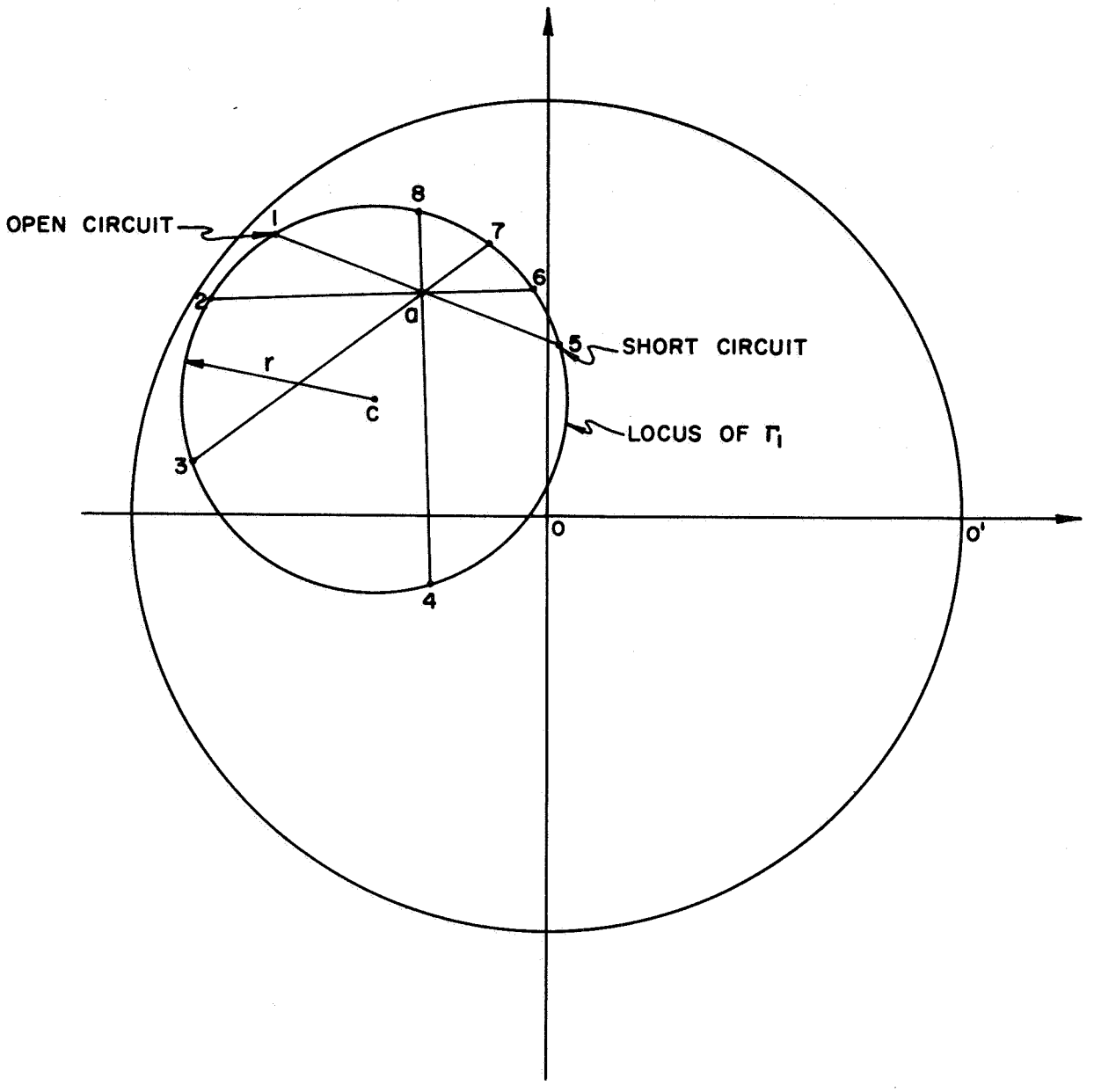

FIG. VIII-1 COMPLEX REFLECTION COEFFICIENT OF PORT 1

measurement error and, similarly, the two redundant chords used to fix point (a) give an additional check against error. (This procedure averages out experimental error, and is the chief advantage of the method over that of, for example, using only the short circuit and open circuit points.)

Having determined points a and c, S_{11} is determined by connecting these points with line $\overline{ac}$ and drawing $\perp$'s to this line at a and c, which intersect the circle at b and d, respectively (Fig. VIII-2). The intersection of line $\overline{bd}$ with line $\overline{ac}$ at point $\underline{q}$ then determines $S_{11}=\overline{0\underline{q}}$ as measured on the chart.

A line is now drawn through the open circuit point (point #5) and $\underline{q}$ (Fig. VIII-3) intersecting the circle at point e. This point is then used to construct the diameter $\overline{ec}$. The constructions are then completed by drawing a $\perp$ to $\overline{ac}$ at $\underline{q}$, intersecting the circle at f (Fig. VIII-3).

The scattering coefficients are then determined as follows:

$$S_{11} = |\overline{0\underline{q}}| \; \angle(\overline{0\underline{q}}, \; \overline{00'})$$

$$S_{12} = \frac{|\overline{\underline{q}f}|}{r} \; \frac{\angle(\overline{ec}, \; \overline{00})}{2}$$

$$S_{22} = \frac{|\overline{\underline{q}c}|}{r} \; \angle(\overline{ec}, \; \overline{\underline{q}c})$$

(For clarity, the angles of S_{12} and S_{22} are also shown in Fig. VIII-3 and that of S_{11} in Fig. VIII-2.)

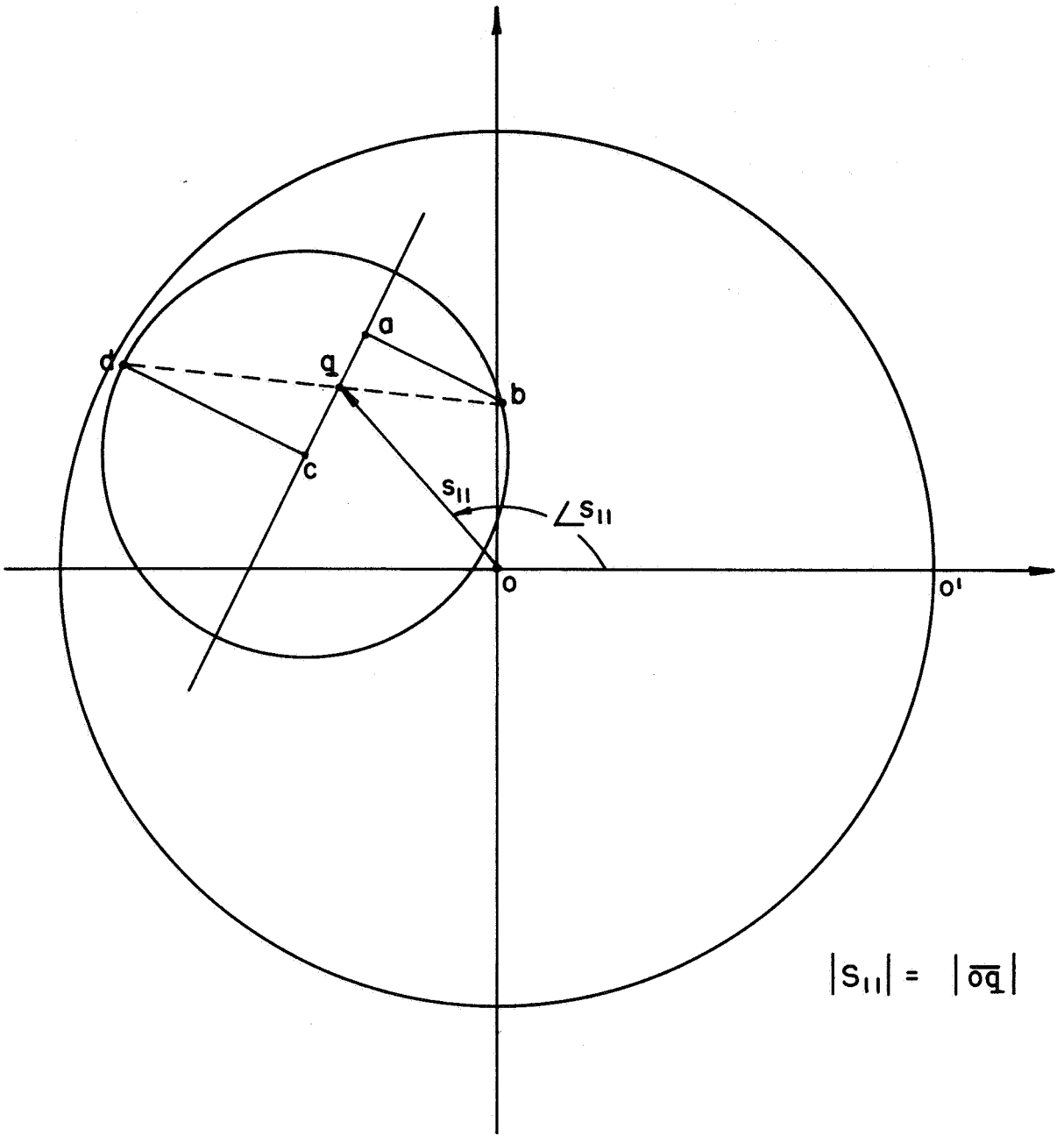

FIG. VIII-2 GRAPHICAL CONSTRUCTION TO OBTAIN S_{11}

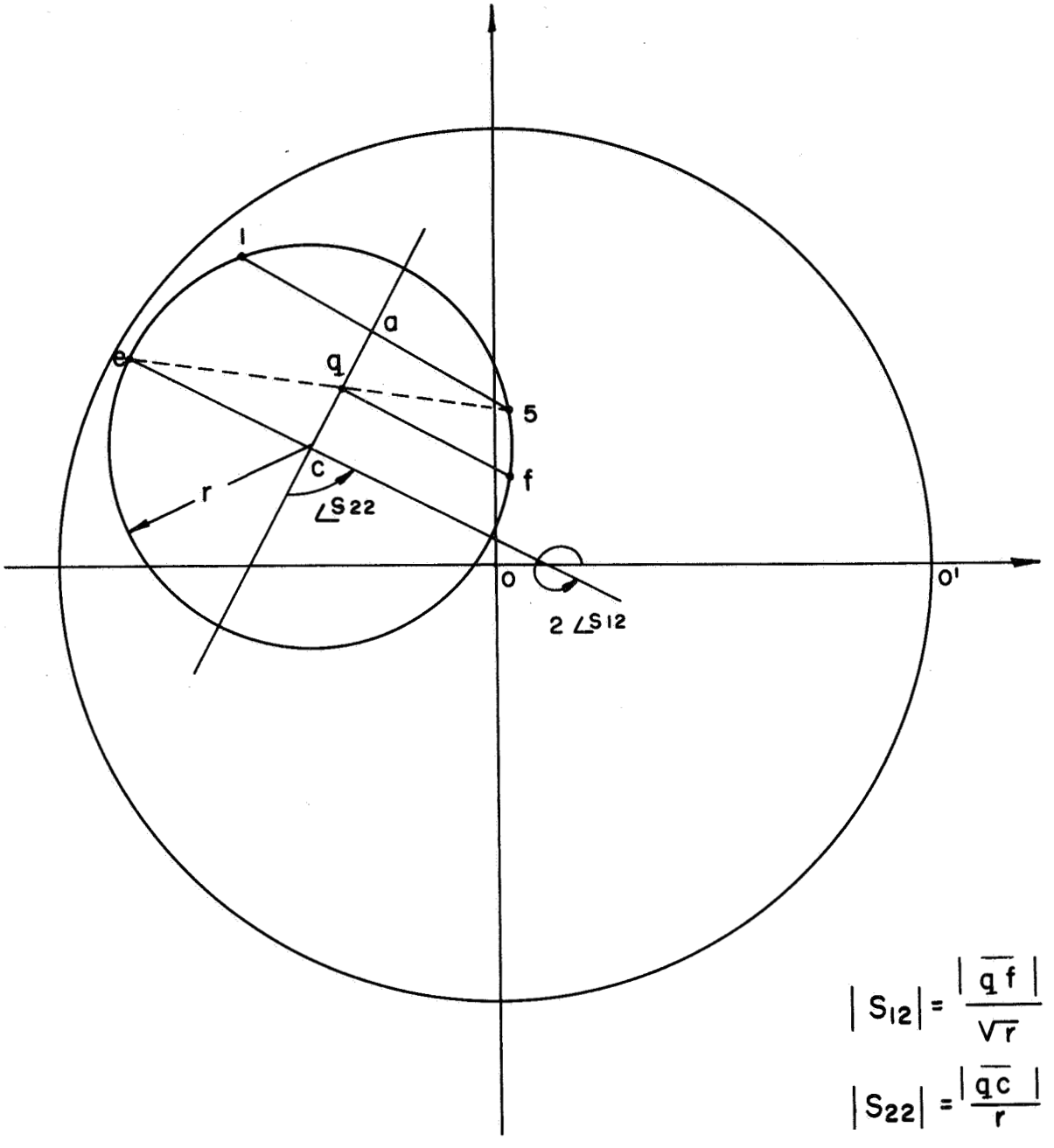

$$|S_{12}| = \frac{|\overline{qf}|}{\sqrt{r}}$$

$$|S_{22}| = \frac{|\overline{qc}|}{r}$$

FIG. VIII-3 GRAPHICAL CONSTRUCTION TO OBTAIN S_{12} & S_{22}

A typical set of data and associated circle constructions at one frequency in the measured range is given in Table VIII-1 and Fig. VIII-4, respectively.

TABLE VIII-1

COMPLEX SCATTERING COEFFICIENTS DETERMINED FROM CONSTRUCTIONS IN FIG. VIII-4

S_{ij}	MAGNITUDE	ARGUMENT
S_{11}	.59	81.5°
S_{12}	.67	-31.5°
S_{22}	.18	46.5°

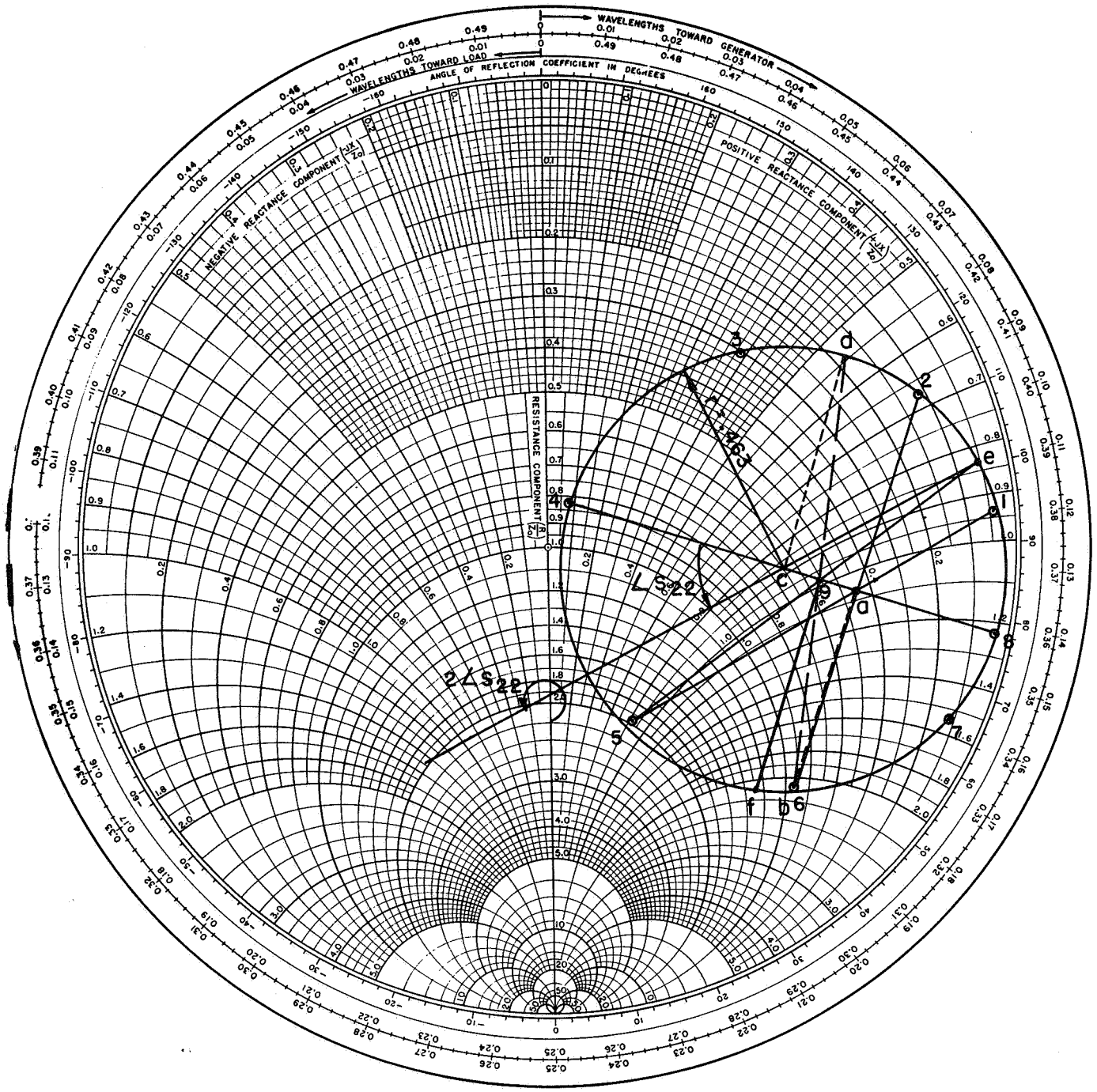

FIG. VIII-4 TYPICAL SCATTERING MATRIX MEASUREMENT DATA

APPENDIX IX

DIFFICULTIES ASSOCIATED WITH DETERMINING WAVEGUIDE ADMITTANCE FROM COAXIAL LINE ADMITTANCE

It is, of course, possible to determine a "measured" value of normalized waveguide input admittance, $y_{in}=y_2$, by using the measured normalized admittance, y_1, in the coaxial line and the measured scattering matrix elements of the network by means of the relations

$$y_{in} = y_2 = \frac{1-\Gamma_2}{1+\Gamma_2} \tag{1}$$

$$\Gamma_2 = \frac{1}{S_{22} - \dfrac{S_{12}^2}{S_{11}-\Gamma_1}} \tag{2}$$

$$\Gamma_1 = \frac{1-y_1}{1+y_1} \tag{3}$$

One can then compare the "measured" value of y_2 obtained from (1) with that computed from theory, using (22) of the text and the computed values of external admittance. This was done for the non-coated case, Fig. IX-1, and only for the measured values of y_2 for the coated case, Fig. IX-2 and IX-3.

Unfortunately for the subject antenna, such a comparison is meaningless for two reasons:

(a) The magnitude of Γ_2 is nearly unity, $|\Gamma_2|\approx 1$, so that for a given fixed percentage measurement error in

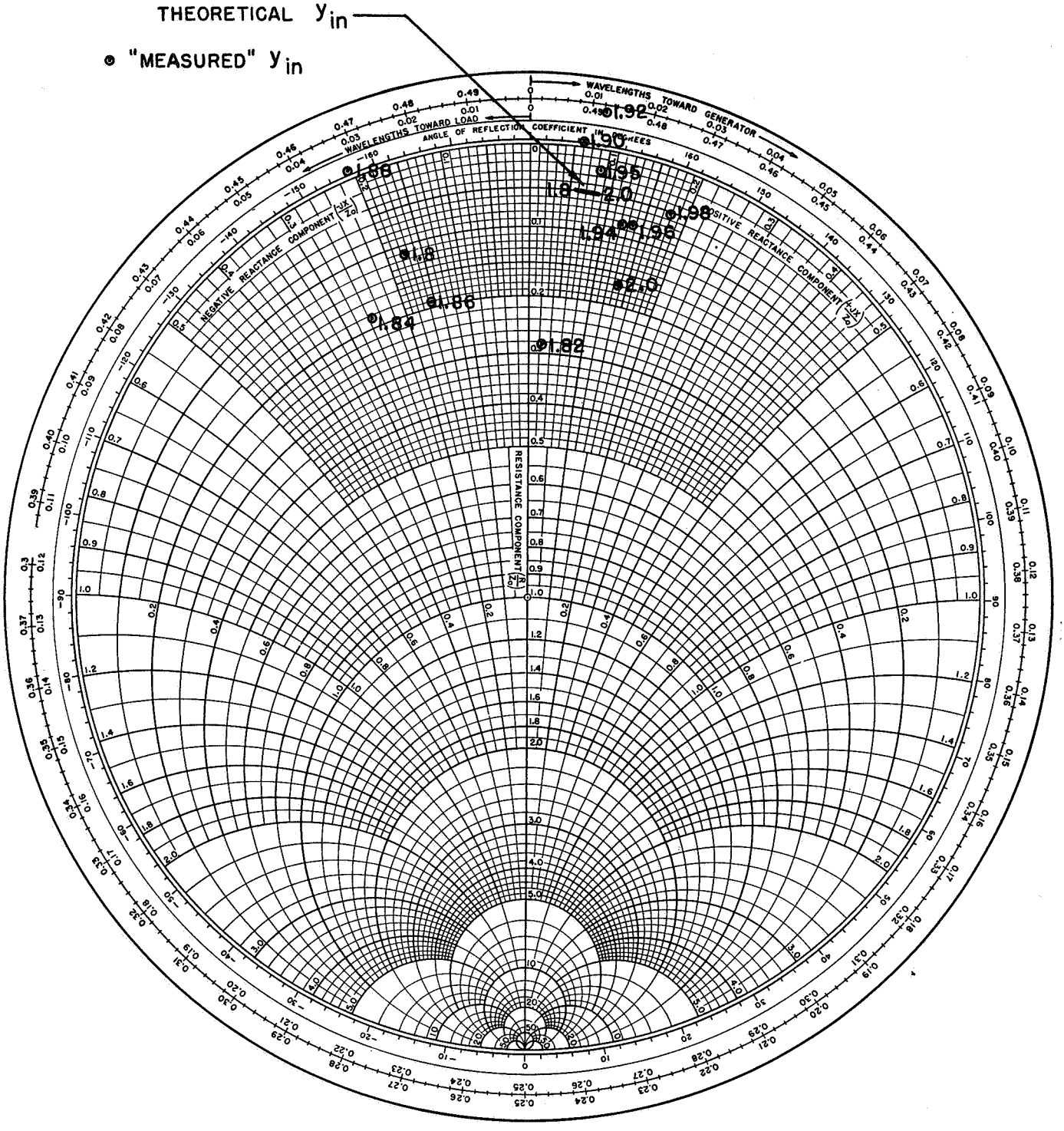

FIG. IX-1 THEORETICAL AND MEASURED NORMALIZED WAVEGUIDE INPUT ADMITTANCE – NO COATING

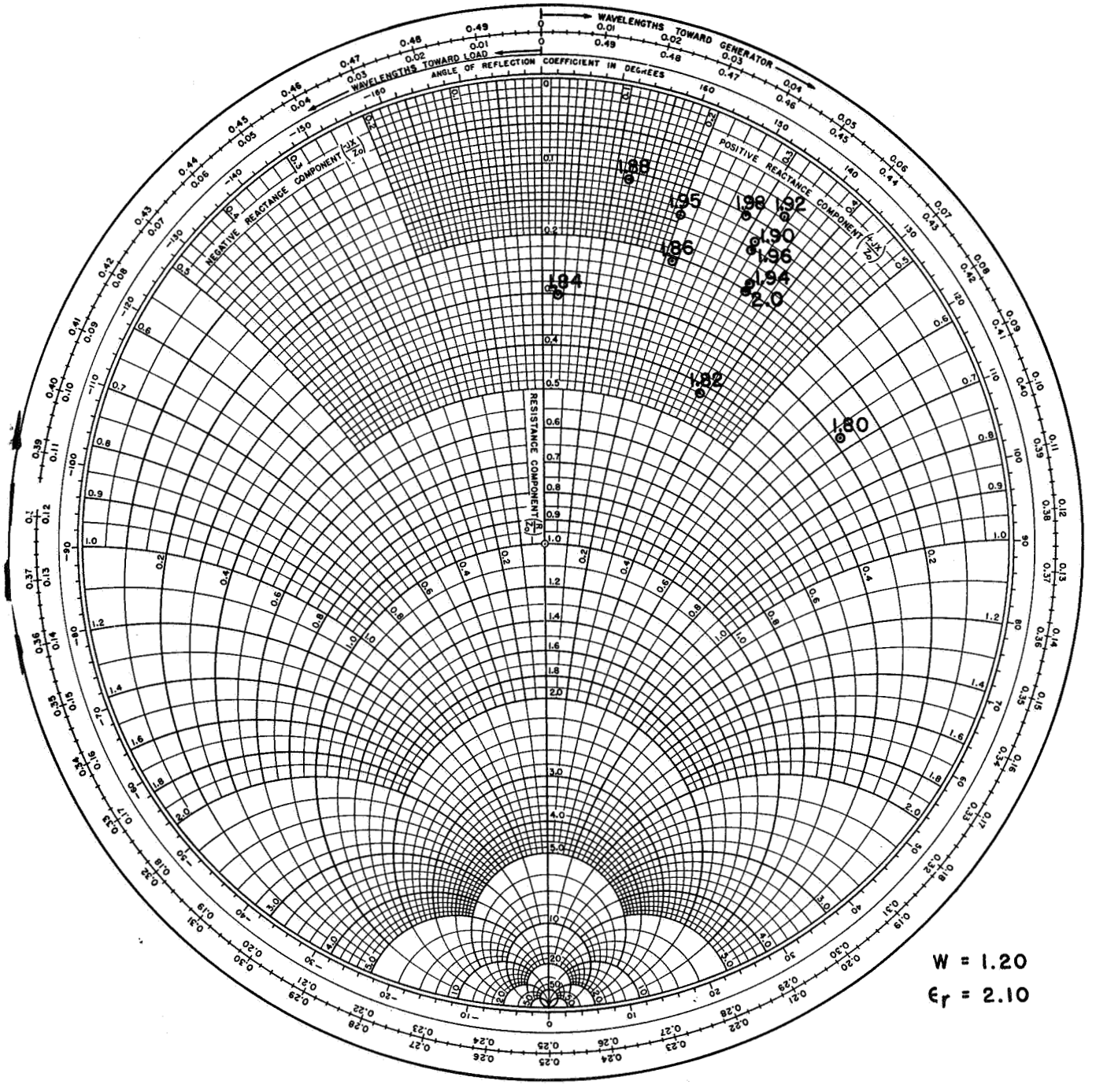

FIG. IX-2 MEASURED NORMALIZED WAVEGUIDE INPUT ADMITTANCE — TEFLON COATING

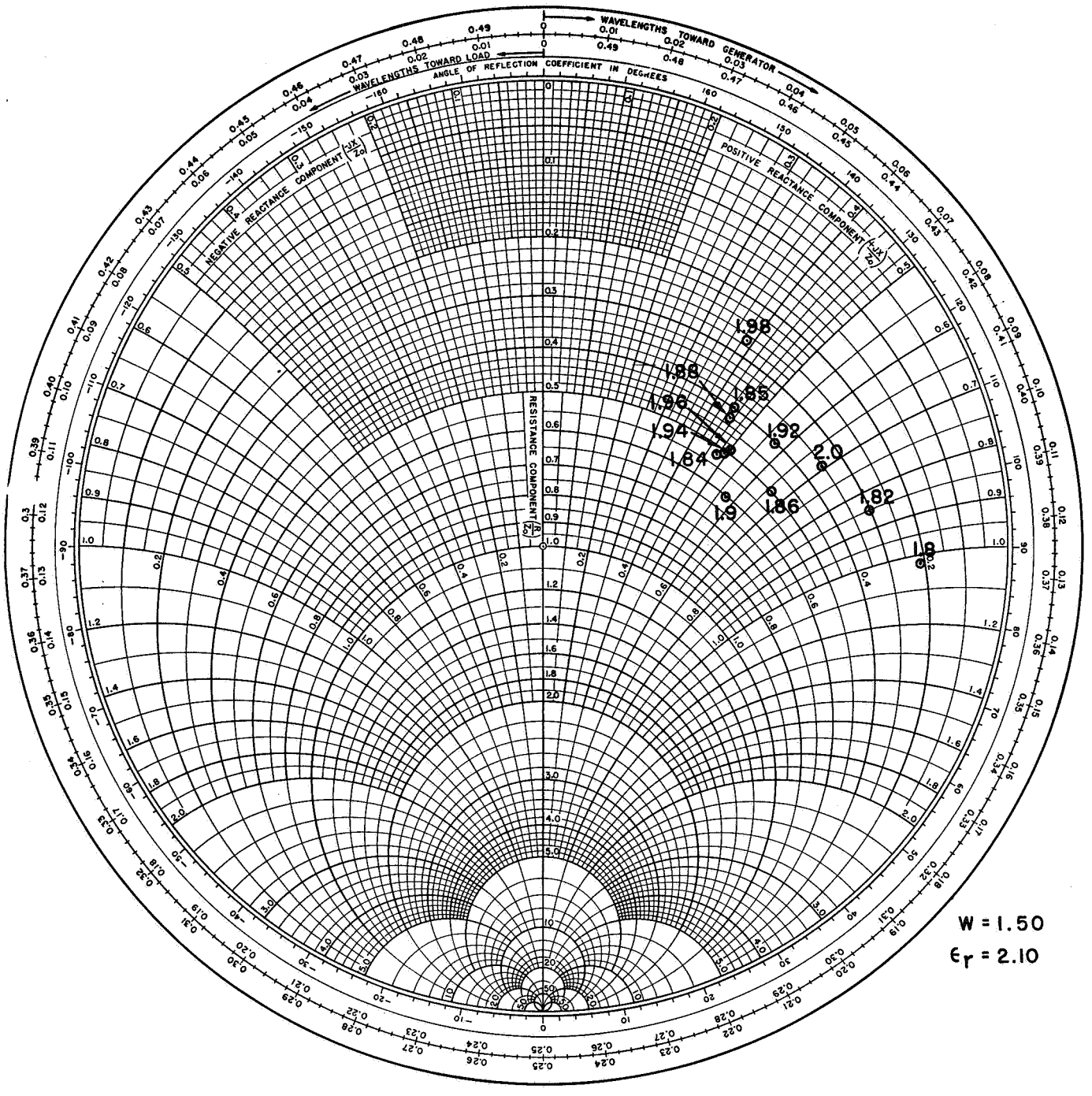

FIG. IX-3 MEASURED NORMALIZED WAVEGUIDE INPUT ADMITTANCE – TEFLON COATING

$\left|\frac{\Delta\Gamma_2}{\Gamma_2}\right|$, $|\Delta\Gamma_2|$ can be large. This is seen by noting from a Smith Chart, that an error circle centered about a given value of $|\Gamma_2|$ has a larger radius for increasing $|\Gamma_2|$. This leads to larger differences in the admittance y_2 for a given measurement accuracy in $|\Delta\Gamma_2/\Gamma_2|$ with increasing $|\Gamma_2|$.

(b) The percentage error in Γ_2 can actually be amplified, as compared to that in Γ_1. This is seen from the relation (2) which gives the ratio of percentage error in Γ_2, $|\Delta\Gamma_2/\Gamma_2|$, to that of the percentage error in Γ_1, $|\Delta\Gamma_1/\Gamma_1|$, as

$$\frac{\left|\frac{\Delta\Gamma_2}{\Gamma_2}\right|}{\left|\frac{\Delta\Gamma_1}{\Gamma_1}\right|} = \frac{|\Gamma_1|}{|\Gamma_2|}\,\frac{|1-S_{22}\Gamma_2|^2}{|S_{12}|^2} \tag{4}$$

A plot of this ratio is given in Fig. IX-4 using the measured values of $|\Gamma_1|$, S_{12} and S_{22}, and the theoretical value of $|\Gamma_2|$. It is seen that this ratio can exceed unity. Thus, for example, for an assumed 10% measurement accuracy in the coaxial line (i.e., $|\Delta\Gamma_1/\Gamma_1| = 0.10$) the accuracy in $|\Delta\Gamma_2/\Gamma_2|$ can approach 50%.

Thus, from point (b) above, it might be thought that the only meaningful frequency range to compare theory with experiment would be that for which the above ratio was well below unity. It is true that in this range the comparison would be better (and is, in fact, better as seen from Fig. IX-1); however, point (a) above still causes trouble, i.e., too much scattering of the measured points for y_2, as seen from Figs. IX-1,2 and 3.

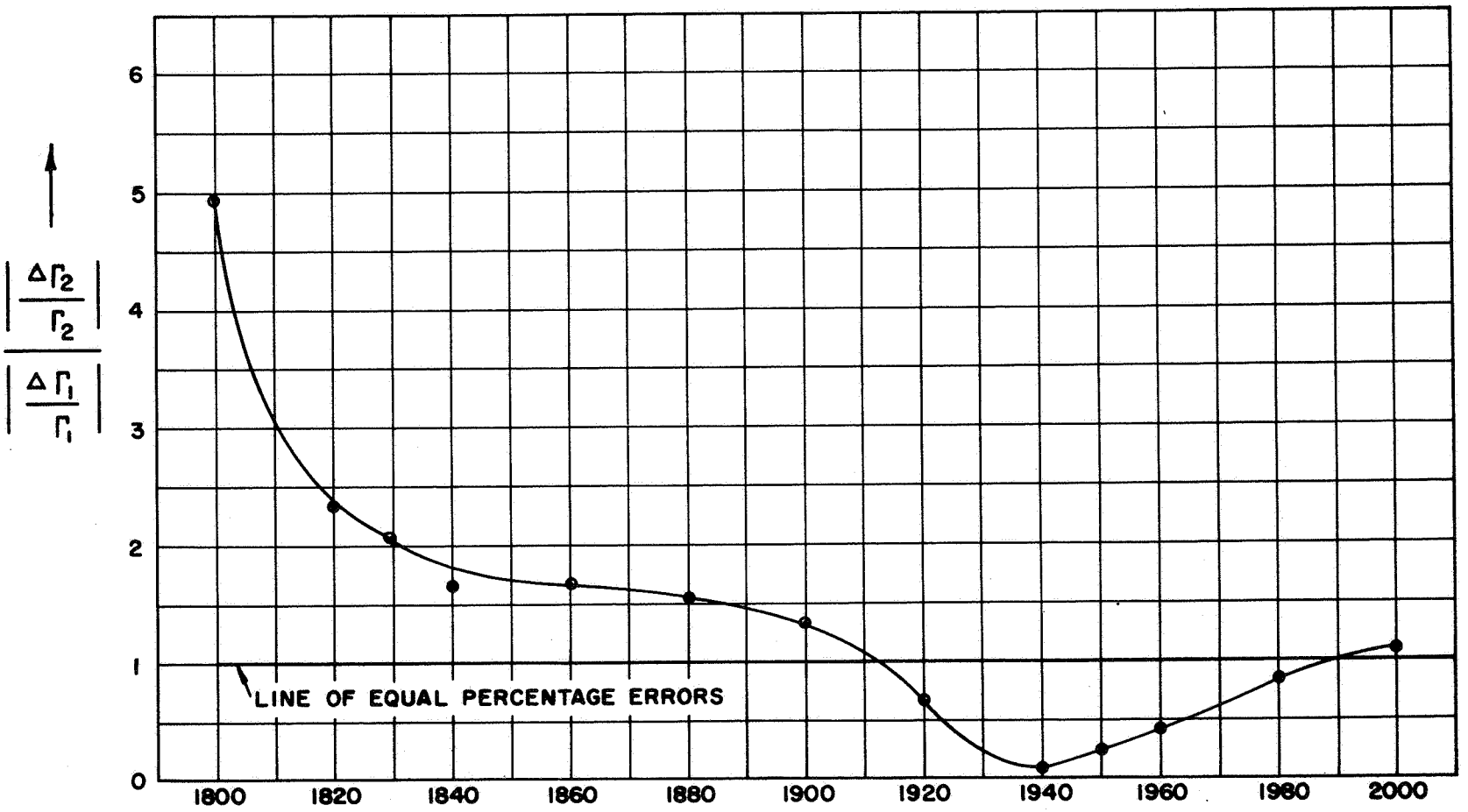

FIG. IX-4 RATIO OF PERCENTAGE ERROR IN Γ_2 (REFLECTION COEFFICIENT IN WAVEGUIDE) TO PERCENTAGE OF ERROR IN Γ_1 (REFLECTION COEFFICIENT IN COAXIAL LINE)

Because of these two factors, it is concluded that only the measurements made in the coaxial line should be used to compare with theory.

APPENDIX X

FORTRAN PROGRAM FOR COMPUTATION OF EXTERNAL ADMITTANCE - NO COATING

a. Formulation of the Problem and Computational Procedure

The program described here approximates the values of two real valued functions, $g_c = G(C)$ and $b_c = B(C)$, for specified values of the independent variable C. These two functions are defined by

$$g_c = G(C) = K_G \cdot \sum_{m=0}^{\infty} A_m \cdot I_{G,m} \tag{1}$$

and

$$b_c = B(C) = K_B \cdot \sum_{m=0}^{\infty} A_m \cdot (I_{1,m} - I_{2,m}). \tag{2}$$

Furthermore,

$$K_G = \frac{8}{\pi \cdot C^4 \cdot \beta^2}, \text{ where } \beta = \frac{\ell}{a}; \tag{3}$$

$$K_B = \frac{4}{C^3 \cdot \beta^2}, \quad \text{where } \beta = \frac{\ell}{a}; \tag{4}$$

$$A_m = \begin{cases} \frac{1}{2} & \text{for } m = 0, \\ \left[\dfrac{\sin\left(\frac{m \cdot \phi_0}{2}\right)}{\left(\frac{m \cdot \phi_0}{2}\right)} \right]^2 & \text{for } m = 1, 2, \ldots; \end{cases} \tag{5}$$

$$I_{G,m} = \int_0^1 F_m (y, C)\, dy; \tag{6}$$

$$I_{1,m} = \int_1^{\infty} E_{1,m} (t, C)\, dt; \tag{7}$$

and

$$I_{2,m} = \int_0^1 F_{2,m} (y, C)\, dy. \tag{8}$$

Using the transformation $y = \frac{1}{t}$, the integral in (7) can be rewritten in the form:

$$I_{l,m} = \int_0^1 F_{l,m}(y, C)\, dy. \tag{7'}$$

The program uses the form (7') to approximate the values of $I_{l,m}$. More detailed information concerning the definition and evaluation of integrand functions is given in Section e of this appendix.

A. The program approximates the values of G(C) by finite sums

$$S_{G,m'} = K_G \cdot \sum_{m=0}^{m'} A_m \cdot Q_{G,m}\ , \tag{9}$$

where:

(i) K_G and A_m are given by (3) and (5), respectively

(ii) $Q_{G,m}$ represents an approximation to $I_{G,m}$;

and

(iii) m' is automatically determined during the execution of the program by the following rule: given the input quantities ε_{SG} and m'_{max}, either m' is the smallest positive integer $m(\leq m'_{max})$ such that

$$|S_{G,m} - S_{G,m-1}| \leq \varepsilon_{SG} \cdot |S_{G,m}| \tag{10}$$

or else $m' = m'_{max}$.

For each m, a recursive version of the Simpson integration scheme is used to approximate the value of $I_{G,m}$ by the finite sequence $Q_{G,m}^{(1)}, Q_{G,m}^{(2)}, \ldots, Q_{G,m}^{(n')}$. The nth approximation $Q_{G,m}^{(n)}$ is based on the subdivision of the basic interval of integration, [0,1], into n subintervals of equal length, $h = 2^{-n}$.

As $h \to 0$, the truncation error of such an approximation is of the order h^4.

For each m, the number $Q_{G,m} = Q_{G,m}^{(n')}$ represents the accepted approximation to $I_{G,m}$. Here, n' is determined automatically using the following rule: either n' is the smallest positive integer $n(\leq n'_{max})$ such that

$$|Q_{G,m}^{(n)} - Q_{G,m}^{(n-1)}| \leq \varepsilon_{IG} \tag{11}$$

or else $n' = n'_{max}$. The numbers ε_{IG} and n'_{max} are input quantities.

B. The values of B(C) are approximated by finite sums

$$S_{B,m''} = K_B \cdot \sum_{m=0}^{m''} A_m \cdot (Q_{1,m} - Q_{2,m});$$

where:

(i) K_B and A_m are given by (4) and (5), respectively;

(ii) $Q_{1,m}$ and $Q_{2,m}$ are approximations of $I_{1,m}$ and $I_{2,m}$, respectively; and

(iii) m" is automatically determined during the execution of the program by the following rule: given the input numbers ε_{SB} and m''_{max}, either m" is the smallest positive integer $m(\leq m''_{max})$ such that

$$|S_{B,m} - S_{B,m-1}| \leq \varepsilon_{SB}|S_{B,m}| \tag{12}$$

or else $m'' = m''_{max}$.

The values of $I_{1,m}$ and $I_{2,m}$ are approximated by $Q_{1,m} = Q_{1,m}^{(n_1)}$ and $Q_{2,m} = Q_{2,m}^{(n_2)}$, respectively, in the same way as the

values of I_G were approximated by $Q_{G,m} = Q_{G,m}^{(n')}$ except that we now use two pairs of controls. The input numbers ε_{I1} and $n_{1,max}$ control the choice of n_1 in $Q_{1,m}^{(n_1)}$. Similarly, ε_{I2} and $n_{2,max}$ are used to determine n_2 in $Q_{2,m}^{(n_2)}$. To remind the reader, $n_{1,max}$ and $n_{2,max}$ are used to determine the lower bounds, $h_1 = 2^{-n_{1,max}}$ and $h_2 = 2^{-n_{2,max}}$, on the discretization step in numerical approximation of $I_{1,m}$ and $I_{2,m}$, respectively.

C. The values of $F_{1,m}(y,C)$ and $F_{2,m}(y,C)$ depend not only on y and C but also on two additional constant parameters, $\beta = (\frac{\ell}{a})$ and ϕ_0. They are called constant parameters because their values are normally $\beta = 2.388$ and $\phi_0 = 0.1687$. Since β and ϕ_0 are input quantities, their values may be modified subject to certain constraints.

b. Organization and Characteristics of the Program

A. The programming language used is FORTRAN IV for the IBM 7094 computer. The program does all computational arithmetic in SP (single precision) floating point mode. All input/output quantities are either integers or SP floating point numbers (i.e., the I- or E-format specifications are used for their conversion, respectively).

B. The program consists of a main program and eleven subroutine type subprograms. The FORTRAN names of the latter are SQIG, SQIB1, SQIB2, SINTGR, FINTGR, BESSK, BEJYM, BESSJZ, BESSJ1, BESSYZ, and BESSY1. The block diagram in Fig. 1 below shows the structural and logical interdependence of these twelve components constituting the program; it also briefly indicates their main functions.

Remark: The latest version of the program contains three subroutine type subprograms not listed above and not shown in the block diagram on the next page. Their FORTRAN names are SABJYM, SABKM, and HMBJYM. All three of them are called by (entered from) the integrand function subprogram FINTGR. The function of these additional subprograms is to evaluate high order and/or small argument expressions formed from the Bessel functions used in computation of the integrand (see Section e). They were added to the program because our regular procedure to do the above mentioned task often led to the floating point overflow.

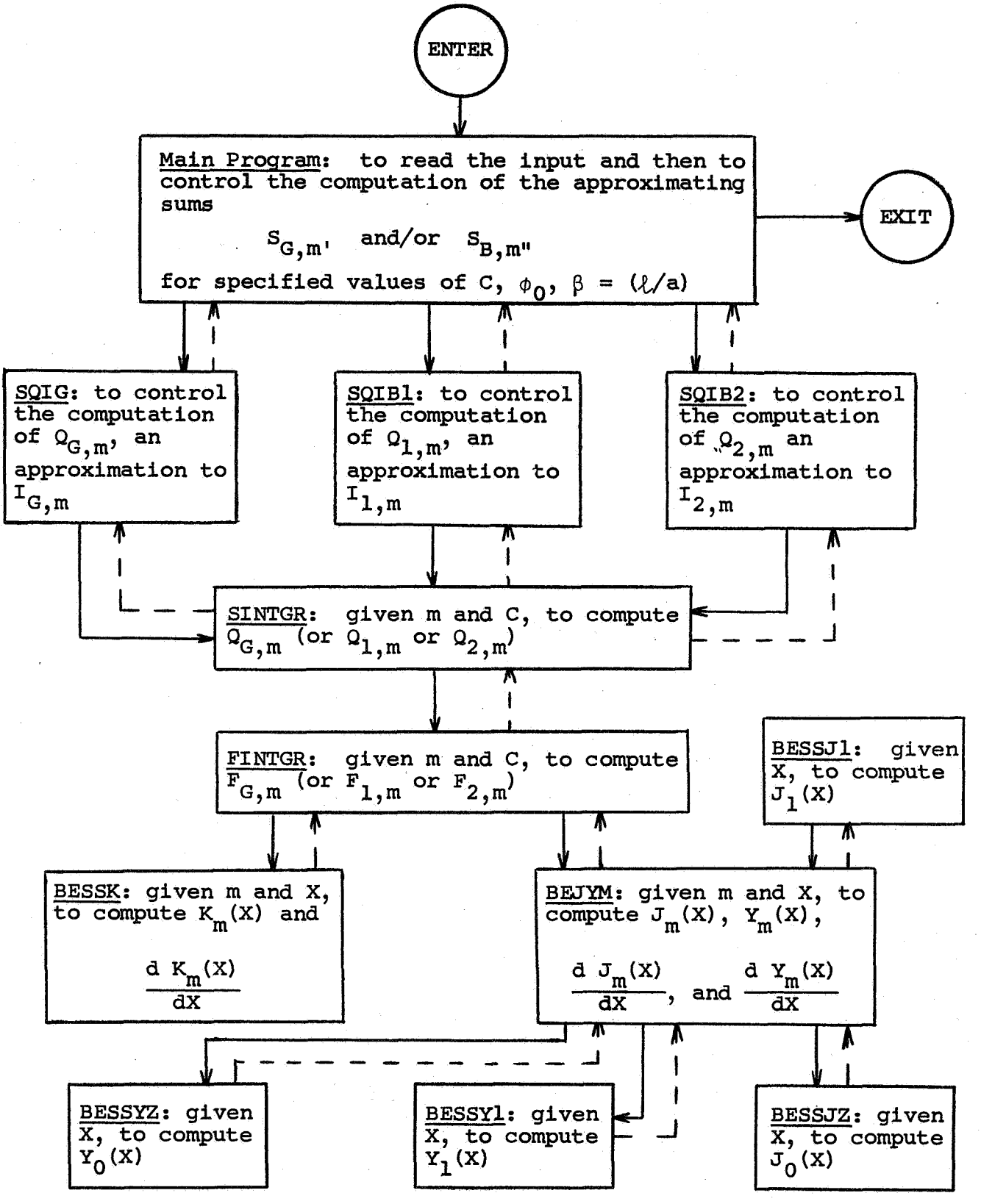

Fig. X-1. Block Diagram of the Program - No Coating

c. Input

A machine job may consist of one or several runs. The input data deck for such a job will then consist of the same number of input data subdecks, one for each run. Each subdeck must always contain the cards no. 1, 2, and 3 (the enumeration of input cards is shown below in format description). The card no. 4 must be present if and only if KG, the flag to compute g_c, is nonzero in the second card. Similarly, the card no. 5 must be present if and only if KB, the flag to compute b_c, is nonzero in the second card.

A. The Format of Input Cards

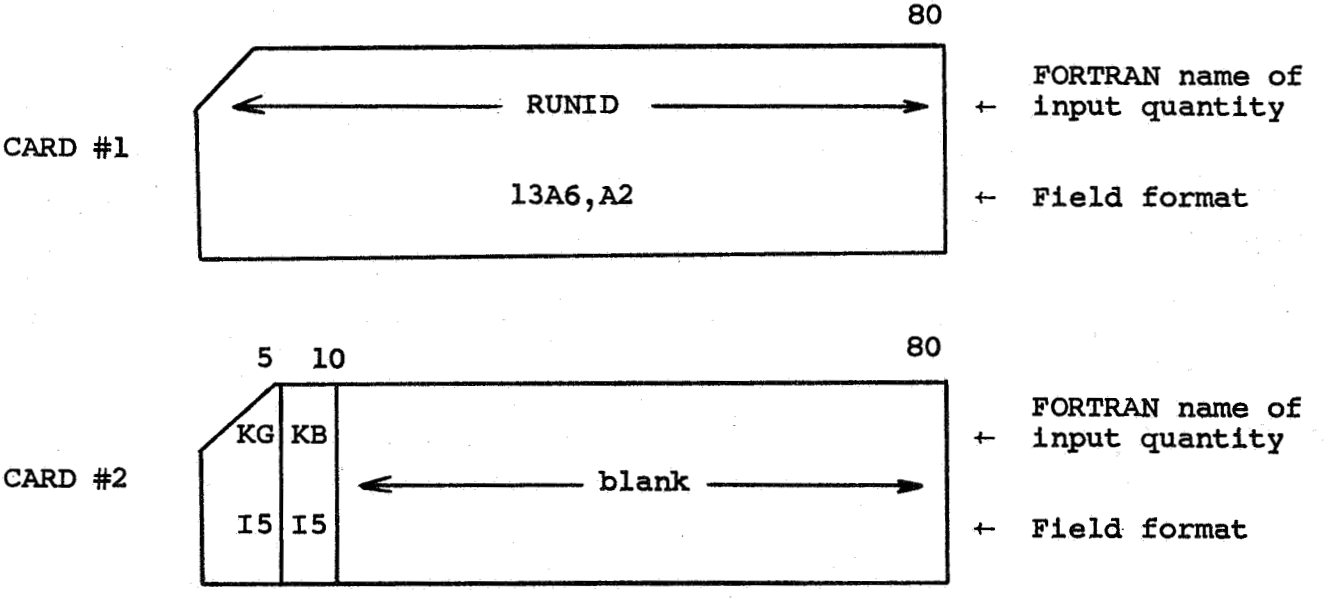

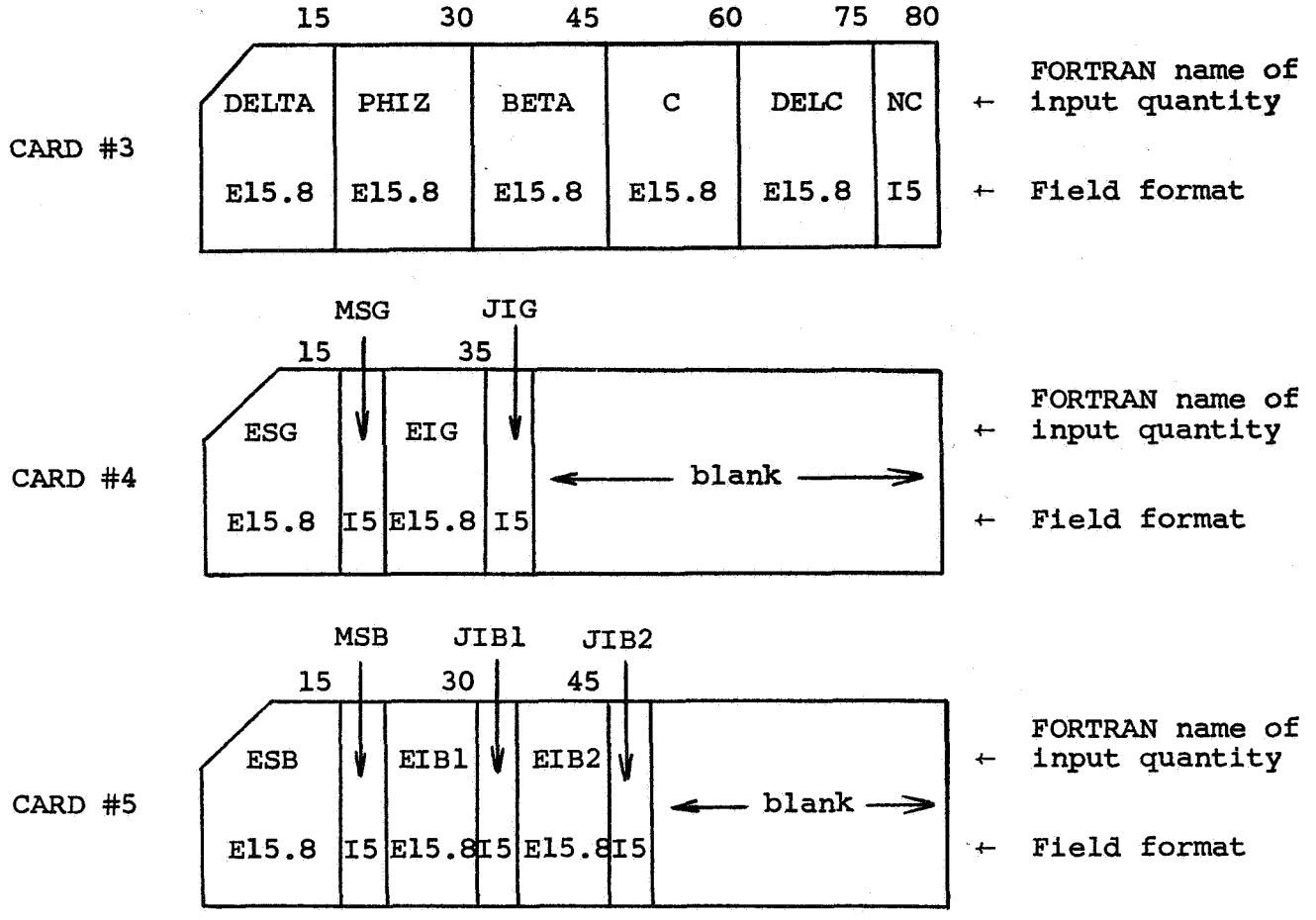

B. Input Quantities and Their Restrictions

CARD #1:

RUNID ← An alphameric message identifying the run; remark: this card may be blank (however, it must be present).

CARD #2

KG ← The g_c-computation control: g_c will be approximated only if KG > 0.

(a) KG = 1 will cause the writing of the basic output only.

(b) KG = 2, in addition to (a), will cause the writing of the term by term computation of the approximating sum.

(c) KG $\geq$ 3, in addition to (a) and (b), will display the details of numerical quadrature process for each term of the approximating sum.

KB ← The b_c-computation control: b_c will be approximated only if KB > 0; further information concerning the usage of positive values of KB can be found above in the explanation of KG (for that purpose merely replace KG by KB and g_c by b_c).

CARD #3:

DELTA ← δ determines the length of the subinterval over which the factor function Q of $F_{G,m}$ (or $F_{2,m}$) will be evaluated by a special procedure (Q contains a removable singularity at an interior point, $y = y_s$, of this subinterval). Warning: use $10^{-5} \leq \delta \leq 10^{-2}$.

PHIZ ← ϕ_0, a physical parameter of the system under analysis (normally, $\phi_0 = 0.1687$).

BETA ← $\beta = (\frac{\ell}{a})$, a physical parameter of the system under analysis (normally, $\beta = 2.388$).

C ← Initial value of C. Warning: C must be ≥ 0.5.

DELC ← ΔC, the increment of C to be used. Warning: ΔC must be > 0.

NC ← n_c, the number of distinct values of C at which g_c and/or b_c should be approximated. Warning n_c must be a positive integer.

CARD #4 (control parameters for approximation of g_c):

ESG ← ε_{SG}, the convergence criterion used to determine m' for approximating sums $S_{G,m'}$. Warning: ε_{SG} must be > 0.

MSG ← m'_{max}, where $m'_{max} + 1$ is the maximum number of terms allowed in $S_{G,m'}$. Warning: m'_{max} must be a positive integer.

EIG ← ε_{IG}, the convergence criterion used to determine the proper number of subintervals in computation of $Q_{G,m}$. Warning: ε_{IG} must be > 0.

JIG ← n'_{max}, where $2^{n'_{max}}$ determines the maximum number of subintervals allowed in computation of $Q_{G,m}$. Warning: n'_{max} must be a positive integer.

CARD #5 (control parameters for approximation of b_c):

ESB ← ε_{SB}, the convergence criterion used to determine m" for approximating sums $S_{B,m"}$. Warning: ε_{SB} must be > 0.

MSB ← $m"_{max}$, where $m"_{max} + 1$ is the maximum number of terms allowed in $S_{B,m"}$. Warning: $m"_{max}$ must be a positive integer.

EIB1 ← ε_{I1}, the convergence criterion used to determine the proper number of subintervals in computation of $Q_{1,m}$. Warning: ε_{I1} must be > 0.

JIB1 ← $n_{1,max}$, where $2^{n_{1,max}}$ determines the maximum number of subintervals allowed in computation of $Q_{1,m}$. Warning: $n_{1,max}$ must be a positive integer.

EIB2 $\leftarrow \varepsilon_{I2}$, the convergence criterion used to determine the proper number of subintervals in computation of $Q_{2,m}$.
Warning: ε_{I2} must be > 0

JIB2 $\leftarrow n_{2,max}$, where $2^{n_{2,max}}$ determines the maximum number of subintervals allowed in computation of $Q_{2,m}$.
Warning: $n_{2,max}$ must be a positive integer.

C. The following values are recommended for control parameters.

(i) For approximation of g_c and/or b_c, set $\delta = 10^{-4}$.

(ii) For approximation of g_c only, set:

$KG = 2$,

$\varepsilon_{SG} = 10^{-5}$,

$m'_{max} = 10$,

$\varepsilon_{IG} = 10^{-6}$,

$n'_{max} = 9$.

(iii) For approximation of b_c only, set:

$KB = 2$,

$\varepsilon_{SB} = 10^{-5}$,

$m''_{max} = 37$,

$\varepsilon_{I1} = 10^{-6}$,

$n_{1,max} = 9$ or 10,

$\varepsilon_{I2} = 10^{-6}$,

$n_{2,max} = 8$ or 9.

Such a choice of control parameters should correctly approximate g_c to 5-6 most significant digits and b_c to 4-6 most significant digits (assuming that the physical parameters $\beta (=\frac{\ell}{a})$ and ϕ_0 have been given with at least the same amount of accuracy). Typically, the approximation of one value of g_c will then take about 0.5 minute and of b_c about 1.5 minutes of the IBM 7094 time. The sum approximating b_c converges much more slowly than that for g_c. In our experimental runs, a choice of $\varepsilon_{SG} = 10^{-5}$ always caused the approximating sum $S_{G,m'}$ to converge with $m' = 5$. On the other hand, the recommended choice of control parameters for approximation of b_c required the computation of about 35 terms.

The reader should be warned that an improper combination of control parameters may easily lead to a very poor accuracy or an excessive amount of computing time required.

d. Output

Next we shall explain the labels appearing in the output listing of the program. The intermediate output of the numerical quadrature subroutine SINTGR which is written only when the value of the KG- or KB-control signal is ≥ 3 has not been included here: a display of this output was needed to debug the program and find proper values for control parameters. Thus it is of little interest to a typical user of the program.

A. Input quantities used by both parts of the program:

KG : the g_c-computation control flag;

KB : the b_c-computation control flag;

DELTA : δ, a control parameter;

PHIZ : ϕ_0;

BETA : $\beta = \frac{\ell}{a}$;

C : C;

DELC : ΔC;

NC : n_c.

B. The output written by the g_c-part of the program can be classified as follows: (1) the g_c-input (written if KG $\geq$ 1); (2) preliminary output (written for each value of C if KG $\geq$ 1); (3) final output (written, if KG $\geq$ 1, for each value of C after computing the corresponding approximation of g_c); and (4) intermediate output (written, if KG $\geq$ 2, for every new term of the sum approximating g_c/K_G).

B.1. The g_c-input:

ESG : ε_{SG};

MSG : m'_{max};

EIG : ε_{IG};

JIG : n'_{max}.

B.2. Preliminary output:

C1 : $C \cdot \beta$, where $\beta = \frac{\ell}{a}$;

C2 : $C \cdot \beta/2$;

YS : $y_S = \pi/(C \cdot \beta)$, the point of removable singularity in the factor Q of the integrand function;

C3 : y_S^2;

CG : $K_G = 8/(\pi . C^4 . \beta^2)$;

YA : y_a } (i) $y_a < y_S < y_b$ and (ii) Q is evaluated
YB : y_b } by a special procedure over the interval $y_a \leqq y \leqq y_b$;

DELY : Δy, a quantity used in determination of y_a and y_b.

B.3. Final output:

C : the value of C for which g_c has been approximated by $S_{G,m'}$;

G(C) : $S_{G,m'}$;

ERR : $S_{G,m'} - S_{G,m'-1}$;

RERR : $(S_{G,m'} - S_{G,m'-1})/S_{G,m'}$;

M : m', where m'+1 is the total number of terms used to evaluate $S_{G,m'}$.

B.4. Intermediate Output:

M : the value of the term subscript m, where m + 1 is the number of terms in the partial sum $\bar{S}_{G,m} = S_{G,m}/K_G$;

SG : $\bar{S}_{G,m}$;

ERR : $\bar{S}_{G,m} - \bar{S}_{G,m-1}$;

RERR : $(\bar{S}_{G,m} - \bar{S}_{G,m-1})/\bar{S}_{G,m}$;

AM : A_m;

QIG : $Q_{G,m}$.

C. The written output of the b_c-part of the program can be classified into: (1) the b_c input (written if KB $\geq$ 1); (2) preliminary output (written for each new value of C if KB $\geq$ 1); (3) final output (written, if KB $\geq$ 1, for each value of C after computing the corresponding approximation of b_c); and (4) intermediate output (written, if KB $\geq$ 2, for every new term of the sum approximating b_c/K_B).

C.1. The b_c-input:

ESB : ε_{SB};

MSB : m''_{max};

EIB1 : ε_{I1};

JIB1 : $n_{1,max}$;

EIB2 : ε_{I2};

JIB2 : $n_{2,max}$;

C.2. Preliminary output:

C1 : $C \cdot \beta$, where $\beta = \frac{\ell}{a}$;

C2 : $C \cdot \beta/2$;

YS : $y_s = \pi/(C \cdot \beta)$, the point of removable singularity in the factor Q of the integrand in $I_{2,m}$;

C3 : y_s^2;

CB : $K_B = 4/(C^3 \cdot \beta^2)$;

YA : y_a } (i) $y_a < y_s < y_b$ and (ii) Q is evaluated by a special procedure over the interval $y_a \leq y \leq y_b$;
YB : y_b }

DELY : Δy, a quantity used in determination of y_a and y_b.

C.3. Final output:

C : the value of C for which b_c has been approximated by $S_{B,m''}$;

B(C) : $S_{B,m''}$;

ERR : $S_{B,m''} - S_{B,m''-1}$;

RERR : $(S_{B,m''} - S_{B,m''-1})/S_{B,m''}$.

B.4. Intermediate output:

M : the value of the term subscript m, where m + 1 is the number of terms in the partial sum $\bar{S}_{B,m} = S_{B,m}/K_B$;

SB : $\bar{S}_{B,m}$;

ERR : $\bar{S}_{B,m} - \bar{S}_{B,m-1}$;

RERR : $(\bar{S}_{B,m} - \bar{S}_{B,m-1})/\bar{S}_{B,m}$;

AM : A_m;

QIB1 : $Q_{1,m}$;

QIB2 : $Q_{2,m}$;

QIB : $Q_{1,m} - Q_{2,m}$.

e. Computation of Integrand Functions

1. The function $F_m(y, C)$ used in

$$I_{G,m} = \int_0^1 F_m(y, C)\, dy \tag{13}$$

is defined by

$$F_m(y, C) = \frac{Q^2}{[(J_m'(X))^2 + (Y_m'(X))^2]} ; \tag{14}$$

where:

$$Q = \begin{cases} \dfrac{\cos[\frac{C}{2}\cdot\beta\cdot y]}{y^2 - (\pi/C\cdot\beta)^2} & \text{if } y < y_a \text{ or } y > y_b \\ -\dfrac{(\frac{C}{2}\cdot\beta)^2}{\pi} & \text{if } y_a < y < y_b, \end{cases} \tag{15}$$

$$X = C \cdot \sqrt{1-y^2} , \tag{16}$$

and

$$J_m'(X) = \frac{dJ_m(X)}{dX} \quad \text{and} \quad Y_m'(X) = \frac{dY_m(X)}{dX} . \tag{17}$$

Remarks:

(a) $\beta = \frac{\ell}{a}$,

(b) y_a and y_b are the computed end points of a special interval such that $y_a < y_s < y_b$, where $y_s = \frac{\pi}{C\cdot\beta}$.

In the program, $F_m(y, C)$ is then evaluated by the following formula:

$$F_m(y, C) = \begin{cases} 0 & \text{if } X = 0 \\ Q^2/[(J_m'(X))^2+(Y_m'(X))^2] & \text{if } X > 0. \end{cases} \quad (18)$$

2. The function $F_{2,m}(y, C)$ appearing in

$$I_{2,m} = \int_0^1 F_{2,m}(y, C) \quad (19)$$

is defined by

$$F_{2,m}(y, C) = \frac{(\sqrt{1-y^2}) \cdot Q^2 \cdot [J_m(X) \cdot J_m'(X)+Y_m(X) \cdot Y_m'(X)]}{[(J_m'(X))^2+(Y_m'(X))^2]}; \quad (20)$$

where Q, X, $J_m'(X)$, and $Y_m'(X)$ are given by the equations (15) through (17).

The following formula is used to evaluate $F_2(y, C)$ in the program:

$$F_{2,m}(y, C) = \begin{cases} 0 & \text{if } X = 0 \\ Q^2 \cdot [(\sqrt{1-y^2} \cdot Y_m(X))/Y_m'(X)] \cdot [(1+N_m(X))/(1+D_m(X)] & \text{if } X > 0. \end{cases} \quad (21)$$

Here,

$$N_m(X) = \left[\frac{J_m(X)}{Y_m(X)}\right] \cdot \left[\frac{J_m'(X)}{Y_m'(X)}\right] \quad (22)$$

and

$$D_m(X) = \left[\frac{J_m'(X)}{Y_m'(X)}\right]^2 . \quad (23)$$

3. The function $F_{l,m}(y, C)$ appearing in

$$I_{l,m} = \int_1^{\infty} E_{l,m}(t,C)\,dt = \int_0^1 F_{l,m}(y, C)\,dy \tag{24}$$

is defined (after the transformation $t = \frac{1}{y}$) by

$$F_{l,m}(y, C) = (y\sqrt{1-y^2})\cdot\bar{Q}^2\cdot\frac{K_m(\bar{X})}{K_m'(\bar{X})}\,, \tag{25}$$

where:

$$\bar{X} = \frac{C}{y}\cdot\sqrt{1-y^2}\,, \tag{26}$$

$$K_m'(\bar{X}) = \frac{d\,K_m(\bar{X})}{d\bar{X}}\,, \tag{27}$$

$$y_S = \frac{\pi}{C\cdot\beta} \tag{28}$$

and

$$\bar{Q} = \frac{\cos[\frac{C}{2}\cdot\beta\cdot\frac{1}{y}]}{1-(y\cdot y_S)^2}\,. \tag{29}$$

The following procedure is then used to evaluate $F_{l,m}(y, C)$ in the program:

$$F_{l,m}(y, C) = \begin{cases} 0 & \text{if } y = 1 \\ \bar{Q}^2\cdot[(y\sqrt{1-y^2})\cdot(\frac{K_m(\bar{X})}{K_m'(\bar{X})})] & \text{if } y > 1. \end{cases} \tag{30}$$

The procedure to evaluate $[(y\sqrt{1-y^2})\cdot(K_m(\bar{X})/K_m'(\bar{X})]$ depends on the values of m and $\bar{X}$.

APPENDIX XI

FORTRAN PROGRAM FOR COMPUTATION OF EXTERNAL CONDUCTANCE - TEFLON COATING

a. Formulation of the Problem and Computational Procedure

A. The values of the external conductance function

$$G(C,W) = K(C,\beta) \cdot \sum_{m=0}^{\infty} A_m \cdot I_m$$

are approximated by finite sums

$$S_M = K(C, \beta) \cdot \sum_{m=0}^{M} A_m \cdot Q_m,$$

where:

(i) $K(C, \beta) = \frac{32}{\pi^3 C^4 \beta^2}$,

(ii) $A_m = \begin{cases} \frac{1}{2} & \text{for } m = 0 \\ \left[\frac{\sin(\frac{m\phi_0}{2})}{(\frac{m\phi_0}{2})}\right]^2 & \text{for } m = 1, 2, \ldots , \end{cases}$

and

(iii) Q_m is a numerical approximation to

$$I_m = \int_0^1 F_m (y; C, W)\, dy.$$

The reader is referred to APPENDIX A for details concerning the integrand function F_m. We shall mention here, however, that the value of $F_m(y; C, W)$ depends not only on y, C, W but also on three additional constant parameters, $\beta (= \frac{\ell}{a})$, ϕ_0, and ε_r. Thus, to be more precise, G(C, W) and S_m are functions of

(i) the variable parameters C, W

and

(ii) the constant parameters β, ϕ_0, and ε_r. Normally, the values of the parameters belonging to class (ii) will be:

$$\beta = 2.388, \quad \phi_0 = 0.1687, \quad \text{and } \varepsilon_r = 2.10.$$

Since they have to be specified as input quantities anyway, their values may be modified by the user as explained in Section III.

B. M, the number of terms in the approximating sum S_M, is automatically determined during the execution of the program as follows: given the input quantities ε_S (> 0) and m_{max}, the number M is either the smallest positive integer m ($\leqq m_{max}$) such that

$$|S_m - S_{m-1}| \leqq \varepsilon_S \cdot r,$$

where

$$r = \begin{cases} 1 & \text{if } |S_m| \leqq 1 \\ |S_m| & \text{if } |S_m| > 1, \end{cases}$$

or else, if the above convergence criterion fails for $m \leqq m_{max}$, $M = m_{max}$.

C. A recursive version of the Simpson rule based on an incomplete Romberg integration scheme [27] is used to approximate the integral I_m for each value of m by a sequence of numbers $Q_m^{(1)}$, $Q_m^{(2)}$,.., $Q_m^{(N)}$. The nth approximation, $Q_m^{(n)}$, is based on the subdivision of the basic interval of

integration, [0, 1], into 2^n subintervals of equal length, $h = 2^{-n}$. As $h \to 0$, the truncation error of such an approximation is of the order of h^4.

For each m, the element $Q_m^{(N)}$ is accepted as the final approximation to I_m, where N is determined automatically as follows: either N is the smallest positive integer n, $n_{min} + 1 \leq n \leq n_{max}$, such that

$$|Q_m^{(n)} - Q_{m-1}^{(n-1)}| \leq \varepsilon_I$$

or else, in case of a convergence failure, N is set equal to n_{max}. The numbers n_{min}, n_{max}, and ε_I are input quantities.

D. Each evaluation of the integrand $F_m(y; C, W)$ requires several evaluations of the Bessel functions $J_m(X)$ and $Y_m(X)$, and of their derivatives w.r. to X, $J_m'(X)$ and $Y_m'(X)$. Here X is a function of y and several input parameters. For that purpose, double precision subroutines BESS, BESJ, and BESY have been developed. To evaluate $J_m(X)$ and $Y_m(X)$, they use numerical methods similar to those discussed in reference [28]. The derivatives of the Bessel functions $J_m(X)$ and $Y_m(X)$ are then computed by the recursive formulas

$$J_m'(X) = -J_{m+1}(X) + \frac{m}{X} \cdot J_m(X) \quad \text{for } m = 0, 1, \ldots$$

and

$$Y_m'(X) = -Y_{m+1}(X) + \frac{m}{X} \cdot Y_m(X) \quad \text{for } m = 0, 1, \ldots .$$

The subroutines BESS, BESJ, and BESY were checked out independently from the main program for all ranges of the values of m and x used in the computation of G(C, W). The results agreed with tabulated values, [22], through 7-8 most significant digits.

b. Organization and Characteristics of the Program

A. The program was written using FORTRAN IV for the IBM 7094 computer. All computational arithmetic is internally handled in DP (= double precision) floating point mode. All input/output quantities are either integers or DP floating point numbers (i.e., the I- or D- format specifications are used for their conversion, respectively).

B. The program consists of a main program and six subroutine type subprograms whose FORTRAN names are: ERRX, SINTGR, FINTGR, BESS, BESJ, and BESY.

The block diagram below shows the structure and logical interdependence of the program and explains briefly the function of each subprogram.

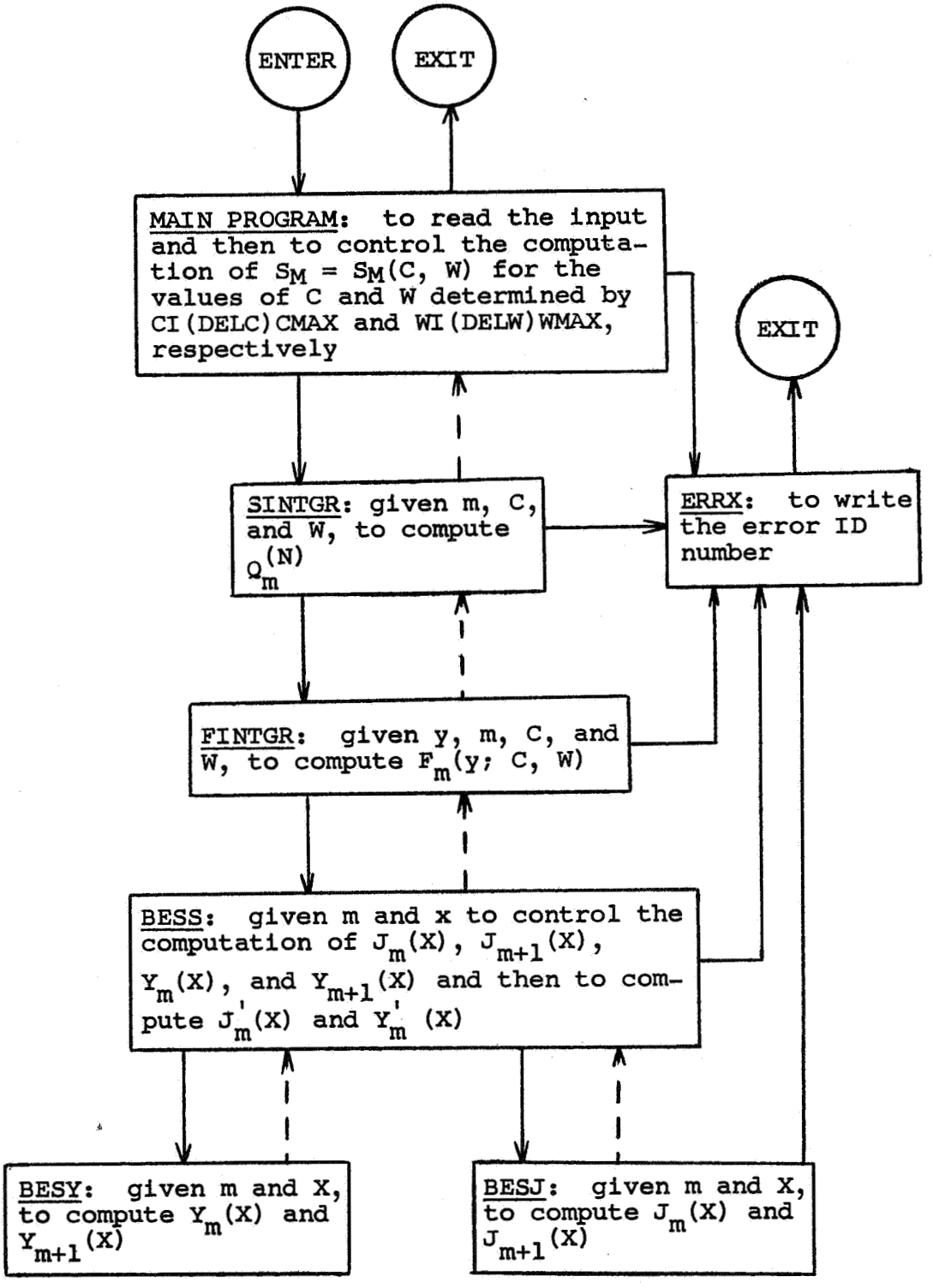

Fig. XI-1. Block Diagram of the Program - Coating

c. Input and Usage

A machine job may consist of one or several runs. Thus the input data deck must contain the corresponding number of input data subdecks, one for each run. Each subdeck consists of five cards.

A. The Format of Input Cards

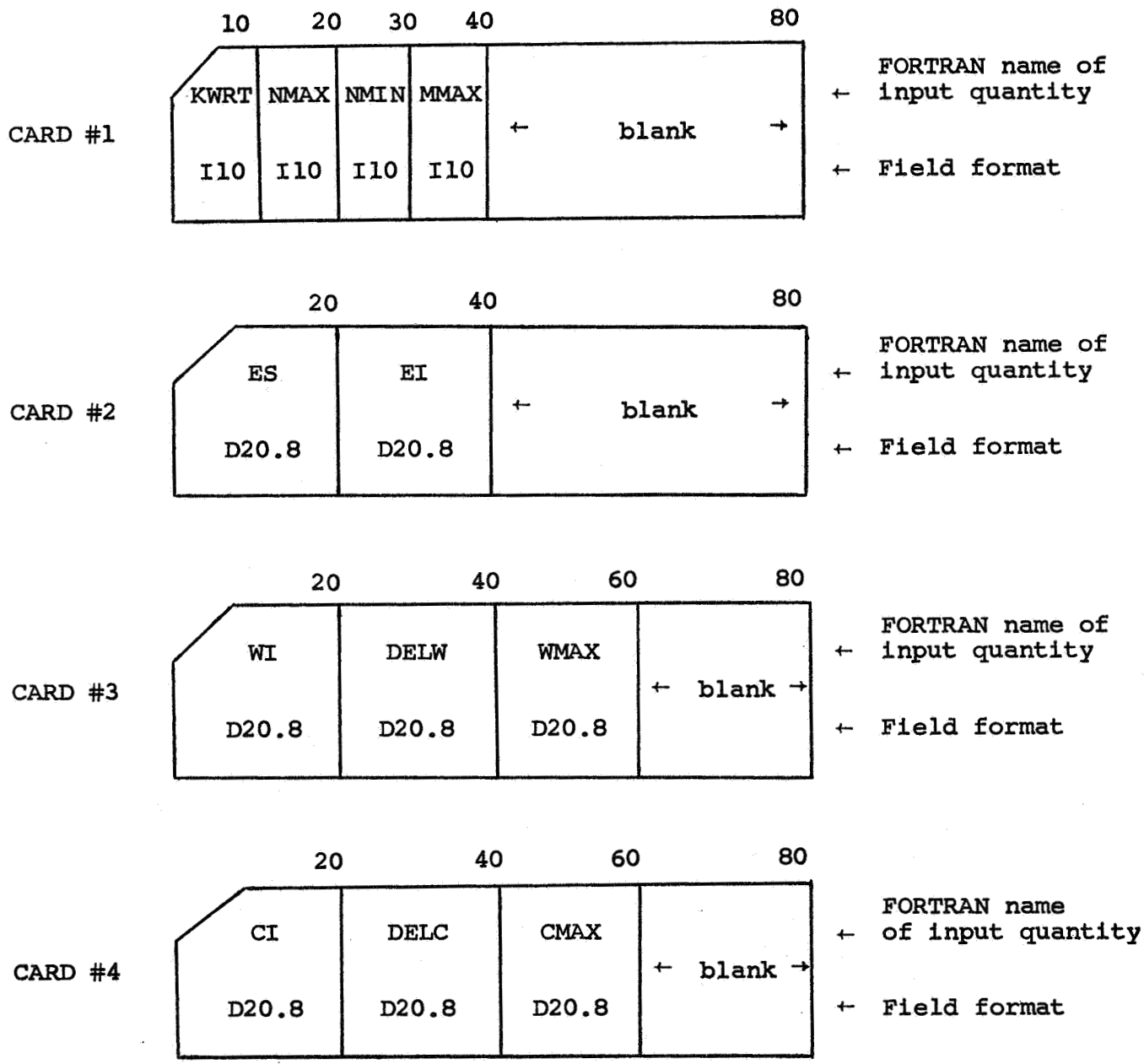

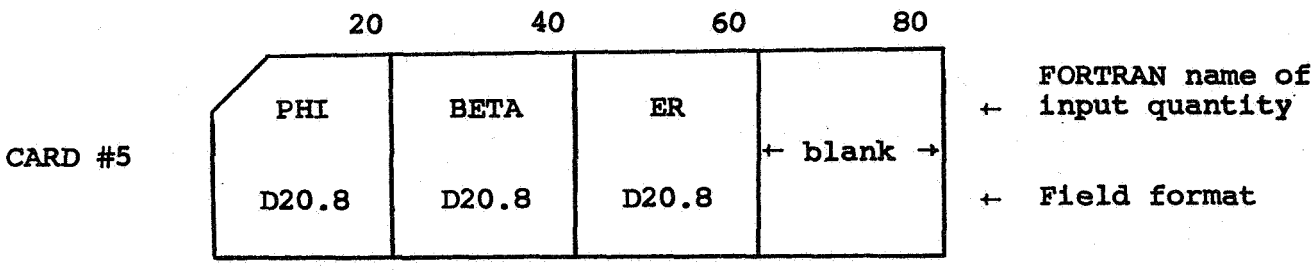

B. Input Quantities and Their Restrictions

The input cards # 1 and 2 contain the program execution controls; the cards # 3, 4, and 5 contain parameters used in the computation of G(C, W).

CARD #1:

KWRT ← the write-control flag:

(a) KWRT = 0 will cause the writing of the basic output only;

(b) KWRT = 1, in addition to (a), will cause the writing of the numerical quadrature convergence process.

(c) KWRT = 2, in addition to (a) and (b), will display the details of the computation of the integrand function, F_m, for each (y, C, W).

NMAX ← n_{max} is used to define $h_{min} = 2^{-n_{max}}$, the smallest permissible subinterval for numerical quadrature. Warning: if n_{max} is < 5, it will be automatically corrected to 5.

NMIN ← n_{min} is used to define $h_{max} = 2^{-(n_{min}+1)}$, the largest permissible subinterval for numerical quadrature. Warning: if n_{min} is < 2, it will be automatically corrected to 2.

MMAX ← m_{max}, where m_{max} + 1 is the largest permissible number of terms in S_M. Warning: m_{max} must be $\geq$ 1.

CARD #2:

ES ← ε_S, the convergence criterion for the approximations S_1, S_2,... of G(C, W). Warning: ε_S must be > 0.

EI ← ε_I, the convergence criterion for the approximations $Q_m^{(1)}$, $Q_m^{(2)}$,... of I_m. Warning: ε_I must be > 0.

CARD #3:

WI ← W_I, the initial (smallest) value of W. Warning: W_I must be $\geq$ 0.5.

DELW ← ΔW, the increment of W to be used. Warning: ΔW must be > 0.

WMAX ← W_{max}, the last (largest) value of W. Warning: W_{max} must be $\geq$ W_I.

CARD #4:

CI ← C_I, the initial (smallest) value of C. Warning: C_I must be $\geq$ 0.5.

DELC ← ΔC, the increment of C to be used. Warning: ΔC must be > 0.

CMAX ← C_{max}, the last (largest) value of C. Warning: C_{max} must be $\geq$ C_I.

CARD #5:

PHI $\leftarrow \phi_0$; warning: ϕ_0 must be > 0.

BETA $\leftarrow \beta = (\frac{\ell}{a})$; warning: β must be > 0.5.

ER $\leftarrow \varepsilon_r$ must be $\geqq$ 1.05.

Furthermore, the values of C, W, and ε_r must always satisfy the following constraints:

(a) $0 < CW \leqq 4$,

(b) $0 < CW \sqrt{\varepsilon_r} \leqq 4$,

(c) $0 < C \sqrt{\varepsilon_r} \leqq 4$;

otherwise, the subroutine BESY (in its present form) will fail.

C. The following values are recommended for the control:

the write-control flag KWRT = 0 or 1,

$n_{max} = 9$ or 10,

$n_{min} = 3$,

$m_{max} = 10$,

$\varepsilon_I = 10^{-6}$ or 10^{-5}, and

$\varepsilon_S = 10^{-5}$.

Such a choice of control parameters should approximate G(C, W) correctly to 5-6 most significant digits (assuming that the physical parameters $\beta = (\ell/a)$, ϕ_0, and ε_r have been given with at least the same degree of accuracy). Typically, the computation of a value of G(C, W) will then require one to three minutes of computer time.

The user is warned to be careful about modifying the values of n_{max} and ε_I. Since the number of integration subintervals in the approximation of I_m may be equal up to $2^{n_{max}}$, a slight increase in n_{max} may result in an excessive increase of computing time. On the other hand, making ε_I too small may cuase a frequent usage of $2^{n_{max}}$ subintervals in numerical integration.

In our experimental runs, $\varepsilon_S = 10^{-5}$ caused the sums S_m to converge at m = 6 for all combinations of other parameters.

D. Compliance with the input constraints listed above should always terminate the execution of the program in a normal exit. In the event that the execution terminated in one of the error exits identified by its ID number, the user is advised to localize (in the listing of the source program) the statement causing the transfer of control to the error exit subprogram ERRX. This can be done by noting that ERRX is called by

```
CALL ERRX(K),
```

where K is the ID number of the error: the value of K is always written in an error message.

d. Output

Next we shall explain the labels appearing in the output listing of the program. Such a label often but not always is the FORTRAN name of the variable whose value appears under it. Output quantities additionally written when the write-control flag KWRT is ≥ 2 are not discussed below: a user normally should not apply KWRT ≥ 2 since this results in an excessive amount of written output.

A. Preliminary output quantities (always written following the listing of the input):

C1 : $C \cdot \beta$, where $\beta = \frac{\ell}{a}$;

C2 : $\frac{C}{2} \cdot \beta$;

YS : $y_S = \frac{\pi}{C \cdot \beta}$, the value of y at which the factor Q of the integrand function $F_m(y; C, W)$ has a removable singularity;

YSL: $\max(0, y_S - \delta)$, where δ is a programmed parameter;

YSR: $\min(1, y_S + \delta)$, where δ is the same programmed parameter as in YSL;

C3 : y_S^2;

CG : $K(C, \beta) = 32/(\pi^3 C^4 \beta^2)$;

C4 : $\varepsilon_r - 1$;

C5 : $(C \cdot W)^2$

C6 : $(\varepsilon_r - 1)^2$;

QS : $-(C \cdot \beta/2)^2/\pi$, the value of Q at $y = y_S$;

CW : $C \cdot W$.

B. Intermediate output after the computation of the mth term (written under any value of KWRT for m = 0, 1, 2,...,M):

M : m, where m + 1 is the number of terms in the current approximation, $\bar{S}_m$, to $G(C, W)/K(C, \beta)$;

SG : $\bar{S}_m = \frac{S_m}{K(\beta,C)}$, the current approximation to $G(C, W)/K(C, \beta)$;

AM : A_m, the coefficient of the last term of $\bar{S}_m$;

QI : $Q_m = Q_m^{(N)}$, the approximation to I_m used in the last term of $\bar{S}_m$;

ERR : $\bar{S}_m - \bar{S}_{m-1}$;

RERR : $(\bar{S}_m - \bar{S}_{m-1})/\bar{S}_m$.

C. Final output after computation of an approximation to G(C, W) for given C and W (written under any value of KWRT):

G(C,W) : S_M, the accepted approximation to G(C, W);

C : the value of C used in the computation of S_M;

W : the value of W used in the computation of S_M;

M : M, where M + 1 is the total number of terms in S_M;

ERR : $S_M - S_{M-1}$;

RERR : $(S_M - S_{M-1})/S_M$.

C. Intermediate output of the numerical quadrature subroutine SINTGR after the computation of the nth approximation to I_m (written only under KWRT $\geq$ 1 for each m and all n = 1, 2,...,N):

N : the current value of n;

1./2.**N : $(\frac{1}{2})^n$, the length of the subinterval corresponding to the current value of n;

TRAPZ : $T_m^{(n)}$, the trapezoidal approximation to I_m for the current value of n;

ERR(TRAPZ) : $T_m^{(n)} - T_m^{(n-1)}$;

SIMPS : $Q_m^{(n)}$, the Simpson approximation to I_m for the current value of n;

ERR(SIMPS) : $Q_m^{(n)} - Q_m^{(n-1)}$.

e. Computation of the Integrand Function $F_m(y, C, W)$

A proper procedure (computational algorithm) to evaluate I_m is a necessary condition for a successful approximation of $G(C, W)$. We shall outline briefly the procedure used by us for that purpose: its main objective is to depress the accumulation of round-off errors and to navigate around possible floating point overflows.

In order to simplify the notation, we shall omit subscripts, superscripts, and arguments wherever clarity will allow us to do that. In this respect we are somewhat aided by the fact that each evaluation of $F_m(y; C, W)$ is carried out for a given and fixed set of numbers m, y, C, W, ϕ_0, $\beta(=\frac{\ell}{a})$, and ε_r.

In the program we use the following computational procedure to evaluate $F_m(y; C, W)$:

$$F = ((A_3 \cdot Q^2) \cdot (\frac{F_N}{F_D})) \cdot \frac{1}{S^2} \cdot \tag{1}$$

First,

$$Q = \begin{cases} (\dfrac{\cos(\frac{C}{2} \cdot \beta \cdot y)}{y + y_S}) \cdot (\dfrac{1}{y - y_S}) & \text{if } |y-y_S| > \delta \\ -(\dfrac{C \cdot \beta}{2})^2 \cdot \dfrac{1}{\pi} & \text{if } |y-y_S| \leq \delta \end{cases} \tag{2}$$

where:

$$y_S = \frac{\pi}{C \cdot \beta}, \quad \beta = \frac{\ell}{a}, \tag{3}$$

and δ is a programmed parameter (its FORTRAN name is DELTA) which has been set equal to 10^{-3}.

Next,

$$S = \begin{cases} |Y'| \cdot \sqrt{\left(\frac{J'}{Y'}\right)^2 + 1} & \text{if } |J'| \leq |Y'| \\ |J'| \cdot \sqrt{\left(\frac{Y'}{J'}\right)^2 + 1} & \text{if } |J'| > |Y'| \end{cases} \tag{4}$$

where:

$$J = J_m(X),\ Y = Y_m(X),\ X = CW\sqrt{1-y^2} \tag{5}$$

and

$$J' = \frac{d\ J_m(X)}{dX}, \quad Y' = \frac{d\ Y_m(X)}{dX}\ . \tag{6}$$

The eight A-expressions, including A_3 used above in F, must be evaluated at the beginning of the procedure for computing F. They are defined as follows:

$$A_1 = \varepsilon_r - y^2;$$

$$A_2 = 1 - y^2;$$

$$A_3 = (\varepsilon_r - y^2) \cdot (1 - y^2);$$

$$A_4 = \varepsilon_r \sqrt{1 - y^2}$$

$$A_5 = \sqrt{\varepsilon_r - y^2}\ ;$$

$$A_6 = \sqrt{1 - y^2}\ ;$$

$$A_7 = (m \cdot y \cdot (\varepsilon_r - 1))^2;$$

$$A_8 = (C \cdot W)^2 \cdot A_3.$$

Finally,

$$F_N = A_8 \cdot (E_1^2 + E_2^2) + E_7 \tag{7}$$

and

$$F_D = [A_8 \cdot (E_1 \cdot E_3 - E_2 \cdot E_4) - E_5]^2 + [A_8 (E_1 \cdot E_4 + E_2 \cdot E_3) - E_6]^2; \tag{8}$$

where:

$$E_1 = A_4 \cdot \bar{U} \cdot (\frac{J}{S}) - A_5 \cdot \bar{V} \cdot (\frac{J'}{S}),$$

$$E_2 = A_4 \cdot \bar{U} \cdot (\frac{Y}{S}) - A_5 \cdot \bar{V} \cdot (\frac{Y'}{S}),$$

$$E_3 = A_6 \cdot \bar{T} \cdot (\frac{J}{S}) - A_5 \bar{L} \cdot (\frac{J'}{S}),$$

$$E_4 = A_6 \cdot \bar{T} \cdot (\frac{Y}{S}) - A_5 \bar{L} \cdot (\frac{Y'}{S}),$$

$$E_5 = A_7 \cdot \bar{V} \cdot \bar{L} \cdot [(\frac{J}{S})^2 - (\frac{Y}{S})^2], \text{ and}$$

$$E_6 = A_7 \cdot \bar{V} \cdot \bar{L} \cdot [2 \cdot (\frac{J}{S}) \cdot (\frac{Y}{S})] .$$

In the E-expressions above, the quantities S, J, Y, J', Y' have already been defined earlier by (4), (5), and (6). Thus, it remains to define $\bar{U}$, $\bar{V}$, $\bar{L}$, and $\bar{T}$. They are:

$$\bar{U} = J_m(\frac{Z}{W}) \cdot Y_m'(z) - J_m'(z) \cdot Y_m(\frac{Z}{W}) ,$$

$$\bar{V} = J_m(\frac{Z}{W}) \cdot Y_m(z) - J_m(z) \cdot Y_m(\frac{Z}{W}) ,$$

$$\bar{L} = J_m(z) \cdot Y_m'(\frac{Z}{W}) - J_m'(\frac{Z}{W}) \cdot Y_m(z) , \text{ and}$$

$$\bar{T} = J_m'(z) \cdot Y_m'(\frac{Z}{W}) - J_m'(\frac{Z}{W}) \cdot Y_m'(z) ;$$

where:

$$z = CW\sqrt{\varepsilon_r - y^2} \ .$$

In the expressions above, a prime denotes differentiation with respect to the entire argument within the parentheses.

APPENDIX XII

FORTRAN PROGRAM FOR SCATTERING MATRIX EQUATION

a. Computation of Γ_1 from Γ_2, S_{11}, S_{12}, and S_{22}, via

$$\Gamma_1 = S_{11} + \frac{S_{12}^2 \Gamma_2}{1 - S_{22}\Gamma_2} .$$

```
B6. +READY          LIST
 101. =       CF    PROGRAM GAMMA1
 102. =           1 CONTINUE
 103. =       CF    READ 0,SM11,SA11,SM12,SA12,SM22,SA22
 104. =       CF    READ 0,GM2,GA2
 105. =             PI=3.141593
 106. =             ARB=180.0/PI
 107. =             SA11=SA11/ARB
 108. =             SA12=SA12/ARB
 109. =             SA22=SA22/ARB
 110. =             GA2=GA2/ARB
 111. =             AR=SM22*COS(SA22)*GM2*COS(GA2)-SM22*SIN(SA22)*GM2*SIN(GA2)
 112. =             AI=SM22*COS(SA22)*GM2*SIN(GA2)+SM22*SIN(SA22)*GM2*COS(GA2)
 113. =             AM=SQRT(AI*AI+AR*AR)
 114. =             AA=ATAN2(AI,AR)
 115. =             BR=1.-AM*COS(AA)
 116. =             BI=-(AM*SIN(AA))
 117. =             BM=SQRT(BR*BR+BI*BI)
 118. =             BA=ATAN2(BI,BR)
 119. =             CM=SM12*SM12
 120. =             CA=2.*SA12
 121. =             DR=CM*COS(CA)*GM2*COS(GA2)-CM*SIN(CA)*GM2*SIN(GA2)
 122. =             DI=CM*COS(CA)*GM2*SIN(GA2)+CM*SIN(CA)*GM2*COS(GA2)
 123. =             DM=SQRT(DR*DR+DI*DI)
 124. =             DA=ATAN2(DI,DR)
 125. =             EM=DM/BM
 126. =             EA=DA-BA
 127. =             GR=SM11*COS(SA11)+EM*COS(EA)
 128. =             GI=SM11*SIN(SA11)+EM*SIN(EA)
 129. =             GM=SQRT(GR*GR+GI*GI)
 130. =             GA=ATAN2(GI,GR)*ARB
 131. =             PRINT 100,GM,GA
 132. =         100 FORMAT(7H MAG. =,1F12.6,8H PHASE =,1F12.6)
 133. =             GO TO 1
 134. =           2 CONTINUE
 135. =             END
 136.
 136.
```

b. Computation of Γ_2 from Γ_1, S_{11}, S_{12}, and S_{22}, via

$$\Gamma_2 = \frac{1}{S_{22} - \frac{S_{12}^2}{S_{11}-\Gamma_1}}$$

```
                LIST
101. =      CF  PROGRAM GAMMA
102. =        1 CONTINUE
103. =      CF  READ 0,S11,T11,S12,T12,S22,T22
104. =      CF  READ 0,G1,TG1
105. =          PI=3.141593
106. =          ARB=180./PI
107. =          T11=T11/ARB
108. =          T12=T12/ARB
109. =          T22=T22/ARB
110. =          TG1=TG1/ARB
111. =          AC=S11*COS(T11)-G1*COS(TG1)
112. =          AS=S11*SIN(T11)-G1*SIN(TG1)
113. =          AM=SQRT(AC*AC+AS*AS)
114. =          AA=ATAN2(AS,AC)
115. =          CM=S12*S12/AM
116. =          CA=2.*T12-AA
117. =          FC=S22*COS(T22)-CM*COS(CA)
118. =          FS=S22*SIN(T22)-CM*SIN(CA)
119. =          GM=1./SQRT(FC*FC+FS*FS)
120. =          GA=-(ATAN2(FS,FC)*ARB)
121. =          PRINT 100,GM,GA
122. =      100 FORMAT(7H MAG. =,1F10.6,7HPHASE =,1F10.6)
123. =          GO TO 1
124. =        2 CONTINUE
125. =          END
126.
```

126.

LIST OF MAJOR SYMBOLS

a	Outer radius of metal cylinder.
b	Outer radius of dielectric cylinder.
c	Speed of light in vacuum (3.10^8 meters/sec.).
C	Circumference of metal cylinder in free space wavelengths ($C=2\pi a/\lambda_v$).
$\mathbb{E}$	Vector electric field intensity, volts/meter.
E_ϕ	Component of $\mathbb{E}$ in ϕ direction, etc.
$\bar{E}_{\phi m}(h)=\bar{E}_\phi$	Transform of E_ϕ.
$E_o=\vec{E}_o(1+\Gamma_2)=\frac{V_o}{w}=$	Electric field across center of slot.
ε_v	Permittivity of vacuum ($1/36\pi\cdot10^9$ coulombs/meter).
ε_r	Relative dielectric constant of coating.
f	Frequency, cycles/sec.
h	Wave number in axial, z, direction.
$\mathbb{H}$	Vector magnetic field intensity, amperes/meter.
H_z	Component of $\mathbb{H}$ in z direction.
$H_{zm}(h)=\bar{H}_z$	Transform of H_z
$H_m^{(2)}(X)=J_m(X)-jY_m(X)$	Hankel function of second kind, order m, argument X.
$I_m(X)$	Modified Bessel function of first kind, order m, argument X.
$J_m(X)$	Bessel function of first kind, order m, argument X.
$K_m(X)$	Modified Bessel function of second kind, order m, argument X.
ℓ	Length of slot = internal width of waveguide.
m	Mode number (integer values, m=0,1,2...).
N	Index of refraction of coating ($N=\sqrt{\varepsilon_r}$).
p	Wave number in air region in radial, ρ, direction, $p^2=h^2-\beta_v^2$.
L.H.S.	Left hand side.
R.H.S.	Right hand side.

LIST OF SYMBOLS (Continued)

S_{11}, S_{12}, S_{22}	Scattering matrix elements.
u	Wave number in coating region in radial, ρ, direction, $u^2=\beta_v^2\varepsilon_r-h^2$.
u_v	Wave number in air region in radial, ρ, direction, $u_v^2=\beta_v^2-h^2$, $u_v^2=-p^2$.
V_o	Voltage across center of slot.
w	Slot width = internal height of waveguide.
W	b/a
$y=h/\beta_v$	Normalized wave number in axial direction.
y_c	Normalized external admittance ($y_c=Y_c\eta_v$).
Y_c	External admittance, mhos.
Y_{10}	Characteristic wave admittance of TE_{10} mode.
$y_{in}=y_2$	Normalized input waveguide admittance = $Y_{in}\eta_v = \frac{1-\Gamma_2}{1+\Gamma_2}$.
y_1	Normalized input coaxial line admittance = $\frac{1-\Gamma_1}{1+\Gamma_1}$.
$\beta_v=\omega\sqrt{\mu_v\varepsilon_v}$	Propagation factor in free space.
β_1	Propagation factor of TE_{10} mode.
ϕ_o	Angular slot width ($\phi_o = \frac{w}{a}$).
Γ_1	Complex reflection coefficient in coaxial line.
Γ_2	Complex reflection coefficient in waveguide.
$\eta_v=\sqrt{\frac{\mu_v}{\varepsilon_v}}$	Characteristic impedance of vacuum (120π ohms).
λ_v	Free space wavelength = c/f, meters.
$\omega=2\pi f$	Angular frequency.

All other symbols are defined as they are introduced.

REFERENCES

[1] J. R. Wait, "Electromagnetic Radiation from Cylindrical Structures", Pergamon Press, New York, N.Y., 1959, Chapter 16.

[2] C. M. Knop and C. T. Swift, "A Note on the Radiation Conductance of an Axial Slot on a Cylinder", Journal of Research, Radio Science, Vol. 69D, No. 3, March,1965, pp. 447-451.

[3] "Research Study of some RAM Antennas", Final Report on NASA Contract NAS1-4623, June, 1965, pp. II-67.

[4] Ibid, pp. II-6 to II-9.

[5] "Bessel Functions, Part I and Part II", in British Association Mathematical Tables, Cambridge University Press, London, England, Vols. 6 and 10, 1952 and 1958.

[6] R. S. Elliott, "Azimuthal Surface Waves on Circular Cylinders", J. Appl. Phys., 26, (4), pp. 368-376 (April,1955).

[7] C. H. Walter, "Travelling Wave Antennas", McGraw-Hill Book Co., 1965, pp. 363-366.

[8] J. R. Baechle, "The Effects of Curvature on Travelling Wave Antennas", Ph.D. Thesis, Ohio State University, Columbus, Ohio, Dec.,1963.

[9] C. T. Swift and C. M. Knop, "Equatorial Patterns of an Axially Slotted Cylinder Coated with a Critically Dense Plasma", IEEE Trans., Vo. AP-12, No. 4, July, 1964, pp. 498-502.

[10] Reference 3, pp. II-74 - II-82.

[11] R. N. Ghose, "Microwave Circuit Theory and Analysis", McGraw-Hill Book Co., N.Y., 1963, pp. 211-212.

[12] G. A. Deschamps, "Application of Non-Euclidean Geometry to the Analysis of Waveguide Junctions", URSI-IRE Spring Meeting, 1952.

[13] G. A. Deschamps, "Determination of Reflection Coefficients and Insertion Loss of a Waveguide Junction", J. Appl. Phys., Vol. 24, No. 8, pp. 1046-1050, August, 1953.

[14] J. E. Storer, L. S. Sheingold and S. Stein, "A Simple Graphical Analysis of a Two-port Waveguide Junction", Proc. IRE, Vol. 41, No. 8, pp. 1004-1013, Aug.,1953.

[15] C. T. Swift, "Radiation Patterns of a Slotted Cylinder Antenna in the Presence of an Inhomogeneous Lossy Plasma", Trans. IEEE, Vol. AP-12, No, 6, PP. 728-738, Nov.,1964; see also Trans. IEEE, Vol. AP-13, No. 6, p. 999.

[16] R. E. Collin, "Field Theory of Guided Waves", McGraw Hill Book Co., 1960, pp. 477-480.

[17] J. Y. Savard, "Higher-Order Cylindrical Surface-Wave Modes", IEEE Trans. MTT, Vol. MTT-15, No. 3, pp. 151-155, (March,1967).

[18] W. Hersch, "The Surface Wave Aerial", IEE Monograph, No. 363E, Feb.,1960, (Also Proc. IEE, 107, Part C, Sept.,1960).

[19] H. M. Barlow and J. Brown, "Radio Surface Waves", Oxford at the Clarendon Press, 1962. In particular, the sentence starting with:Hersch (1)... in the last paragraph of p. 69 is incorrect.

[20] F. B. Hildebrand, "Advanced Calculus for Engineers", Prentice-Hall, Inc., N.Y., 1949, pp. 161.

[21] Ibid, pp. 520-521.

[22] M. Abramowitz and I. A. Stegan, "Handbook of Mathematical Functions", National Bureau of Standards, Applied Mathematics Series 55, June, 1964.

[23] G. L. Ragan, "Microwave Transmission Circuits", Vol. 9, MIT Rad. Lab. Series, pp. 339-361, McGraw-Hill, 1946. (Also Boston Tech. Publishers, Inc., 1964).

[24] R. F. Harrington, "Time Harmonic Electromagnetic Fields", McGraw-Hill Book Company, N.Y., 1961, pp. 177-180, and problem 4-33, p. 195.

[25] Robin M. Chisholm, "The Characteristic Impedance of Trough and Slab Lines", IRE Trans. on MTT, July, 1956, pp. 166-172.

[26] E. Jahnke and F. Emde, "Tables of Functions", Dover Publications, N.Y., 1945, pp. 32-35, Part IV.

[27] E. L. Stiefel, "An Introduction to Numerican Analysis", Academic Press, New York, 1963.

[28] "System/360 Scientific Subroutine Package-Version II - Programmer's Manual", IBM Corporation, 1967.

ACKNOWLEDGEMENTS

In addition to the major contributors listed on the cover of the report, the following acknowledgements are in order:

Andrew Corporation

G. J. Bischak for assistance in the initial formulation of antenna design details.

T. Charlton for many technical discussions; in particular, to those dealing with azimuthal surface waves.

L. Hansen for the initial conception and work on the loop-T Bar antenna feed, and supervision of antenna construction.

A. G. Holtum for discussions relating to scattering matrix measurements.

G. Machay, Jr. for performing all the model shop work, from initial prototype to completed model.

R. F. H. Yang for discussions relating to antenna feed details.

S. Rubis for partial supervision of the model shop work.

Illinois Institute of Technology Research Institute

Dr. V. Gylys who performed all the numerical analysis and programming described in Appendix X and XI.

"The aeronautical and space activities of the United States shall be conducted so as to contribute . . . to the expansion of human knowledge of phenomena in the atmosphere and space. The Administration shall provide for the widest practicable and appropriate dissemination of information concerning its activities and the results thereof."

—NATIONAL AERONAUTICS AND SPACE ACT OF 1958

NASA SCIENTIFIC AND TECHNICAL PUBLICATIONS

TECHNICAL REPORTS: Scientific and technical information considered important, complete, and a lasting contribution to existing knowledge.

TECHNICAL NOTES: Information less broad in scope but nevertheless of importance as a contribution to existing knowledge.

TECHNICAL MEMORANDUMS: Information receiving limited distribution because of preliminary data, security classification, or other reasons.

CONTRACTOR REPORTS: Scientific and technical information generated under a NASA contract or grant and considered an important contribution to existing knowledge.

TECHNICAL TRANSLATIONS: Information published in a foreign language considered to merit NASA distribution in English.

SPECIAL PUBLICATIONS: Information derived from or of value to NASA activities. Publications include conference proceedings, monographs, data compilations, handbooks, sourcebooks, and special bibliographies.

TECHNOLOGY UTILIZATION PUBLICATIONS: Information on technology used by NASA that may be of particular interest in commercial and other non-aerospace applications. Publications include Tech Briefs, Technology Utilization Reports and Notes, and Technology Surveys.

Details on the availability of these publications may be obtained from:

SCIENTIFIC AND TECHNICAL INFORMATION DIVISION

NATIONAL AERONAUTICS AND SPACE ADMINISTRATION

Washington, D.C. 20546